

Centre for Doctoral Training in Controlled Quantum Dynamics  
Department of Physics, Imperial College London

---

# Entanglement and quantum clocks in curved spacetime

Maximilian P. E. Lock

September 2018

---

Submitted in partial fulfilment of the requirements for the degree of  
Doctor of Philosophy



## Originality and copyright declarations

Unless otherwise acknowledged or referenced, the contents of this thesis are the author's own original work, conducted as part of a PhD program at Imperial College, and have not been submitted for any degree requirement at this or any another university. Some of the work described in this thesis has been previously presented in the early and late stage assessment of the PhD program, and either has been, or will be, reported in a number of publications. A list of relevant publications by the author can be found later in this document.

The copyright of this thesis rests with the author and is made available under a Creative Commons Attribution Non-Commercial No Derivatives licence. Researchers are free to copy, distribute or transmit the thesis on the condition that they attribute it, that they do not use it for commercial purposes and that they do not alter, transform or build upon it. For any reuse or redistribution, researchers must make clear to others the licence terms of this work.

Maximilian Lock

September 2018

## Abstract

In this thesis, we investigate how motion through a curved spacetime background affects a system's dynamics, specifically the entanglement contained between its degrees of freedom, and our ability to use the system as a clock.

We incorporate both quantum theory and general relativity using quantum field theory in curved spacetime, localising the field by boundaries to describe e.g. an optical cavity. We derive the effect of boundary motion on the state of the field contained therein. A moving boundary can create particles from the vacuum in a phenomenon known as the dynamical Casimir effect; we give a description of the effect in curved spacetime. Reconsidering a common scenario, now adopting the Schwarzschild metric, we find novel particle-production resonances due to the curvature. We also discuss a potential enhancement of the effect in the phonon field of a Bose-Einstein condensate.

We apply these results to a quantum model of the famous light-clock thought experiment. After motivating and reviewing the model, we show for Gaussian clock states that the discrepancy between two such clocks is state-independent, and separates into classical and quantum effects. We numerically investigate the discrepancy when one clock is held in a gravitational field and the other falls a certain distance, finding quantitative and qualitative differences from the case of classical pointlike observers. We further show that the quantum and classical effects respectively increase and decrease in magnitude with increasing gravitational field strength.

We then study entanglement in a number of drop-tower scenarios, considering entanglement generated between field modes within an apparatus, and the degradation of an initially entangled state, both between spatially separated parties, and between modes contained within one apparatus. We quantify the effect via the negativity or the entanglement fidelity, as appropriate to each case. We present numerical investigations into the entanglement generated/degraded, finding novel features compared to previous investigations of non-inertial motion in flat spacetime, and discuss our results in the context of recent experiments on the subject.

*“You start doing research at birth, and you should never stop.”*

---

Kenneth G. Wilson [1]

## Acknowledgements

It’s an enormous privilege to be able to devote my time to something as fascinating as scientific research, even if the knowledge of this privilege sometimes gets lost in the day-to-day. Through this work I’ve been given the invaluable opportunity to travel great distances and meet many brilliant people. This was possible due to opportunities afforded to me that are not available to everyone. Aside from the accidents of birth from which I benefit, I was also supported in the past by financial programs aimed at encouraging the education of young people from low-income families - programs which are sadly no longer in place. It’s no exaggeration to say that without these, I wouldn’t even have made it to the starting line of my PhD.

In my opinion, we’re often far more dependent on one another than we would like to believe, and as a result, the following list of acknowledgements is necessarily incomplete. First, thanks are due to my family, old and new. In particular, thanks to my brother Dom for an act of kindness 16 years ago whose consequences include this thesis, and to my son Ned, for teaching me the meaning of unconditional love, and for reminding me that we’re all born as scientists. I’d also like to thank the Pratersauna WG for giving me a loving home, Karishma for always being there for me, Claude and Pauli for making sure I don’t take everything too seriously, and to Val, a constant source of love, comfort and encouragement. Thank you.

I’d also like to thank everyone involved with the Controlled Quantum Dynamics CDT for the training, opportunities and experience provided to me. My heartfelt thanks go to the members of cohort 5 for their companionship, and the great times we spent together, in particular Dan Goldwater and John Selby for many wonderful scientific discussions, but even more so for the warmth of their friendship. On the Vienna side, I’m deeply grateful to my friends in my former group for their camaraderie, especially Tupac Bravo Ibarra, Luis Cortés Barbado, Richard Howl and Dom Šafránek for being generous with their time when I bugged them with various odd questions. I’d also like to express my gratitude to Marcus Huber for

his support, his encyclopaedic knowledge, and his laid-back attitude, as well as to Nico Friis for his regular scientific guidance, but more importantly his indomitable good mood, his cheerful optimism, and his understanding of sarcasm. My thanks are of course also due to my supervisor Ivette Fuentes, for bringing me to Vienna, for providing me with fantastic opportunities, and for leaving me the freedom to grow.

Finally, like the proverbial tree falling in the woods, an unread thesis might be said to have never existed at all - an awfully demotivating prospect, given the enormous expenditure of time and effort required to write it. My last acknowledgement is therefore to you, dear reader, for lending me your eyes. I hope you find something stimulating.

## Publications

The following publications are associated with the work described in this thesis:

- I “Dynamical Casimir effect in curved spacetime” [2]
- II “Relativistic quantum clocks” [3]
- III “Frequency spectrum of an optical resonator in a curved spacetime” [4]
- IV “Quantum and classical effects in a light-clock falling in Schwarzschild geometry” [5]
- V “Generation and degradation of entanglement in a drop-tower” [6]

## List of figures

3.1	An illustration of the division of bipartite states into separable, entangled, PPT and bound entangled. The * denotes that the indicated set may not contain all bound entangled states. . . . .	39
5.1	A cartoon of $\sin[\omega_m(r_*(r) - r_*(r_1))]$ for $m = 1$ and $m = 2$ , in the case of no (orange) and strong (blue) curvature (as quantified by $r_S$ ). This illustrates how the curvature “pulls” the modes towards the gravitating body in the Schwarzschild $r$ -coordinate. . . . .	70
6.1	The fractional difference between the readings of dropped and stationary clocks in the case of pointlike, ideal clocks (dashed line), and classical light clocks (solid line), as a function of $t$ . Their negative values indicate that the dropped clocks experience less time passing than the stationary ones. Curves shown for $L_0 = 1$ m and a fall of 110 m to the surface of the Earth. . . . .	80
6.2	The overall (a) and small-time-scale (b) quantum contribution (i.e. $\theta_B^{Qu}/\theta_A$ ) to the fractional phase discrepancy between the clocks during a fall of 110 m to the surface of the Earth. This contribution acts to increase the difference in phase between the two clocks. For comparison, $\mathcal{F}_{\text{ext}} \approx -10^{-5}$ at the end of the motion. . . . .	82
6.3	The approximately linear behaviour of the fractional classical ( $\mathcal{F}_{\text{ext}}$ , red) and quantum ( $\theta_B^{Cl}/\theta_A$ , blue) contributions to the difference in phase between $A$ and $B$ , as a function of the spacetime curvature (i.e. Schwarzschild radius), after a fall of 110 m to the surface of the Earth. Note that, since these phase differences are negative, the rising (falling) curve is decreasing (increasing) in magnitude. For comparison, the Schwarzschild radius of the Earth is $r_S \sim 1$ cm. . . .	83
7.1	The negativity between modes in a single cavity, initially in the vacuum state, after a fall of 110 m to the surface of the Earth. . . . .	89

7.2	Entanglement degradation, as quantified by $\mathcal{N}^{(2)}$ as a function of the mode number $m$ of the dropped cavity's initial state. This is shown for an initial Bell state $ \Phi^+\rangle$ (orange), as well as for initial two-mode squeezed vacuum states with a squeezing parameter of magnitude 1/2 (blue) and 1/10 (green). . . . .	92
7.3	The evolution of the entanglement degradation throughout the fall (in terms of the Schwarzschild time coordinate $t$ ) for an initial Bell state $ \Phi^+\rangle$ (orange), as well as for initial two-mode squeezed vacuum states with a squeezing parameter of magnitude 1/2 (blue) and 1/10 (green), with $m = 10$ in all cases. . . . .	92
7.4	Mode dependence of the reduction in entanglement fidelity after the fall for the four initial states. . . . .	97
7.5	The evolution of $F_{\Phi^+}^{(2)}$ (black) and $F_{\Psi^+}^{(2)}$ (blue) throughout the fall, with $m = 1$ and $n = 2$ . The inset shows the small-scale oscillations of these quantities, which for $F_{\Psi^+}^{(2)}$ are of a sufficient amplitude and frequency to give the blue curve the appearance of a band. . . . .	97

# Contents

<b>Abstract</b>	<b>4</b>
<b>Acknowledgements</b>	<b>4</b>
<b>Publications</b>	<b>6</b>
<b>List of figures</b>	<b>7</b>
<b>I Context and framework</b>	<b>15</b>
<b>1 Introduction</b>	<b>16</b>
1.1 Motivation . . . . .	16
1.2 Structure of the thesis . . . . .	18
<b>2 Quantum field theory in curved spacetime</b>	<b>20</b>
2.1 Curved spacetime . . . . .	21
2.1.1 Geometry . . . . .	21
2.1.2 Kinematics . . . . .	22
2.1.3 Time-symmetric spacetimes . . . . .	22
2.1.4 The Schwarzschild metric . . . . .	23
2.2 Quantising the scalar field on a curved background . . . . .	24
2.2.1 A real scalar field on a classical background . . . . .	25
2.2.2 Quantising the field for inertial observers in flat spacetime . . . . .	27
2.2.3 Quantisation for general observers in general spacetimes . . . . .	28
2.2.4 Quantising a real massless scalar field on the Schwarzschild spacetime . . . . .	32
2.2.5 Bogoliubov transformations . . . . .	33

<b>3</b>	<b>Entanglement and the covariance matrix formalism</b>	<b>37</b>
3.1	Entanglement . . . . .	38
3.1.1	Negativity . . . . .	39
3.1.2	Entanglement fidelity . . . . .	39
3.2	Gaussian-state quantum mechanics . . . . .	40
3.2.1	From a bosonic field to Continuous variables . . . . .	40
3.2.2	Gaussian states and the covariance matrix formalism . . . . .	41
3.2.3	Examples . . . . .	42
3.2.4	Bogoliubov transformations of Gaussian states . . . . .	45
3.2.5	Symplectic eigenvalues . . . . .	46
3.3	Entanglement in continuous-variable quantum mechanics . . . . .	46
3.4	Entanglement and QFT . . . . .	47
<b>4</b>	<b>Quantum, relativistic, and relativistic quantum clocks</b>	<b>50</b>
4.1	Time in general relativity . . . . .	50
4.2	Time in quantum mechanics . . . . .	52
4.2.1	Pauli's theorem . . . . .	52
4.2.2	Finite-dimensional quantum clocks . . . . .	53
4.2.3	Parameter estimation . . . . .	53
4.2.4	Event-times . . . . .	54
4.2.5	Atomic clocks . . . . .	54
4.2.6	The quantum hourglass . . . . .	55
4.3	Relativistic quantum clocks . . . . .	55
4.4	The quantum light clock . . . . .	56
4.4.1	The model . . . . .	56
4.4.2	Review of results . . . . .	57
4.4.3	Summary . . . . .	59
<b>II</b>	<b>Space-time curvature effects in quantum systems</b>	<b>61</b>
<b>5</b>	<b>Boundary motion and the Dynamical Casimir Effect</b>	<b>62</b>
5.1	Introduction . . . . .	62
5.2	A brief overview of the DCE . . . . .	63
5.3	Stationary boundaries . . . . .	65

5.4	The effect of boundary motion . . . . .	66
5.5	Example: an oscillating boundary in the presence of a massive body . . . . .	69
5.6	Curved-spacetime DCE in BEC systems . . . . .	72
5.7	Conclusion and Discussion . . . . .	73
<b>6</b>	<b>Quantum and classical effects in a falling light-clock</b>	<b>75</b>
6.1	Introduction . . . . .	75
6.2	Classical and quantum effects on the clock time . . . . .	76
6.3	A falling quantum clock . . . . .	79
6.3.1	The scenario . . . . .	79
6.3.2	Classical clocks and proper times . . . . .	79
6.3.3	The quantum contribution to the phase discrepancy . . . . .	80
6.3.4	Curvature dependence . . . . .	81
6.4	Summary and discussion . . . . .	81
<b>7</b>	<b>Entanglement generation and degradation in curved spacetime</b>	<b>86</b>
7.1	Introduction . . . . .	86
7.2	Scenario 1: generation of entanglement in a single dropped box . . . . .	88
7.3	Scenario 2: degradation of entanglement between separated partners . . . . .	90
7.3.1	Setup . . . . .	90
7.3.2	Negativity for an initial Bell state . . . . .	90
7.3.3	Negativity for an initial two-mode squeezed vacuum states . . . . .	91
7.3.4	Results and discussion . . . . .	92
7.4	Scenario 3: change in entanglement fidelity within a single apparatus . . . . .	94
7.4.1	Setup . . . . .	94
7.4.2	Perturbative transformation of the entanglement fidelity . . . . .	94
7.4.3	Correlated states . . . . .	95
7.4.4	Anticorrelated states . . . . .	96
7.4.5	Results and discussion . . . . .	96
7.5	Conclusion . . . . .	98
<b>III</b>	<b>Conclusion, appendices and bibliography</b>	<b>100</b>
<b>8</b>	<b>Conclusion</b>	<b>101</b>
8.1	Summary . . . . .	101
8.2	Taking things further . . . . .	103

<b>Bibliography</b>	<b>104</b>
<b>A Notation and abbreviations</b>	<b>122</b>
<b>B The Bogoliubov transformation for constant-length motion</b>	<b>124</b>
<b>C The Bogoliubov transformation for boundary motion in a static 3+1D spacetime</b>	<b>128</b>
<b>D Unitary form of perturbative Bogoliubov transformations</b>	<b>129</b>



## Part I

# Context and framework

# Chapter 1

## Introduction

### 1.1 Motivation

Entanglement is quintessentially quantum, and studying it in a relativistic context has yielded a number of interesting results. For example, it is not in general Lorentz-invariant [7, 8], and is present between spacelike-separated regions of the vacuum [9], a fact which may hold clues about the quantum properties of spacetime itself [10]. Time, on the other hand, is already at the heart of the conflict between general relativity and quantum theory (see e.g. [11]). This thesis presents our modest efforts in exploring these two topics. Specifically, we examine how the presence of spacetime curvature modifies the evolution of quantum states in a system undergoing some motion, and how this in turn affects the system’s use as a time reference, and as a carrier of entanglement. We introduce the study of entanglement and quantum clocks from a relativistic perspective in more technical detail in Sections 3.4 and 4.3 respectively. Although there are contexts where these two aspects are discussed in relation to each other (e.g. [12, 13]), we consider them separately, believing each to be a fertile ground in which to examine the interplay of relativity and quantum theory.

To do this, we need a framework incorporating both quantum mechanics and general relativity. Restricting ourselves to the consideration of energy scales accessible in current (or near-future) experiments, and situations where the spacetime curvature is relatively low (as on the surface of the Earth), we do not need a full theory of quantum gravity, and we can instead employ the semiclassical methods of Quantum Field Theory (QFT) in curved spacetime, as described in Chapter 2. By “semi-classical”, we mean that quantum matter and radiation are embedded in a given curved spacetime, the latter being subject to the classical Einstein’s equations.<sup>1</sup>

---

<sup>1</sup>This is distinct from “semiclassical gravity” where one obtains the spacetime metric by inserting

QFT in curved spacetime also allows us to describe quantum fields from the perspective of non-inertial observers, leading to predictions of novel phenomena related to acceleration, namely the Unruh effect [14] and the Dynamical Casimir Effect (DCE) [15]. It is worth emphasising that these effects are both quantum mechanical and relativistic in nature, and cannot be derived by, for example, simply inserting a relativistic proper time into the Schrödinger equation of quantum mechanics. To fully include (classical) relativity into the quantum dynamics, one needs QFT in curved spacetime.

In recent years, aspects of quantum information have been integrated into QFT in curved spacetime in a collection of research efforts known as relativistic quantum information. This has allowed, for example, investigations into the effect of spacetime dynamics [16, 17] and non-inertial motion in flat spacetime [18, 8, 19, 20] on quantum entanglement (see Section 3.4), and the potentially detrimental [21, 22] or advantageous [23, 24] consequences of this effect for some quantum information applications. A particularly fruitful branch of relativistic quantum information is the incorporation of quantum metrology into a relativistic setting [25, 26], with a number of potential applications including the detection of gravitational waves in small-scale Bose-Einstein Condensate (BEC) experiments [27]. This framework has been used to consider the measurement of time by quantum clocks undergoing non-inertial motion, which is of particular relevance to this thesis, and is reviewed in Section 4.4.2.

We will mostly consider curvature effects on quantum states of the electromagnetic field, though we will also briefly discuss phononic states in a BEC. The field states will serve as the clocks and carriers of entanglement, which we will describe using aspects of continuous-variable quantum information. To construct localised states, we will consider the fields to be confined by boundaries, as in an optical cavity. We then need a way to calculate the transformation of the field state as a result of moving these boundaries through curved spacetime. Our results in this regard, described in Chapter 5, form the cornerstone of this thesis. Throughout our work, and particularly in the discussion of clocks, we rely upon the notion of operationalism. This is the principle that physical concepts be defined with respect to the operations by which they must be measured [28]. After all, “quantum phenomena do not occur in a Hilbert space, they occur in a laboratory” [29]. We will discuss the notion of operationalism a little more in Section 4.1, in the context of relativity.

Given the difference in the scales at which quantum theory and general relativity are usually applied, one may ask what we expect to gain by examining their overlap. Our response to such a question is threefold. Firstly, we point to the onward march

---

the average stress-energy tensor of a field state into the Einstein equations.

of technology. Modern timekeeping is precise enough to detect gravitational time dilation over a distance of 2 cm at the Earth's surface [30], part of a trend of exponentially increasing precision [31]. Considering this in tandem with the potential for improved timekeeping by exploiting quantum entanglement [32, 33], we argue that it will one day be necessary to consider general relativity when discussing the metrology of time. We give more details on this argument in Section 4.2.5. On the other hand, though harder to quantify in a single number, our ability to manipulate entanglement is also improving, driven by the expansion of the field of quantum information theory and the pursuit of a quantum computer [34].

Our second response is to point out the possibility of new technologies and experiments. There are already proposals to use effects which are both quantum and relativistic in order to measure the Schwarzschild radius of the Earth [35], or to make an accelerometer [36], for example. See [37] for a review of experiments carried out or proposed which employ both quantum and general relativistic features. Furthermore, there are practical questions which we cannot answer with quantum mechanics and general relativity separately. For example, what happens if we distribute entanglement across regions with differing spacetime curvatures (a scenario in which experimental investigations have recently begun [38]), or how do we synchronise a collection of distributed (potentially space-based) quantum clocks? The answers to these questions may be relevant for proposals to use correlated networks of orbiting atomic clocks for entanglement-assisted GPS [32], or to search for dark matter [39]

Finally, there is a strong motivation from the perspective of fundamental science to investigate the nature of time and entanglement at the overlap of general relativity and quantum theory. Beyond the intrinsic interest of exploring a coherent combination of the two most fundamental theories in physics, finding a quantum relativistic conception of time may be of relevance when using quantum clocks to test the equivalence principle [40, 41] and to single out general relativity from the family of gravitational theories obeying this principle [42], for example. As noted above, investigations of entanglement in a relativistic context have the potential to advance research into the quantum structure of spacetime, which we discuss in more detail in Section 3.4.

## 1.2 Structure of the thesis

The first part of this thesis consists of introductory chapters, presenting the relevant concepts, and reviewing the context necessary to make sense of the work presented later. Since our work combines disparate fields, and the theses of older

students are often used to introduce newer students to an area of research, special care has been taken to present this background in a pedagogical way, and it may therefore be of less interest to the more experienced reader. Chapter 2 lists some useful formulas and results from the general theory of relativity, before describing the pertinent aspects of QFT in curved spacetime, paying particular attention to the observer-dependence of a given quantisation of the field. In Chapter 3, we define entanglement and describe its quantification, as well as introducing some relevant tools from continuous-variable quantum mechanics (specifically regarding Gaussian states) and the description of entanglement in this context, before reviewing entanglement in the context of relativistic field theory. The different conceptions of time in quantum mechanics and general relativity are discussed in Chapter 4, exploring the contrast between them, and reviewing a relativistic quantum clock model which will be the workhorse for later results.

The presentation of our own work begins in the second part. First, as noted above, we need a way to describe the transformation of quantum states of the field due to the motion of the boundaries confining it. Chapter 5 gives exactly this, laying the groundwork for later chapters. The method is laid out in general, before being applied to a well-known scenario in flat spacetime, giving a novel effect when one includes background curvature, as well as recovering known results. We sketch a treatment of the same scenario applied to a BEC system, finding a potential augmentation of the effect. With that in place, Chapter 6 expounds our investigation into the use of a quantum clock to measure time in a curved background, re-examining the clock model referred to above, and finding separate classical and quantum effects on the clock time, the former arising due to the clock's finite extent. This is explored numerically in a droptower scenario, contrasting both quantitatively and qualitatively with the case of ideal pointlike clocks in general relativity. In Chapter 7, motivated by recent experimental efforts [43], we again consider the droptower, now examining the generation of entanglement between field modes contained within a single apparatus, as well as the degradation of entangled states between two systems (one dropped and one fixed), and within a single dropped apparatus. We examine the similarities and the differences in the generation/degradation of entanglement compared to investigations of the effect of non-inertial motion in flat spacetime.

The final part, Chapter 8 presents our concluding remarks, summarising our results and describing some limitations, as well as giving some possible future directions. A first step in one of those directions is given in Appendix D. We give a test and an extension of the results presented in Chapter 5 in Appendices B and C respectively. All acronyms, and much of the notation will be defined as they are introduced, but for reference, Appendix A contains a list of both.

## Chapter 2

# Quantum field theory in curved spacetime

In this chapter we sketch the necessary background in general relativity and QFT in curved spacetime, as well as considering some examples and identities which will be of use later. A more complete introduction to these subjects can be found in [44, 45] (general relativity) and [46, 47, 48, 49] and Section 14.2 of [45] (QFT in curved spacetime). We first review some geometric notions and their application in describing kinematics in a curved spacetime, before briefly discussing a notion of symmetry which is of fundamental importance to the work described in this thesis. The Schwarzschild spacetime is then introduced, and used to illustrate these notions, and two relevant classes of observer are highlighted. This is followed by a description of the process of quantising a real scalar field (a spin-0, and therefore bosonic, field) in curved spacetime, and how this relates to observers. We then return to the Schwarzschild spacetime, showing how to quantise the massless field far away from the spacetime's event horizon in a couple of cases, and to which observers these quantisations relate. Finally, we describe how different field quantisations, for example according to different observers, can be related to one other.

Here and throughout this thesis, we use a mostly-plus metric signature, and set  $c = \hbar = 1$ , except where it is useful to reintroduce them in order to compare magnitudes. Furthermore, we only consider spacetimes which are globally hyperbolic, i.e. causally well-behaved in the sense that the present determines the future (see e.g. [45], Section 8.3, for a technical definition).

## 2.1 Curved spacetime

The general theory of relativity describes gravity as the effect of the non-Euclidean geometry of spacetime, and gives a prescription for determining this geometry given the distribution of energy in that spacetime (Einstein's equations). In this thesis, we do not consider the latter, asking only how the presence of a given geometry affects the evolution of quantum states.

### 2.1.1 Geometry

In the mathematical formalism of general relativity, points in a spacetime constitute a manifold. At each point of the manifold one can define tangent and cotangent vector spaces, and physical objects are then encoded into tensors, that is, multilinear maps acting on multiple copies of these vector spaces. For example, in coordinates with components  $x^\mu$ , a tensor  $T$  is written

$$T = T^{\mu\dots\nu}{}_{\alpha\dots\beta} \partial_\mu \otimes \dots \otimes \partial_\nu \otimes dx^\alpha \otimes \dots \otimes dx^\beta \quad (2.1)$$

where  $\partial_\mu := \frac{\partial}{\partial x^\mu}$  and  $dx^\alpha$  are bases for the tangent and cotangent spaces respectively,  $\otimes$  denotes the tensor product between vector spaces, and we use the Einstein summation convention, where repeated indices indicate summation. We will use the common notation, whereby a single element of a tensor, written with free indices, is used to refer to the entire tensor (i.e.  $T^{\mu\dots\nu}{}_{\alpha\dots\beta}$  for the example above) and a coordinate and its label are used interchangeably in the partial derivative (e.g.  $\partial_{x^0} := \partial_0$ ). An inner product between vectors in the tangent space is defined via the (symmetric) metric tensor  $g_{\mu\nu}$  (whose components are in general functions of the coordinates), giving a notion of distances and angles between vectors. The inverse metric is denoted  $g^{\mu\nu}$ . Indices are lowered and raised by contraction with the metric and its inverse respectively. Coordinate-invariant distances in a spacetime with metric  $g_{\mu\nu}$  are given by the line element

$$ds^2 = g_{\mu\nu} dx^\mu dx^\nu \quad (2.2)$$

A class of metrics which will be important later are those which are separable in temporal and spatial coordinates, by which we mean that there exist some coordinates  $x^\mu = (t, \mathbf{x})$  (with the bold font indicating a spatial 3-vector) such that the line element can be written in the form

$$ds^2 = -N(t, \mathbf{x})^2 dt^2 + G_{ab}(t, \mathbf{x}) dx^a dx^b, \quad (2.3)$$

where Latin indices indicate that the sum should be taken over only the spatial coordinates.  $N(t, \mathbf{x})$  is known as the lapse function. Vectors are defined in the tangent space of a given point in the manifold, so to relate vectors in different tangent spaces, and therefore at different points in spacetime, we use the connection determined by the Christoffel symbols

$$\Gamma^\mu{}_{\alpha\beta} = \frac{1}{2}g^{\mu\sigma}(\partial_\alpha g_{\sigma\beta} + \partial_\beta g_{\alpha\sigma} - \partial_\sigma g_{\alpha\beta}). \quad (2.4)$$

The connection allows us to define tensor derivatives of vectors  $V^\mu$  and covectors  $V_\mu$ , such as the covariant derivative:

$$\nabla_\mu V^\nu = \partial_\mu V^\nu + \Gamma^\nu{}_{\mu\sigma} V^\sigma, \quad (2.5a)$$

$$\nabla_\mu V_\nu = \partial_\mu V_\nu - \Gamma^\sigma{}_{\mu\nu} V_\sigma. \quad (2.5b)$$

For a scalar quantity  $\phi$ , the covariant derivative reduces to the usual partial derivative  $\nabla_\mu \phi = \partial_\mu \phi$ .

### 2.1.2 Kinematics

The four-acceleration (or “absolute” acceleration) of an object following a worldline  $\mathcal{C}$  defined by the coordinate functions  $x^\mu(\tau)$ , with affine parameter  $\tau$  and tangent vector  $u^\mu = \frac{dx^\mu}{d\tau}$ , is

$$a^\mu := u^\nu \nabla_\nu u^\mu = \frac{d^2 x^\mu}{d\tau^2} + \Gamma^\mu{}_{\alpha\beta} \frac{dx^\alpha}{d\tau} \frac{dx^\beta}{d\tau}. \quad (2.6)$$

The proper acceleration experienced by the object is  $a = \sqrt{a^\mu a_\mu}$ . An inertial object (i.e. one with zero four-acceleration) follows a worldline satisfying the geodesic equation, which is obtained by setting the left-hand side of Equation (2.6) to zero. We recall that  $u^\mu$  encodes the object’s energy and momentum. Adopting the “clock postulate”, discussed in Section 4.1, we identify the time measured by an observer following the curve  $x^\mu(\tau)$  with the affine parameter  $\tau$ , which we refer to as the proper time. This is related to the line element along the curve by  $d\tau^2 = -ds^2$ , i.e.

$$\tau = \int_{\mathcal{C}} \sqrt{-g_{\mu\nu}(x) dx^\mu dx^\nu}. \quad (2.7)$$

### 2.1.3 Time-symmetric spacetimes

Continuous symmetries of a spacetime are associated with a Killing vector (the latter generating, in the Lie theory sense, the corresponding element of the symmetry

group), and correspond to conservation laws via Noether's theorem. A vector  $\xi^\mu$  is Killing if it satisfies

$$\nabla_\mu \xi_\nu + \nabla_\nu \xi_\mu = 0. \quad (2.8)$$

If the metric is independent of a particular coordinate, say  $x^\rho$ , so that  $\partial_\rho g_{\mu\nu} = 0$ , then  $\xi^\mu = \delta^\mu_\rho$  is a Killing vector. If a vector  $V^\mu$  satisfies  $g_{\mu\nu} V^\mu V^\nu < 0$ , it is said to be timelike. Combining these statements, we see that if a metric has a time-translation symmetry, so that it is independent of a temporal coordinate  $x^0$ , then  $\partial_0$  is a timelike Killing vector<sup>1</sup>. Conversely, given a timelike Killing vector, we can find coordinates such that  $\xi^\mu = (1, \mathbf{0})$ , and Equation (2.8) then ensures that the metric is independent of that temporal coordinate. Denoting these coordinates  $x^\mu = (t, \mathbf{x})$ , the family of observers with  $u^\mu$  proportional to  $\xi^\mu$ , i.e.  $u^\mu = ((-g_{00}(\mathbf{x}))^{-1/2}, \mathbf{0})$ ,<sup>2</sup> therefore have proper times  $\tau$  such that  $\frac{\partial}{\partial \tau} = (-g_{00})^{-1/2} \partial_t$ . This fact will be of particular relevance in the following section, where it will be related to an observer's definition of the particle content of a quantum field. If a spacetime (or a patch thereof) admits a Killing vector which is everywhere timelike, it is referred to as stationary. If, in addition, the metric can be written such that the line element takes the form given in Equation (2.3), the spacetime (or patch thereof) is referred to as static.

#### 2.1.4 The Schwarzschild metric

In later chapters, we will make use of the Schwarzschild metric, whose corresponding line element can be written in spherical coordinates as

$$ds^2 = -f(r)dt^2 + \frac{1}{f(r)}dr^2 + r^2 d\Omega^2, \quad (2.9)$$

where  $d\Omega^2 = d\theta^2 + \sin^2 \theta d\varphi^2$ ,  $f(r) := 1 - \frac{r_S}{r}$  and the Schwarzschild radius is  $r_S = 2GM$ , with  $G$  and  $M$  respectively denoting the gravitational constant and the mass of a black hole. Far from the black hole's horizon (i.e.  $r \gg r_S$ ) This spacetime can be used to model a spherically-symmetric gravitating body with mass  $M$ . Ignoring the effect of the Earth's rotation, we will use this spacetime to model physics at and near the planet's surface. We note that this spacetime is static. The metric is independent of  $t$  and therefore  $\xi^\mu = \delta_t^\mu$  satisfies condition (2.8), i.e.  $\partial_t$  is a timelike Killing vector<sup>3</sup>.

An experimenter at rest with respect to the surface of the Earth, i.e. with fixed

<sup>1</sup>where the vector is written in the form given in Equation (2.1).

<sup>2</sup>The necessity of this form is a consequence of the normalisation of the tangent vector  $g_{\mu\nu} u^\mu u^\nu = -1$ .

<sup>3</sup>This is no longer true for  $r < r_S$ , but we only consider  $r \gg r_S$  in this thesis.

$(r, \theta, \varphi) = (r_0, \theta_0, \varphi_0)$ , is referred to as a “shell” observer. From the normalisation of  $u^\mu$ , we see that such an observer has the four-velocity  $u_{shell}^\mu = (f(r_0)^{-1/2}, \mathbf{0})$ , and so in an interval of coordinate time  $t$ , the observer experiences a proper time

$$\tau_{shell} = \sqrt{f(r_0)}t. \quad (2.10)$$

The shell observer is related to the timelike Killing vector  $\partial_t$  in the manner discussed in Section 2.1.3, and we have  $\frac{\partial}{\partial \tau_{shell}} = f(r_0)^{-1/2} \partial_t$ . Now, since the coordinate acceleration  $\frac{du^\mu}{d\tau} = 0$ , from the right-hand side of Equation (2.6), we see that the only the connection (i.e. geometric) term contributes to the four-acceleration, and a shell observer then experiences the proper acceleration

$$a_{shell} = \frac{r_s}{2r_0^2} \frac{1}{\sqrt{f(r_0)}}. \quad (2.11)$$

This example highlights the difference between the proper, coordinate and four-acceleration.

A second type of observer who will be relevant in later chapters is the “drip” observer, who starts at rest at, say,  $(r, \theta, \varphi) = (r_0, \theta_0, \varphi_0)$  and falls freely for a period of time. Solving the geodesic equation (Equation (2.6) with  $a^\mu = 0$ ), one finds

$$u_{drip}^\mu = \left( \frac{\sqrt{f(r_0)}}{f(r)}, -\sqrt{f(r_0) - f(r)}, 0, 0 \right), \quad (2.12)$$

and therefore in an interval of coordinate time  $t$ , the drip observer then experiences a proper time

$$\tau_{drip} = \sqrt{\frac{r_0}{r_s}} \left[ \sqrt{r(r_0 - r)} + r_0 \arccos \left( \sqrt{\frac{r}{r_0}} \right) \right] \quad (2.13)$$

where  $r(t)$  is determined by

$$\frac{dr}{dt} = -f(r) \sqrt{1 - \frac{f(r)}{f(r_0)}}. \quad (2.14)$$

## 2.2 Quantising the scalar field on a curved background

QFT is a framework for describing systems of identical particles, where particle number is a dynamical quantity. It came about in large part from efforts to make quantum theory compatible with special relativity [50]. In it, particles are described as the quantised excitations of the field. We follow the common canonical quantisation procedure for free fields [51], which we summarise here:

1. Specify a Lagrangian for a classical field, usually on the grounds of certain

symmetries.

2. Apply the principle of extremal action to find equations of motion for the field.
3. Associate the set of solutions to these equations with modes, and express the field as a linear combination of these solutions;
4. Find the canonical momentum corresponding to the field, and obtain the Hamiltonian via the Legendre transform.
5. Associate the field and its momentum with operators, and impose that their equal-time commutators (or anticommutators for fermionic fields) are equal to  $i\hbar$  multiplied by the Poisson bracket of the corresponding classical quantities (a prescription formalised by Dirac [52]).
6. Decompose the field operator into creation and annihilation operators associated with each classical solution (i.e. mode), subject to the usual (anti)commutation relations.
7. Use the creation and annihilation operators to define a ground (vacuum) state and a Fock space for each mode.

In QFT in curved spacetime, the general theory of relativity is incorporated by “embedding” quantum fields in a classical curved spacetime. The resulting semiclassical theory is then analogous to the treatment of quantum matter subjected to classical electromagnetic radiation (for example in the treatment of the Rabi problem), and just as in the latter theory, the reaction of the classical field to the quantum matter is ignored. We will consider a real scalar field, which corresponds to uncharged spin-0 particles, such as the Higgs boson and certain composite particles (neutral scalar mesons), and is the simplest of the fields commonly studied in QFT. More relevant to the work described in this thesis, however, is the capacity of the massless real scalar field to model the electromagnetic field when the effect of polarisation is neglected [53], as well as the acoustic excitations of a BEC while taking into account a curved spacetime background [54, 55]. We will mostly consider the former application, considering BECs only briefly in Section 5.6.

### 2.2.1 A real scalar field on a classical background

Giving up the global Lorentz symmetry of Minkowski-space QFT, and instead demanding only local covariance, one finds the general Lagrangian density for a real scalar field  $\Phi$  with mass  $m$ , embedded in a spacetime with metric  $g_{\mu\nu}$ , to be [47]

$$\mathcal{L} = \frac{1}{2} (-g)^{1/2} \{ g^{\mu\nu} (\nabla_\mu \Phi) (\nabla_\nu \Phi) - [m^2 + \zeta R] \Phi^2 \}, \quad (2.15)$$

where  $g := |\det(g_{\mu\nu})|$ ,  $\zeta$  is an arbitrary numerical factor,  $R$  is the Ricci scalar curvature, and where all quantities except for  $m$  and  $\zeta$  are in general functions of the spacetime coordinates. Here we choose  $\zeta = 0$  (so called “minimal coupling”). Applying the principle of extremal action to Equation (2.15), one arrives at the generally covariant Klein-Gordon equation

$$[\square + m^2] \Phi = 0 \quad (2.16)$$

with  $\square := g^{\mu\nu} \nabla_\mu \nabla_\nu = (-g)^{-1/2} \partial_\mu [(-g)^{1/2} g^{\mu\nu} \partial_\nu]$ . Equation (2.16) being linear, its solutions form a vector space. Let  $\{\phi_k\}$  denote a basis to this space, with each  $k$  representing a set of numbers (collectively referred to as a mode) labelling the solution. Since the differential operator in Equation (2.16) contains only real quantities, it follows that  $\{\phi_k^*\}$  (where  $*$  denotes the complex conjugate) must also be solutions. The general solution is then given as a linear combination of each mode,

$$\Phi = \sum_k [a_k \phi_k + a_k^* \phi_k^*], \quad (2.17)$$

where  $a_k$  are arbitrary complex coefficients and  $\sum_k$  denotes either integration or summation over  $k$  depending its continuous or discrete nature. The orthonormality of elements of the basis is defined with respect to the inner product [47]

$$(f_1, f_2) := -i \int_\Sigma d\sigma (-g_\Sigma)^{1/2} n^\mu [f_1 (\partial_\mu f_2^*) - (\partial_\mu f_1) f_2^*], \quad (2.18)$$

where  $\Sigma$  is a spacelike hypersurface with future-directed unit normal  $n^\mu$  and induced metric  $g_\Sigma$ . The product defined by (2.18) satisfies all the properties of a Hermitian inner product except for positivity, i.e. we can have  $(f, f) < 0$ , as we shall see. Using the property of global hyperbolicity mentioned earlier, it can be shown that (2.18) is independent of  $\Sigma$  [47].

Given a metric written in the form determined by Equation (2.3), the Klein-Gordon inner product becomes [14]

$$(f_1, f_2) = -i \int d\mathbf{x} \frac{\sqrt{G}}{N} [f_1 (\partial_t f_2^*) - (\partial_t f_1) f_2^*], \quad (2.19)$$

where  $G := \det G_{ab}$ . Here the spacelike hypersurface  $\Sigma$  is given by  $t = \text{const}$ , and the product is therefore independent of  $t$ . Furthermore, we can define the conjugate momentum to each mode solution by [14]

$$\Pi_k(t, \mathbf{x}) := \frac{\sqrt{G(t, \mathbf{x})}}{N(t, \mathbf{x})} \partial_t \phi_k(t, \mathbf{x}), \quad (2.20)$$

and the conjugate momentum to the general solution  $\Phi$  is then  $\Pi := \int_k \Pi_k$ .

To quantise the field, we need a prescription for constructing an algebra of operators and a Hilbert space from the classical solution given in Equation (2.17). In particular, we will need physical grounds on which to choose one basis of solutions over another.

### 2.2.2 Quantising the field for inertial observers in flat spacetime

Let us briefly consider the set of inertial reference frames in Minkowski (flat) spacetime, each described in the usual rectangular system of coordinates. In these cases, we have  $g_{\mu\nu} = \text{diag}(-1, 1, 1, 1)$ , and the operator  $\square$  takes the same form in each frame. Denoting any such frame by  $(t, \mathbf{x})$ , there is a “natural” choice for the basis of solutions:

$$\phi_{\mathbf{k}}(t, \mathbf{x}) = N_{\mathbf{k}} e^{-i(\omega_{\mathbf{k}} t - \mathbf{k} \cdot \mathbf{x})} \quad (2.21)$$

where the (continuous) mode label is the wavevector  $\mathbf{k}$ ,  $\omega_{\mathbf{k}} = m^2 + |\mathbf{k}|^2$  and  $N_{\mathbf{k}} = 1/\sqrt{2\omega_{\mathbf{k}}(2\pi)^3}$  is a normalisation constant.

From Equation (2.20), we find the conjugate field  $\Pi = \partial_t \Phi$  and promote<sup>4</sup>  $\Phi$  and  $\Pi$  to operators. Imposing the canonical commutation relations on them (the Dirac prescription mentioned above) leads to the promotion of  $a_{\mathbf{k}}$  to an operator (with  $a_{\mathbf{k}}^* \rightarrow a_{\mathbf{k}}^\dagger$ ) satisfying the bosonic commutation relation

$$\left[ a_{\mathbf{k}}, a_{\mathbf{k}'}^\dagger \right] = \delta(\mathbf{k} - \mathbf{k}'), \quad (2.22)$$

where  $[\cdot, \cdot]$  is the commutator and  $\delta(\mathbf{x})$  is the Dirac distribution. A vacuum state can be defined by  $a_{\mathbf{k}} |0\rangle = 0 \forall \mathbf{k}$ . One can then construct a Fock space in the usual way, by defining a single-particle Hilbert space, and then taking the (appropriately symmetrised) direct sum of each tensor power of this single-particle space [56]. The states with definite particle number in each mode form a basis for the Fock space, a state with  $n$  particles in mode  $\mathbf{k}$  being denoted by  $|n_{\mathbf{k}}\rangle$ . The  $a_{\mathbf{k}}$  and  $a_{\mathbf{k}}^\dagger$  are then interpreted as ladder operators for particle-number states:

$$a_{\mathbf{k}}^\dagger |n_{\mathbf{k}}\rangle = \sqrt{n_{\mathbf{k}} + 1} |(n+1)_{\mathbf{k}}\rangle, \quad (2.23a)$$

$$a_{\mathbf{k}} |n_{\mathbf{k}}\rangle = \sqrt{n_{\mathbf{k}}} |(n-1)_{\mathbf{k}}\rangle. \quad (2.23b)$$

The number of particles in mode  $\mathbf{k}$  is associated with the operator  $a_{\mathbf{k}}^\dagger a_{\mathbf{k}}$ . Under a Lorentz transformation such that  $k^\mu = (\omega_{\mathbf{k}}, \mathbf{k}) \rightarrow k'^\mu = (\omega_{\mathbf{k}'}, \mathbf{k}')$ , an  $n$ -particle

<sup>4</sup>By “promoting” something to an operator, we mean that we associate an operator with it, and in an abuse of notation, use the original quantity to denote the associated operator.

Fock state of mode  $\mathbf{k}$  then transforms to an  $n$ -particle Fock state of mode  $\mathbf{k}'$  (and the vacuum state is unchanged). Consequently, all inertial observers agree on the number of particles in the field. For general observers and/or general spacetimes, we will see that this is no longer the case.

### 2.2.3 Quantisation for general observers in general spacetimes

When quantising the field in the previous section, we could have chosen a different basis of solutions than the one given by Equation (2.21). Indeed, one can arbitrarily combine the elements of one basis in order to construct a new one. Is it then natural to ask why this particular basis was used, and if another would have been equally valid. We will now see that these questions are particularly relevant when quantising the field in curved spacetime. Since the vacuum state (and thence the notion of particles) was defined with respect to the set of modes, the choice of basis has physical consequences, and must therefore be made based upon a physical condition. Before continuing, we note that in flat spacetime, every inertial frame's time coordinate  $t$  is associated with the timelike Killing vector  $\partial_t$ .

#### A physical condition determining a basis of modes

Let  $(t, \mathbf{x})$  now denote coordinates in any stationary spacetime, such that  $\partial_t$  is a timelike Killing vector; the metric is therefore independent of  $t$  in these coordinates. Consequently, given any solution  $\phi(t, \mathbf{x})$  to the Klein-Gordon equation (2.16),

$$\phi(t + dt, \mathbf{x}) = (1 + dt \partial_t) \phi(t, \mathbf{x}) \quad (2.24)$$

is also a solution, and we can therefore see that the space of solutions forms a representation<sup>5</sup> of the time-translation symmetry group. The generator  $\partial_t$  is the timelike Killing vector itself. If we can find a basis of solutions  $\{\phi_k(t, \mathbf{x})\}$  which diagonalise this operator, i.e. such that

$$\partial_t \phi_k(t, \mathbf{x}) = -i\omega_k \phi_k(t, \mathbf{x}), \quad (2.25a)$$

$$\partial_t \phi_k(t, \mathbf{x})^* = i\omega_k \phi_k(t, \mathbf{x}), \quad (2.25b)$$

for some positive  $\omega_k$ , then we have found a basis whose elements respond to the action of the group by accruing a phase, but not mixing with one another. In other words, we have decomposed the representation of the time-translation symmetry group into a direct sum of one-dimensional irreducible representations. The distinction between

---

<sup>5</sup>More precisely stated, the solutions form the space upon which a group representation acts.

modes is therefore not lost over time, and as a consequence, after quantisation, the Hilbert space constructed at a given time will be consistent with the one constructed at some later time. The mode solutions with eigenvalues  $-i\omega_k$  (respectively  $i\omega_k$ ) are referred to as having positive-frequency (respectively negative-frequency). Equating the inner product (2.18) between two mode solutions at times  $t$  and  $t + dt$ , we find  $[\partial_t \phi_k(t, \mathbf{x}), \phi_{k'}(t, \mathbf{x})] + (\phi_k(t, \mathbf{x}), \partial_t \phi_{k'}(t, \mathbf{x})) = 0$ , and then Equations (2.25) imply

$$-i(\omega_k - \omega_{k'}) (\phi_k(t, \mathbf{x}), \phi_{k'}(t, \mathbf{x})) = 0, \quad (2.26)$$

and so condition (2.25) implies that different modes are orthogonal. By a similar process, one finds that  $(\phi_k(t, \mathbf{x}), \phi_{k'}(t, \mathbf{x})^*) = 0 \forall k, k'$ . We are then free to choose the  $\{\phi_k(t, \mathbf{x})\}$  such that they are orthonormal

$$(\phi_k(t, \mathbf{x}), \phi_{k'}(t, \mathbf{x})) = I_{kk'}, \quad (2.27)$$

where  $I_{kk'}$  is either a Dirac distribution  $\delta(k - k')$ , a Kronecker delta  $\delta_{kk'}$ , or a combination thereof according to the nature and dimension of the label  $k$ . However, from the definition of the inner product (2.18), we must then have  $(\phi_k(t, \mathbf{x})^*, \phi_{k'}(t, \mathbf{x})^*) = -I_{kk'}$ . Nonetheless, if we interpret the operator  $E := i\partial_t$  as corresponding to energy, this negativity, combined with the conditions (2.25), ensures that the energy of a mode

$$(\phi_k(t, \mathbf{x}), E\phi_k(t, \mathbf{x})) = (\phi_k(t, \mathbf{x})^*, E\phi_k(t, \mathbf{x})^*) = \omega_k \quad (2.28)$$

is always positive. This would not have been guaranteed for an arbitrary choice of basis, which underlines the  $\{\phi_k(t, \mathbf{x})\}$  as a physically appropriate choice.

In a static spacetime, the Klein-Gordon equation becomes separable in its spatial and temporal coordinates in such a way that the existence of solutions satisfying (2.25) is guaranteed. For stationary but not static spacetimes, one can nonetheless arrive at a similarly consistent quantum description via algebraic QFT. Specifically, one can demand that, in selecting a representation of the algebra of field operators, one arrives at a one-particle Hilbert space such that the left-hand side of (2.28) is equal to the energy of the corresponding one-particle state (see [57] for a full treatment).

From here we can follow the same procedure as in Section 2.2.2, leading to a Fock space and ladder operators satisfying  $[a_k, a_{k'}^\dagger] = I_{kk'}$ , with a the field operator

$$\Phi = \sum_k [a_k \phi_k + a_k^\dagger \phi_k^*], \quad (2.29)$$

Since  $\phi_k(t + \Delta t, \mathbf{x}) = e^{-i\omega_k \Delta t} \phi_k(t, \mathbf{x})$ , the time-evolution of the free quantised field in the Heisenberg picture is given by  $a_k(t + \Delta t) = e^{-i\omega_k \Delta t} a_k(t)$ .

### Associating a given mode structure with observers

While we have arrived at a quantisation of the field where the mode structure is determined by a physical condition, there remains an ambiguity. There can exist multiple inequivalent timelike Killing vectors associated with a spacetime (as in Minkowski space), resulting in multiple inequivalent quantisations of the field<sup>6</sup>, and we must decide which quantisation is appropriate for a given observer. We do so by noting, as in Section 2.1.3, that there is a family of observers corresponding to each timelike Killing vector, namely those whose worldline has tangent vector  $u^\mu = ((-g_{00}(\mathbf{x}))^{-1/2}, \mathbf{0})$ . Each member of this family has a proper time  $\tau$  such that  $\frac{\partial}{\partial \tau} = (-g_{00})^{-1/2} \partial_t$ . Solutions that are of positive (negative) frequency with respect to a timelike Killing vector are therefore of positive (negative) frequency with respect to the corresponding observers, though different observers will assign different values to these frequencies. We can now finally answer the questions of why the basis of solutions Equation (2.21) was appropriate for inertial observers in flat spacetime, and if there are other possible bases. The answer to the former question is that Equation (2.21) gives the positive (and its conjugate, the negative) frequency solutions with respect to each inertial observer's proper time, and these proper times correspond to timelike Killing vectors. The answer to the latter question is affirmative: consider the timelike Killing vector given by  $\partial_\eta := x\partial_t + t\partial_x$ , where  $t$  and  $x$  respectively refer to the temporal and one spatial coordinate of an inertial frame. This corresponds to the temporal coordinate  $\eta$  of a Rindler frame, used to describe observers undergoing constant proper acceleration (in this case in the  $x$  direction) [58]. Choosing a basis of solutions which diagonalises  $\partial_\eta$ , one arrives at a mode structure, and then a Hilbert space, which is different from the one used for inertial observers. One consequence of this is that the vacuum states differs for inertial and accelerated observers. This leads to a phenomenon known as the Unruh effect<sup>7</sup>. In Section 2.2.5, we will see how to relate quantisations according to different timelike Killing vectors, and therefore different observers, via Bogoliubov transformations.

### Arbitrary observers and non-stationary spacetimes

We have described a procedure for quantising the field when there exists a timelike Killing vector. In non-stationary spacetime, where no such vector exists, there is in general no physical condition dictating specific mode structures, and therefore

<sup>6</sup>Note that these quantisations are inequivalent in the sense that they correspond to different choices of a basis of modes, but they are equivalent in the sense of representation theory - they are related to each other by a unitary transformation.

<sup>7</sup>To arrive at the thermal state predicted in the Unruh effect, one needs an additional concept, specifically the causal horizon generated by uniform acceleration.

specific vacuum states. To make matters worse, while the vacua of a field quantised according to two different timelike Killing vectors are related to each other by a unitary transformation (see Section 2.2.5), in non-stationary spacetimes the possible vacua are unitarily inequivalent. One must therefore abandon the hope of calculating observables via a Hilbert space, and instead use algebraic QFT in curved spacetime (see [59] for a concise introduction and historical overview).

Furthermore, for observers in a stationary spacetime who are not associated with timelike Killing vector fields in the manner described above, the quantisation of the field according to one or another timelike Killing vector does not describe the particle content of the field according to that observer. In this case, one may be able to make statements about how that observer sees a the field via locally-defined quantities such as  $\langle \psi | T_{\mu\nu}(x^\mu(\tau)) | \psi \rangle$ , where  $x^\mu(\tau)$  is the observer's worldline,  $T_{\mu\nu}(x^\mu)$  is the stress-energy tensor of the field and  $|\psi\rangle$  is the field state according to a given quantisation (see [47] for details and a full definition of  $T_{\mu\nu}(x^\mu)$ ).

Finally, there are certain cases where there is a timelike Killing vector associated with the observer of interest before and after a given process, and one can treat such cases as a scattering problem. On the one hand, we have cases where the spacetime is made of three regions: an “in” region where that the spacetime is stationary, a non-stationary middle region, and an “out” region where the spacetime is stationary again, as is the case<sup>8</sup> when calculating the Hawking radiation from a star collapsing into a black hole [60] or particle creation by an expanding universe [61]. On the other hand, as we discuss in Chapter 5, one can consider observers who begin by following a worldline associated with a timelike Killing vector, then undergo some arbitrary motion, before returning to a worldline associated with a timelike Killing vector.

#### 2.2.4 Quantising a real massless scalar field on the Schwarzschild spacetime

We take as an example a real massless scalar field in the Schwarzschild spacetime, which we will use in later chapters. We seek to describe the field far from the horizon  $r \gg r_s$ . Using the “tortoise” coordinate

$$r_* = r + r_S \ln \left| \frac{r}{r_S} - 1 \right|, \quad (2.30)$$

the line element in the Schwarzschild spacetime (Equation (2.9)) becomes

$$ds^2 = f(r)(-dt^2 + dr_*^2) + r^2 d\Omega^2. \quad (2.31)$$

---

<sup>8</sup>The in and out regions in these examples are in fact only asymptotically stationary.

The angular part of metric is the same as in the Minkowski metric (in Spherical coordinates), and the other part is independent of the angular coordinates. Consequently, the angular part of the Klein-Gordon equation (2.16) is separable, and takes the same form as in flat spacetime. We can therefore write the solutions in terms of spherical harmonics  $Y_{lm}(\theta, \varphi)$ , i.e.  $\phi_{lm}(t, r_*, \theta, \varphi) = R_l(t, r_*) \frac{Y_{lm}(\theta, \varphi)}{r}$ , where  $R_l(t, r_*)$  satisfies [45]

$$[\partial_t^2 - \partial_{r_*}^2 + V_l(r)] R_l(t, r_*) = 0 \quad (2.32)$$

with

$$V_l(r) := f(r) \left[ \frac{l(l+1)}{r^2} + \frac{r_S}{r^3} \right]. \quad (2.33)$$

$V_l(r)$  acts as a potential barrier, with a maximum at  $r < \frac{3}{2}r_S$  and tending to zero at  $r = r_S$  and  $r \rightarrow \infty$ . In the regime of interest (far from the event horizon), we can take  $V_l(r) \approx 0$ , and our mode solutions are

$$\phi_{\omega lm}(t, r, \theta, \varphi) \approx N_\omega e^{-i\omega[t-r_*(r)]} \frac{Y_{lm}(\theta, \varphi)}{r}, \quad (2.34)$$

with  $N_\omega = \sqrt{2\pi\omega}$  and  $(\phi_{\omega lm}, \phi_{\omega' l' m'}) = \delta_{ll'} \delta_{mm'} \delta(\omega - \omega')$ . Now, as noted in Section 2.1.4,  $\partial_t$  is a timelike Killing vector, and we have  $\partial_t \phi_{\omega lm} = -i\omega \phi_{\omega lm}$ . Furthermore, a shell observer fixed at  $(r, \theta, \varphi) = (r_0, \theta_0, \varphi_0)$  has a tangent vector parallel to  $\delta_t^\mu$ , and (as also noted in Section 2.1.4) their proper time  $\tau_{shell}$  is such that  $\frac{\partial}{\partial \tau_{shell}} = f(r_0)^{-1/2} \partial_t$ . Consequently, the shell observer agrees with the separation into positive and negative-frequency modes according to the timelike Killing vector  $\partial_t$ , and we can use the mode basis given in Equation (2.34) to quantise the field for this observer according to the procedure described in Section 2.2.3. The total field is then given by a linear combination as in Equation (2.29).

## 2.2.5 Bogoliubov transformations

### Transformation and identities

We can describe the elements of one basis of mode solutions  $\{\tilde{\phi}_k\}$  in another basis  $\{\phi_l\}$  by a linear combination

$$\tilde{\phi}_k = \sum_l (\alpha_{kl} \phi_l + \beta_{kl} \phi_l^*), \quad (2.35)$$

with the inverse relation

$$\phi_l = \sum_k (\alpha_{kl}^* \tilde{\phi}_k - \beta_{kl} \tilde{\phi}_k^*). \quad (2.36)$$

These are referred to as Bogoliubov transformations, and the  $\alpha_{kl}$  and  $\beta_{kl}$  as Bogoliubov coefficients. They allow us to translate between quantisations according to

different timelike Killing vectors, or to describe the “scattering” processes mentioned above. In the former case, the Bogoliubov coefficients are given by  $\alpha_{kl} = (\tilde{\phi}_k, \phi_l)$  and  $\beta_{kl} = -(\tilde{\phi}_k, \phi_l^*)$ . Inserting (2.36) and its complex conjugate into the expansion for field operator (Equation 2.29), we can rewrite the transformation as acting on the ladder operators, giving

$$\tilde{a}_k = \int_l^f (\alpha_{kl}^* a_l - \beta_{kl}^* a_l^\dagger) \quad (2.37)$$

and the inverse transformation

$$a_l = \int_k^f (\alpha_{kl} \tilde{a}_k + \beta_{kl}^* \tilde{a}_k^\dagger). \quad (2.38)$$

These correspond to a class of unitary transformations, e.g.  $\tilde{a}_k = U a_k U^\dagger$ , where the generator of  $U$  is at most quadratic in the  $\{a_l\}$  and  $\{a_l^\dagger\}$ . Indeed, the action of any at-most-quadratic Hamiltonian, such as displacement, squeezing and beam-splitting operations, or any other Gaussian operation in quantum optics (see Chapter 3) can be represented by a Bogoliubov transformation [62]. In Appendix D, we derive expressions for the unitary operator corresponding to a perturbative Bogoliubov transformation.

The possible Bogoliubov transformations are constrained by the following three (equivalent) conditions: the preservation of the canonical commutation relation, the preservation of the orthonormality of the mode bases, and the unitary character of the transformation. These conditions are met if the coefficients  $\alpha_{kl}$  and  $\beta_{kl}$  satisfy the Bogoliubov identities:

$$\int_l^f (\alpha_{ml} \alpha_{nl}^* - \beta_{ml} \beta_{nl}^*) = I_{mn} \quad (2.39a)$$

$$\int_l^f (\alpha_{ml} \beta_{nl} - \beta_{ml} \alpha_{nl}) = 0 \quad (2.39b)$$

As noted above, the vacuum state constructed by the field quantisation with respect to  $\{\tilde{\phi}_k\}$ , i.e. the state  $|\tilde{0}\rangle$  defined by  $\tilde{a}_k |\tilde{0}\rangle = 0 \forall k$ , need not coincide with  $|0\rangle$ , the one constructed by the quantisation with respect to  $\{\phi_k\}$ . We can see this by considering the action of  $\tilde{a}_k$  on the  $|0\rangle$ :

$$\tilde{a}_k |0\rangle = - \int_l^f \beta_{kl}^* a_l^\dagger |0\rangle \neq 0 \quad (2.40)$$

i.e.  $|0\rangle \neq |\tilde{0}\rangle$ . The particle content of the field is therefore an observer-dependent quantity. For example, the vacuum state of the  $\{\tilde{\phi}_k\}$  quantisation contains an aver-

age of

$$\langle n_l \rangle = \sum_k |\beta_{kl}|^2 \quad (2.41)$$

particles in the mode corresponding to  $\phi_l$ . The  $\beta_{kl}$  therefore quantify “particle creation” due to the transformation.

### Matrix form

Let us gather the mode solutions  $\{\phi_l\}$  into a column vector

$$\Psi := \begin{pmatrix} \phi_1 \\ \phi_2 \\ \vdots \\ \phi_1^* \\ \phi_2^* \\ \vdots \end{pmatrix}, \quad (2.42)$$

and define the matrices  $\alpha$  and  $\beta$  as those whose components are given by the coefficients  $\alpha_{kl}$  and  $\beta_{kl}$ . We can then write the Bogoliubov transformation to the new basis  $\{\tilde{\phi}_k\}$  (likewise gathered into the column vector  $\tilde{\Psi}$ ) as a matrix equation  $\tilde{\Psi} = S\Psi$ , with (in block matrix form)

$$S := \begin{pmatrix} \alpha & \beta \\ \beta^* & \alpha^* \end{pmatrix}. \quad (2.43)$$

The Bogoliubov identities (2.39) can then be written

$$SKS^\dagger = K, \quad (2.44)$$

with  $K := \mathbb{1} \oplus (-\mathbb{1})$  where  $\mathbb{1}$  is the identity matrix. This identifies  $S$  as an element of (a complex representation of) the real symplectic group [63, 64], with the symplectic form  $K$ . The corresponding Lie algebra in this representation consists of the matrices  $X$  satisfying

$$XK + KX^\dagger = 0. \quad (2.45)$$

The composition of multiple Bogoliubov transformations is calculated by multiplying the corresponding matrices.

### Perturbative Bogoliubov transformations

Throughout this thesis we will make use of perturbative Bogoliubov transformations, i.e.

$$\alpha_{mn} = \alpha_{mn}^{(0)} + \alpha_{mn}^{(1)} + \alpha_{mn}^{(2)} + \dots \quad (2.46a)$$

$$\beta_{mn} = \beta_{mn}^{(1)} + \beta_{mn}^{(2)} + \dots \quad (2.46b)$$

with  $\alpha_{mn}^{(0)} = G_m \delta_{mn}$  for some  $G_m$ , and where the number in parentheses indicates the order of that term in some small parameter. The Bogoliubov identities can be written order by order, giving

$$|G_m|^2 = 1 \quad (2.47a)$$

$$G_m \alpha_{nm}^{(1)*} = -G_n^* \alpha_{mn}^{(1)} \quad (2.47b)$$

$$G_m \beta_{nm}^{(1)} = G_n \beta_{mn}^{(1)} \quad (2.47c)$$

$$G_m \alpha_{nm}^{(2)*} + G_n^* \alpha_{mn}^{(2)} = -\int_p \left( \alpha_{mp}^{(1)} \alpha_{np}^{(1)*} - \beta_{mp}^{(1)} \beta_{np}^{(1)*} \right) \quad (2.47d)$$

$$G_m \beta_{nm}^{(2)} - G_n \beta_{mn}^{(2)} = -\int_p \left( \alpha_{mp}^{(1)} \beta_{np}^{(1)} - \beta_{mp}^{(1)} \alpha_{np}^{(1)} \right), \quad (2.47e)$$

and  $|0\rangle$  can be related to  $|\tilde{0}\rangle$  by [65]

$$\begin{aligned} |0\rangle = & \left\{ \mathbb{1} + \frac{1}{2} \int_{pq} \left[ \left( V_{pq}^{(1)} + V_{pq}^{(2)} \right) a_p^\dagger a_q^\dagger - \frac{1}{2} |\beta_{pq}^{(1)}|^2 \right] \right. \\ & \left. + \frac{1}{4} \int_{pqrs} V_{pq}^{(1)} V_{rs}^{(1)} a_p^\dagger a_q^\dagger a_r^\dagger a_s^\dagger \right\} |\tilde{0}\rangle \end{aligned} \quad (2.48)$$

where

$$V_{mn}^{(1)} = -G_n^* \beta_{mn}^{(1)*} \quad (2.49a)$$

$$V_{mn}^{(2)} = -G_n^* \beta_{mn}^{(2)*} + G_m^* G_n^* \int_p \beta_{pm}^{(1)*} \alpha_{pn}^{(1)} \quad (2.49b)$$

If we write a state in the quantisation according to  $\{\phi_l\}$  as a combination of its ladder operators acting on its vacuum, then Equations (2.38) and (2.48) give us a way to write that state in the  $\{\tilde{\phi}_k\}$  quantisation. Note that due to the perturbative nature of the transformation, it may be necessary to normalise the state afterwards.

## Chapter 3

# Entanglement and the covariance matrix formalism

In this chapter we will briefly discuss the notion of quantum entanglement and its quantification, before reviewing the covariance matrix formalism for treating Gaussian states. The latter is most often applied in the field of quantum optics in flat spacetime, and this is the context we use to introduce it. Reviews of entanglement and entanglement measures can be found in [66] and [67] respectively, while a pedagogical introduction to continuous-variable quantum mechanics and Gaussian states can be found in [68]. The consideration of Gaussian states allows us to greatly simplify certain calculations; two relevant examples are the evolution of the optical phase of a quantum state (which is necessary for the results described in Chapter 6), and the negativity (a measure of a quantum state's entanglement, introduced in the following section and employed in Chapter 7). We begin by defining entanglement, the negativity of a state and the entanglement fidelity. We then show how a bosonic quantum field can give rise to a continuous-variable Hilbert space, and how observable aspects of the electromagnetic field are related to this description. The covariance matrix formalism is then introduced, and Gaussian states defined, before showing how Bogoliubov transformations of states, discussed in Section 2.2.5, are represented within the formalism. Applying the notions outlined in this chapter to the scalar field discussed in Chapter 2 allows us to explore relativistic effects on the former, and to consider scenarios where the underlying spacetime is curved. To provide a background for later work, we review some studies of entanglement in a relativistic context in Section 3.4

### 3.1 Entanglement

Entanglement is a key feature of quantum mechanics, arising due to a combination of the superposition principle, and the way in which distinct degrees of freedom are composed within the theory. Broadly speaking, the degree of entanglement in a system's state is the extent to which separate descriptions of the system's degrees of freedom fail to describe their totality; for entangled states, “the whole is something beside the parts” [69]. Entanglement is a fungible resource, forming an essential part of numerous quantum information processing and quantum cryptographic applications (see [66]). Its central role in foundational studies of quantum mechanics is exemplified by Bell's theorem, where entanglement is used to discount the possibility of local hidden-variable interpretations of quantum mechanics [70]. It is a necessary feature of any post-quantum theory which encompasses classical physics [71].

We define bipartite entanglement<sup>1</sup> in the following way. A pure state represented by the vector  $|\psi_{AB}\rangle$  in  $\mathcal{H} = \mathcal{H}_A \otimes \mathcal{H}_B$  is called separable when it can be written as a product of states in the subspaces, i.e.  $|\psi\rangle = |\psi_A\rangle \otimes |\psi_B\rangle$ . For a mixed state with density operator  $\rho$  on  $\mathcal{H}$ , the separability condition generalises to

$$\rho_{AB} = \sum_i p_i \rho_A^i \otimes \rho_B^i. \quad (3.1)$$

A state which is not separable is entangled. Given the utility of this nonseparability as a resource, it is of interest to quantify the entanglement contained within a state. The zoo of entanglement measures is discussed in detail in [67]. This quantification is in general a highly non-trivial task, and a comparison of the entanglement content of different states gives rise to structure which is only partially ordered [72]. Of relevance to the task of quantifying entanglement is the Partial Positive Transpose (PPT) criterion, also known as the Peres-Horodecki criterion. A PPT state is one where taking the partial transpose of the density operator with respect to one of the subspaces results in an operator with non-negative eigenvalues. The PPT criterion is the statement that a separable state is necessarily PPT. However, in general, PPT does not imply separability. States which are PPT but not separable cannot be used to distil pure maximally entangled states, a property which is referred to as bound entanglement [66]. The division of bipartite states into these categories is illustrated in Figure 3.1.

---

<sup>1</sup>The multipartite case, i.e. where  $\mathcal{H}$  is a product of more than two subspaces, is not relevant to the work presented in this thesis.

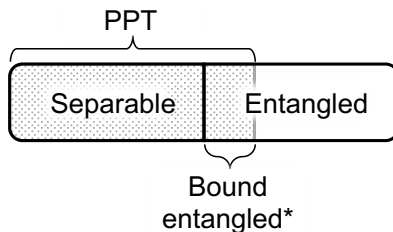


Figure 3.1: An illustration of the division of bipartite states into separable, entangled, PPT and bound entangled. The \* denotes that the indicated set may not contain all bound entangled states.

### 3.1.1 Negativity

The failure of a state to be PPT can be used to define a measure of entanglement, the negativity, as follows:

$$\mathcal{N}(\rho) := \frac{\|\rho^{T_B}\|_1 - 1}{2} = \left| \sum_p \lambda_p^- \right| \quad (3.2)$$

where  $\|A\|_1 := \text{tr}\sqrt{A^\dagger A}$  is the trace norm,  $T_B$  denotes the partial transpose with respect to  $B$ , and  $\lambda_p^-$  are the negative eigenvalues of  $\rho^{T_B}$ . The eigenvalues of  $\rho^{T_B}$  are the same as those of  $\rho^{T_A}$ , and therefore the value of  $\mathcal{N}(\rho)$  does not change if we replace  $\rho^{T_B}$  with  $\rho^{T_A}$  in Equation (3.2). The negativity is by definition 0 for all PPT states (including bound entangled ones). Moreover, it is not additive i.e.  $\mathcal{N}(\rho^{\otimes n}) \neq n\mathcal{N}(\rho)$ . For finite-dimensional systems, the negativity can be efficiently estimated by measurements [73], but for continuous variables, a full state tomography is needed (as in [74]). Operationally, the negativity gives an upper bound to the distillable entanglement and the state's capacity to be used for quantum teleportation [75].

### 3.1.2 Entanglement fidelity

In addition to quantifying the entanglement present within a system, we will find it useful to quantify how this entanglement is affected when the system undergoes some dynamics. To this end, we use the entanglement fidelity, which can be thought of as the fidelity of a process with respect to an initial state; it is the probability that a state undergoing some process would pass a test verifying that it agreed with the initial state (for example according to a joint measurement on  $A$  and  $B$ ) [76]. The entanglement fidelity of a state  $\rho_{AB}$  with respect to a pure entangled state  $|\psi_{AB}\rangle$  is given by [77]

$$F_{\psi_{AB}}[\rho] := \langle \psi_{AB} | \rho | \psi_{AB} \rangle \quad (3.3)$$

## 3.2 Gaussian-state quantum mechanics

### 3.2.1 From a bosonic field to Continuous variables

Given creation and annihilation operators  $a_n$  and  $a_n^\dagger$  for mode  $n$  of the electromagnetic (or indeed any bosonic) field, we can define hermitian quadrature operators by

$$q_n := \frac{1}{\sqrt{2}} (a_n + a_n^\dagger) \quad (3.4a)$$

$$p_n := \frac{-i}{\sqrt{2}} (a_n - a_n^\dagger). \quad (3.4b)$$

These correspond respectively to the real and imaginary parts of a classical wave in the field (see the calculations in Section II.A of [78] for details). They represent observables of the field, and can be measured by the process of homodyne detection [79, 78]. Assuming the mode label  $n$  to be discrete, they satisfy the canonical commutation relation  $[q_m, p_n] = i\delta_{mn}$ . Restricting ourself for now to the consideration of  $N$  modes,<sup>2</sup> we gather the quadratures together into the vector

$$\hat{Q} := (q_1, p_1, q_2, p_2, \dots, q_N, p_N)^T, \quad (3.5)$$

i.e.  $\hat{Q}_{2n-1} := q_n$  and  $\hat{Q}_{2n} := p_n$ , and the canonical commutation relations can then be written

$$[\hat{Q}_m, \hat{Q}_n] = i\tilde{K}_{mn} \quad (3.6)$$

where the matrix  $\tilde{K}$  is a finite-dimensional symplectic form (similar<sup>3</sup> to  $K$  in Section 2.2.5), with components satisfying

$$\tilde{K}_{mn} = \begin{cases} 1 & \text{if } n = m + 1 \\ -1 & \text{if } n = m - 1 \\ 0 & \text{otherwise.} \end{cases} \quad (3.7)$$

Defining the characteristic function of a quantum state  $\rho$  by

$$\chi(Y) := \text{tr} \left[ \rho e^{i\hat{Q}^T \tilde{K} Y} \right], \quad (3.8)$$

<sup>2</sup>Given the dearth of literature on the subject of infinite-mode continuous-variable quantum mechanics, we shall follow the usual procedure of restricting ourself to  $N$  modes, and then tacitly assuming that the relevant quantities generalise straightforwardly as  $N \rightarrow \infty$ .

<sup>3</sup>A truncated version of  $K$  is obtained from  $\tilde{K}$  by the change of basis that takes  $(q_1, p_1, q_2, p_2, \dots, q_N, p_N)^T$  to  $(q_1, q_2, \dots, q_N, p_1, p_2, \dots, p_N)^T$

where  $Y \in \mathbb{R}^{2N}$ , the Wigner function corresponding to that quantum state is given by the Fourier transform [62]

$$W(X) = \frac{1}{(2\pi)^{2N}} \int dY e^{-iX^T \tilde{K} Y} \chi(Y) \quad (3.9)$$

where  $X \in \mathbb{R}^{2N}$ . The components of the vector  $X$  constitute a phase space, corresponding element-by-element to the quadrature operators constituting  $\hat{Q}$ . The Wigner function is then a quasiprobability distribution on that quantum phase space (see e.g. [78]). This gives a description of a physical state which is equivalent to the density operator, and the invertible map between the two descriptions (i.e. Equation (3.9)) is known as the Wigner-Weyl transform [80]. The Wigner function can take negative values, and can only be treated as a joint probability distribution when calculating the marginal probabilities or expectation values of compatible observables, e.g.  $q_n$  and  $p_m$  with  $m \neq n$ . The negativity of the Wigner function is sometimes taken as a signature of non-classicality [81], though there is some ambiguity in this (see e.g. the introduction of [82] and references therein). For example, there are states with positive Wigner functions, but which exhibit quantum entanglement, as we shall see.

### 3.2.2 Gaussian states and the covariance matrix formalism

We now define a vector of first moments  $d$  by

$$d_j := \langle \hat{Q}_j \rangle, \quad (3.10)$$

and a matrix of second moments  $\sigma$  (the covariance matrix) by

$$\sigma_{ij} = \langle \{X_i, X_j\} \rangle - 2 \langle X_i \rangle \langle X_j \rangle, \quad (3.11)$$

where  $\langle A \rangle$  denotes the expectation value of the operator  $A$  with respect to the state of the field, the labels  $i, j$  run from 1 to  $2N$  and  $\{\cdot, \cdot\}$  is the anticommutator. Note that these definitions may differ from other authors by a multiplicative numerical factor. The requirement that the density operator be positive semidefinite, combined with the canonical commutation relations (Equation (3.6)), imply that [68]

$$\sigma + i\tilde{K} \geq 0. \quad (3.12)$$

This expresses the uncertainty relation between the quadratures of a given mode (in the sense of the Robertson relation [83]). Any  $\sigma$  satisfying this inequality corresponds to a physical state [68]. Furthermore, from the definition of  $\sigma$  we have  $\sigma_{ij} = \sigma_{ji}$ ,

and the inequality then implies that  $\sigma > 0$ .

The Gaussian states are those for which the Wigner function takes the form of a Gaussian distribution:

$$W(X) = \frac{1}{\pi^N} \frac{1}{\sqrt{\det \sigma}} e^{-(X-d)^T \sigma^{-1} (X-d)}. \quad (3.13)$$

This is non-negative, and for pure states the Wigner function is strictly non-negative if and only if the state is Gaussian [84]. For this reason the Gaussian states are often referred to as the most classical

In Equation 3.13 one can see that for Gaussian states the Wigner function is completely determined by the first and second moments. Consequently, if we restrict ourselves to Gaussian states and the transformations that preserve their Gaussian character (“Gaussian operations”) then we can describe the state and its evolution by  $d$  and  $\sigma$  alone. This is referred to as the covariance matrix formalism. The first moments encode the average phase and amplitude of the field for each mode. For example the average phase  $\theta$  of mode  $n$  satisfies

$$\tan \theta = \frac{\langle p_n \rangle}{\langle q_n \rangle} = \frac{d_{2n}}{d_{2n-1}}. \quad (3.14)$$

The second moments, on the other hand, encode the variances of each field mode and the correlations between modes (and therefore the entanglement content of the state). Interestingly, the average particle number of a state is in general encoded across both the first and second moments.

Every unitary Gaussian operation is generated by a Hermitian matrix which is an at-most-second-order polynomial in the creation and annihilation operators, and those which are strictly second order can be written in the form of the Bogoliubov transformations introduced in Section 2.2.5 [62]. Conversely, every Bogoliubov transformation can be represented by a unitary operation generated by a second-order Hermitian operator.

The covariance matrix formalism greatly simplifies a number of calculations. For example, taking the partial trace over some modes preserves the Gaussian character of a state, and is represented by simply deleting the corresponding rows and columns from  $\sigma$ , and the corresponding elements of  $d$ .

### 3.2.3 Examples

We now list some examples of Gaussian states and their properties, giving the density operator  $\rho$ , and the first and second moments  $d$  and  $\sigma$  in each case, before describing some relevant non-Gaussian states.

### Vacuum states

As noted in the previous chapter, the vacuum  $|0_n\rangle$  of a mode  $n$  is defined by  $a_n |0_n\rangle = 0$ . The tensor product of the vacuum states for all modes is written  $|0\rangle$ . Any time that a bra or ket is written for a subset of modes, it is implicit that the remaining modes are in the vacuum state. For the vacuum state of mode  $n$ , we have

$$\rho = |0_n\rangle\langle 0_n|, \quad d = 0, \quad \sigma = \mathbb{1}_2, \quad (3.15)$$

where  $\mathbb{1}_2$  is the  $2 \times 2$  identity matrix.

### Coherent states

The coherent state  $|\alpha_n\rangle$  of mode  $n$  is defined as an eigenstate of that mode's annihilation operator, i.e.  $a_n |\alpha_n\rangle = \alpha |\alpha_n\rangle$  for some complex  $\alpha$  (referred to as the displacement parameter). We can then see the vacuum as an example of a coherent state with  $\alpha = 0$ . Coherent states are generated by the action of the displacement operator,  $D_n(\alpha) := e^{\alpha a_n^\dagger - \alpha^* a_n}$  on the vacuum state. We have

$$\rho = e^{-|\alpha|^2} \sum_{s,t=0}^{\infty} \frac{\alpha^{s+t}}{\sqrt{s!t!}} |s_n\rangle\langle t_n|, \quad d = \sqrt{2} \begin{pmatrix} \Re(\alpha) \\ \Im(\alpha) \end{pmatrix}, \quad \sigma = \mathbb{1}_2. \quad (3.16)$$

where  $\Re(\alpha)$  and  $\Im(\alpha)$  denote the real and imaginary parts of  $\alpha$  respectively. The coherent states are sometimes referred to as quasi-classical, as the expectation value of the electromagnetic field evolves as a classical monochromatic wave, and they exhibit minimal fluctuations in the value of the field symmetrically in the quadratures (see e.g. Section 5.3 of [85]). In the Schrodinger picture, the state  $|\alpha_n\rangle$  evolves over a period of time<sup>4</sup>  $t$  according to  $\alpha \rightarrow e^{-i\omega_n t} \alpha$ , where  $\omega_n$  is the frequency of mode  $n$ .

### The two-mode squeezed vacuum

Squeezed states, like coherent states, minimise the uncertainty between field quadratures (and therefore fluctuations of the field). Unlike coherent states however, this uncertainty is not symmetric in the quadratures; one degree of freedom exhibits a greater uncertainty than another, and so the fluctuations are ‘‘squeezed’’ into the former. The two-mode squeezed vacuum is the state resulting from the action of the two-mode squeezing operator, i.e.  $U_{mn}(\zeta) := e^{\zeta(a_m^\dagger a_n^\dagger - a_m a_n)}$ , where, for simplicity we consider the squeezing parameter  $\zeta$  to be real. This is equivalent to choosing

<sup>4</sup>When we consider the field in a curved spacetime, this time will correspond to the timelike Killing vector used to quantise the field.

a particular direction in the quantum phase space along which the quadrature uncertainties are reduced (see [74] for a discussion of the more general case). These states can be generated experimentally using an optical parametric oscillator [74]. We have

$$\rho = \frac{1}{\cosh^2 \zeta} \sum_{s,t=0}^{\infty} (\tanh \zeta)^{s+t} |s_m s_n\rangle \langle t_m t_n|, \quad d = 0, \quad (3.17)$$

$$\sigma = \begin{pmatrix} \cosh(2\zeta) \mathbb{1}_2 & \sinh(2\zeta) \sigma_z \\ \sinh(2\zeta) \sigma_z & \cosh(2\zeta) \mathbb{1}_2 \end{pmatrix},$$

where  $\sigma_z := \text{diag}(1, -1)$  is the Pauli  $z$ -matrix. As we shall see in Section 3.3, these states are entangled across modes  $m$  and  $n$ .

### Thermal state of a single mode

The thermal state (also known as the Gibbs state) is that which maximises the von Neumann entropy for a given mean energy [86], this entropy being defined by

$$S := -\text{tr} [\rho \ln \rho]. \quad (3.18)$$

In the case of a single mode  $n$  of the field, the mean energy is given by  $\text{tr} [\rho \omega_n a_n^\dagger a_n]$ . For the single-mode thermal state, we then have

$$\rho = \frac{1}{Z_n} e^{-\beta \omega_n a_n^\dagger a_n}, \quad d = 0, \quad \sigma = \coth \left( \frac{\beta \omega_n}{2} \right) \mathbb{1}_2, \quad (3.19)$$

where  $Z_n := \text{tr} [e^{-\beta \omega_n a_n^\dagger a_n}]$  and  $\beta := 1/k_B T$  is the usual inverse temperature from statistical mechanics, and where  $k_B$  is Boltzmann's constant. For a free field whose total state is thermal, each subset of modes is also in a Gibbs state. This is the approximate equilibrium state of, for example, an optical cavity weakly coupled to a thermal reservoir.

### Non-Gaussian states

We now give some examples of non-Gaussian states, each of which therefore has a negative Wigner function in some region of the phase space. One important class of such states are the Fock states, which form the usual basis for a Fock space, and are generated by products of creation operators acting on the vacuum, e.g.

$$|s_m t_n\rangle = \frac{(a_m^\dagger)^s}{\sqrt{s!}} \frac{(a_n^\dagger)^t}{\sqrt{t!}} |0\rangle. \quad (3.20)$$

Another set of non-Gaussian states, which will be of use in Chapter 7, are the following

$$|\Phi^+\rangle = \frac{1}{\sqrt{2}} (|0_m 0_n\rangle + |1_m 1_n\rangle) \quad (3.21a)$$

$$|\Phi^-\rangle = \frac{1}{\sqrt{2}} (|0_m 0_n\rangle - |1_m 1_n\rangle) \quad (3.21b)$$

$$|\Psi^+\rangle = \frac{1}{\sqrt{2}} (|0_m 1_n\rangle + |1_m 0_n\rangle) \quad (3.21c)$$

$$|\Psi^-\rangle = \frac{1}{\sqrt{2}} (|0_m 1_n\rangle - |1_m 0_n\rangle) \quad (3.21d)$$

where, for clarity, we have explicitly written the vacuum states of certain modes. Although, these are *prima facie* the Bell states [87], the underlying Hilbert space for each mode is of course not that of qubits. Another notable class of entangled non-Gaussian states are the so-called NOON states  $\frac{1}{\sqrt{2}}(|N_m 0_n\rangle + |0_m N_n\rangle)$ , which have proposed applications in phase metrology [88]. For  $N = 1$  we have a state equivalent to  $|\Psi^+\rangle$ . Finally, we note that superpositions of Gaussian states, such as  $\frac{1}{\sqrt{2}}(|\alpha_n\rangle + |-\alpha_n\rangle)$ , in general lose their Gaussian character, as do Gaussian states from which photons have been coherently added or subtracted [89].

### 3.2.4 Bogoliubov transformations of Gaussian states

After a general Gaussian operation, the first and second moments transform as [62]

$$\begin{aligned} d &\rightarrow \tilde{S}d + b, \\ \sigma &\rightarrow \tilde{S}\sigma\tilde{S}^T \end{aligned} \quad (3.22)$$

where  $b \in \mathbb{R}^{2N}$ , and  $\tilde{S}$  is an element of the (real representation<sup>5</sup> of) the real symplectic group  $\text{Sp}(2N, \mathbb{R})$ , satisfying  $\tilde{S}\tilde{K}\tilde{S}^T = \tilde{K}$ . For a Bogoliubov transformation of the form given in Section 2.2.5, we have  $b = 0$ , and

$$\tilde{S} = \begin{pmatrix} \mathcal{M}_{11} & \mathcal{M}_{12} & \dots & \mathcal{M}_{1N} \\ \mathcal{M}_{21} & \mathcal{M}_{22} & \dots & \mathcal{M}_{2N} \\ \vdots & \vdots & \ddots & \vdots \\ \mathcal{M}_{N1} & \mathcal{M}_{N2} & \dots & \mathcal{M}_{NN} \end{pmatrix}, \quad (3.23)$$

with

$$\mathcal{M}_{mn} := \begin{pmatrix} \Re(\alpha_{mn} - \beta_{mn}) & \Im(\alpha_{mn} + \beta_{mn}) \\ -\Im(\alpha_{mn} - \beta_{mn}) & \Re(\alpha_{mn} + \beta_{mn}) \end{pmatrix}. \quad (3.24)$$

<sup>5</sup>c.f. the complex representation used in Section 2.2.5

One can then take the partial trace over all but the modes of interest by deleting the appropriate entries from the first and second moments. For example, given a single-mode state with initial first and second moments  $d_0^{(n)}$  and  $\sigma_0^{(n)}$ , after enacting a Bogoliubov transformation and tracing out all modes except  $n$ , the new moments are given by [26, 25]

$$d^{(n)} = \mathcal{M}_{nn} d_0^{(n)}, \quad (3.25a)$$

$$\sigma^{(n)} = \mathcal{M}_{nn} \sigma_0^{(n)} \mathcal{M}_{nn}^T + \frac{1}{4} \sum_{s \neq n} \mathcal{M}_{ns} \mathcal{M}_{ns}^T, \quad (3.25b)$$

### 3.2.5 Symplectic eigenvalues

As noted above, the covariance matrix is positive-definite and symmetric. For any symmetric, positive-definite,  $2N \times 2N$  matrix  $\sigma$ , there exists a (unique)  $\tilde{S}_\sigma \in \text{Sp}(2N, \mathbb{R})$  such that [90]

$$\sigma = \tilde{S}_\sigma^T \left[ \bigoplus_{j=1}^N \begin{pmatrix} \nu_j & 0 \\ 0 & \nu_j \end{pmatrix} \right] \tilde{S}_\sigma, \quad (3.26)$$

with  $\nu_j > 0 \forall j$ . The  $N$  values  $\nu_j$  are referred to as the symplectic eigenvalues (or the symplectic spectrum) of  $\sigma$ , and they can be computed by selecting the positive eigenvalues of the matrix  $i\tilde{K}\sigma$ . These allow us to easily compute the negativity of a Gaussian state, as we shall see in the following section.

## 3.3 Entanglement in continuous-variable quantum mechanics

In this section we make a few remarks relevant for later chapters. For a more in-depth review on the subject of entanglement in continuous-variable systems, see [91].

For the Bell states given in Equation (3.21) above, the negativity is  $\mathcal{N}_{Bell} = \frac{1}{2}$ . For qubits, these are the maximally entangled states, but here that is not the case. In contrast with finite-dimensional quantum systems, there are no maximally entangled states in continuous-variable quantum mechanics; given any entangled state it is always possible to construct a more entangled one, as we shall see. The Bell states are nonetheless a resource in continuous-variable systems, and one can in principle use multiple copies of them (e.g. across different pairs of modes, or in different optical cavities) to generate a more entangled state. In addition, although there is no maximally entangled state here, there exists a map between any finite-dimensional

discrete quantum system and some continuous-variable system, allowing any procedure defined on the former can be carried out with the latter [92].

In the quantum phase space, partial transposition of the density matrix with respect to a mode corresponds to flipping the sign of the corresponding “momentum” variable [93], i.e.

$$\rho \rightarrow \rho^{T_n} \iff p_n \rightarrow -p_n, \quad (3.27)$$

where  $T_n$  represents the partial transpose with respect to mode  $n$ . For a two-mode Gaussian state, the first and second moments then transform under the partial transpose as

$$d \rightarrow \Lambda d \quad \text{and} \quad \sigma \rightarrow \Lambda \sigma \Lambda \quad (3.28)$$

where  $\Lambda := \text{diag}(1, 1, 1, -1)$ , and the partial transpose is taken with respect to the mode appearing second in  $d$ . For bipartite Gaussian states, the PPT criterion is both necessary and sufficient for the separability of the state [93] (in contrast with the more general case discussed in Section 3.1). All entangled two-mode Gaussian states then have non-zero negativity, which is given by [91]

$$\mathcal{N}(\sigma) = \max \left\{ 0, \frac{1}{2} \left( \frac{1}{\nu_{min}^{(PT)}} - 1 \right) \right\} \quad (3.29)$$

where  $\nu_{min}^{(PT)}$  is the smallest symplectic eigenvalue of the partially transposed covariance matrix  $\sigma^{(PT)} := \Lambda \sigma \Lambda$ . For the two-mode squeezed vacuum described in Equations (3.17), we then have

$$\mathcal{N}_{TMSV} = \frac{1}{2} \left( e^{2|\zeta|} - 1 \right). \quad (3.30)$$

From this expression, we see that there is in principle no upper bound to the negativity of such a state.

### 3.4 Entanglement and QFT

To provide a context for the results discussed in Chapter 7, we now give a brief overview of some investigations of entanglement in the context of relativistic field theory. Quantum field states can of course exhibit entanglement between observables in different spatial regions, however the degree of entanglement, and the states which are entangled, are perhaps surprising. For example, in Minkowski spacetime, using an algebraic approach, it was found that the outcomes of localised, spacelike-separated measurements on (inertial-observer) vacuum states of both bosonic and fermionic QFTs can violate Bell inequalities [9, 94]. These correlations can be trans-

ferred to a pair of localised, spatially-separated, auxiliary systems [95] in a procedure sometimes referred to as “entanglement harvesting” [96], and decrease rapidly with increasing spatial separation. As a manifestation of this vacuum entanglement, in a similar fashion to EPR-steering in non-relativistic quantum mechanics, local operations in one spatial region can be used to prepare states in another, spacelike-separated, one - a consequence of the Reeh-Schlieder theorem [97].

Much work is dedicated to the computation of the von Neumann entropy of a field state after tracing out the part of the Hilbert space concerning observables in the complement of some spatial region, often referred to as the entanglement entropy (or sometimes geometric entropy) [98]. Lorentz covariance and the strong subadditivity property of the entropy imply that the entanglement entropies associated with two regions of spacetime are necessarily divergent if there exist any correlations (specifically a nonzero mutual information) between their observables [99, 100]. Introducing a regularisation scheme results in an entanglement entropy scaling with the area of the region’s boundary [101, 99]. This contrasts with the volume-scaling that one might expect if the correlations between regions were extensive, and is similar to the area-laws manifested in a number of quantum many-body systems [102]. The resemblance that this bears to the area law of black hole entropy [103, 60] may indicate that the latter is in fact the entanglement entropy resulting from tracing out field degrees of freedom behind the horizon [104, 101]. A suggested covariant generalisation of this area-scaling (in fact a bound to the scaling) has been proposed as a general principle (the “holographic principle”) to be satisfied by any unified theory of matter and spacetime [10]. In this connection, it has been proposed that the structure of space [105] or spacetime [106] emerge due to entanglement.

The necessity of using a metric theory of gravity (i.e. one based on spacetime geometry) is a consequence of the Einstein Equivalence Principle (see e.g. [107], Section 2.1), revealing the relationship between non-inertial motion and spacetime curvature. Given the difficulties in reconciling quantum mechanics and relativity, it is of interest to explore how these two aspects affect something as characteristically quantum as entanglement. Indeed, the effect of non-inertial and gravitational motion on entangled quantum states has recently come under experimental scrutiny [43]. A key result in this context is the Unruh effect, mentioned in Section 2.2.3, whereby an inertial observer who begins uniformly accelerating sees their vacuum state become a thermal state [14]. The observer is causally disconnected from part of the spacetime, leading to the interpretation of the Unruh effect as a manifestation of the vacuum entanglement discussed above [108, 104], though this perspective has been criticised [109]. This example is one of many demonstrating the observer-dependent nature of entanglement [8].

If, instead of the vacuum state, one begins with an entangled state across a pair of momentum modes, non-inertial motion has been shown to degrade the entanglement for scalar [18] and spinor [110] fields. In curved spacetime, the degradation of entanglement across momentum modes due to the presence of a black hole's event horizon has also been analysed for scalar and spinor fields [111, 112]. Entanglement between infalling and outgoing field modes (studied in e.g. [113, 114]) is responsible for the thermal nature of Hawking radiation [60]. This plays an important role in the black hole firewall argument, a proposed resolution to a paradox arising in part from the monogamy of entanglement [115]. The entanglement generated as a result of the expansion of the universe in a Friedmann-Lemaître-Robertson-Walker spacetime has been studied [16]; this encodes information about the history of the spacetime in a way which depends non-trivially on the spin of the field [17].

In Chapter 7, we will note some limitations of the approaches described above, and describe some work attempting to overcome those issues, presenting our own efforts in that context.

## Chapter 4

# Quantum, relativistic, and relativistic quantum clocks

In this chapter we discuss how the notion of time is treated differently in the theory of relativity and in quantum mechanics, before describing the conflict between them, and mentioning some attempts to bridge this gap. We then review the relativistic quantum clock model introduced in [116], a model which we develop further in Chapter 6. We will make occasional references to operationalism, which is incorporated (sometimes implicitly) into many of the approaches discussed below. As noted in Chapter 1, operationalism is the principle that physical concepts be defined with respect to the operations by which they must be measured [28]; it is invoked whenever one attempts to make statements about time by discussing clocks.

### 4.1 Time in general relativity

The general theory of relativity lies within the classical paradigm with respect to the measurements that can be performed, namely that unperformed experiments *do* have results (in contrast with the quantum paradigm [117]). The outcomes of such experiments are not necessarily objective, however, depending on relative motion, as well as the nearby distribution of energy. The theory is built upon the notion of “ideal” clocks and rods, through which the observer gathers information, which they may do to arbitrary accuracy. Einstein’s first work on the subject of relativity [118] begins with a definition of simultaneity via the synchronisation of clocks by means of light signals sent between them. This is the prototypical example of operationalism; one of the earliest texts formalising the concept states that “Einstein, in thus analysing what is involved in making a judgement of simultaneity, and in seizing on the act of the observer as the essence of the situation, is actually adopting a new

point of view as to what the concepts of physics should be, namely, the operational view” [28]. This definition of simultaneity includes a number of assumptions: clocks are pointlike objects following well-defined trajectories in space, and can “tick” with arbitrary precision.

To consider accelerated reference frames, one invokes the “clock hypothesis”<sup>1</sup>, according to which the apparent tick rate of a clock undergoing non-inertial motion equals that of an instantaneously comoving inertial one [119]. A clock with this property is said to be ‘ideal’. The clock hypothesis can be justified by noting that an observer can detect their own non-inertial motion via apparent forces, in contrast to velocity, which is a relative concept. Therefore, given a clock whose rate depends on acceleration in a well-defined manner, one can simply attach an accelerometer to it, and use the resulting measurements to add/subtract time such that the acceleration effect is removed, recovering ideality [120]. Combining this with the constancy of the speed of light, one finds that an ideal clock measures the proper time along its trajectory according to the usual formulas of special relativity. The concept of an ideal clock (and therefore proper time) is then imported into general relativity via Einstein’s equivalence principle [119], and the proper time measured along a clock’s spacetime trajectory is then given by Equation (2.7). Einstein’s equivalence principle is the statement that local experiments conducted by a freely-falling observer cannot detect the presence or absence of a gravitational field (“local” meaning within a small enough volume that the gravitational field can be considered uniform). The phenomenon of gravitational time-dilation predicted by Equation (2.7) (though originally derived from the equivalence principle alone [121]) has been subject to numerous experimental verifications, perhaps the most famous example being the Pound-Rebka experiment [122].

The principle of operationalism also underlies the famous ‘light-clock’ derivation of time dilation due to uniform relative motion, commonly attributed to Einstein, where one considers clocks constituted by two mirrors and a light ray propagating back and forth between them. For non-inertial motion, the orientation of the light clock with respect to the direction of acceleration becomes relevant. In the case where the acceleration is parallel to the plane of the mirrors, the clock can be adapted by the addition of a third mirror [123] in order to recover ideal behaviour. Light clocks whose mirrors are perpendicular to the acceleration deviate from ideality [119], but in a manner that can be made arbitrarily small [124]. In any case, as noted above, such deviations can be measured concurrently and subtracted according to classical physics. In Section 4.4, we will describe a quantum generalisation of this clock.

---

<sup>1</sup>The word “hypothesis” is a misnomer. The clock hypothesis is in fact a postulate (see e.g. Section 16.4 of [44]).

There is a sense in which time is a dynamical variable in general relativity: given a distribution of matter, one solves the Einstein field equations to find the space-time metric, and this in turn determines the proper time each observer experiences. However, the proper time also plays the role of an affine parameter for the corresponding observer's worldline. The role of the clock hypothesis is to assert that these two aspects are identical (up to multiplicative and additive constants). Their identity in flat spacetime and in the absence of acceleration can be asserted by the pithy statement that “good clocks make spacetime trajectories of free particles look straight” [44].

## 4.2 Time in quantum mechanics

### 4.2.1 Pauli's theorem

In quantum theory uncertainty relations between observable quantities combine with the unavoidable backreaction of measurements on the system under interrogation to pose strict limits on observations of physical systems. Arguably the most famous quantum limit to measurability is the Robertson relation, which constrains the uncertainty of a pair of observables via the non-commutativity of their associated self-adjoint operators [125]:

$$\sigma_A \sigma_B \geq \frac{1}{2} |\langle [A, B] \rangle|, \quad (4.1)$$

where  $A$  and  $B$  are the aforementioned operators and  $\sigma_X$  is the standard deviation of the quantity associated with the operator  $X$ . If we ask whether quantum mechanics imposes a limitation of this kind on the measurement of time, we run immediately into a problem. Time is not treated as an observable property of a system in quantum mechanics, but rather it parameterises the dynamics of these properties. If there were to exist a self-adjoint time operator  $\hat{t}$ , it should satisfy (in the Heisenberg picture)  $\frac{d\hat{t}}{dt} = \mathbf{1}$  and consequently  $[\hat{t}, H] = i\hbar$ , where  $H$  is the system Hamiltonian. It was famously shown by Pauli [126] that this criterion implies that  $H$  (or more generally the part of  $H$  acting on the same Hilbert space as  $\hat{t}$ ) has a spectrum equivalent to the real line, thus acting like the non-relativistic momentum operator  $p$ . Consequently, the energy of the system is unbounded below, which is unphysical. While there are some issues with this argument (see e.g. the counterexample proposed in [127]), one can nonetheless rigorously show that the existence of a self-adjoint operator exactly following the  $t$  parameter requires that the Hamiltonian be unbounded below [128].

Possession of a quantum clock with this Hamiltonian<sup>2</sup> would have other non-trivial implications, for example allowing protocols with external control (i.e. time-dependent Hamiltonians) to instead be implemented via a time-independent Hamiltonian, implying that quantum thermal machines can run autonomously with no extra cost [129].

### 4.2.2 Finite-dimensional quantum clocks

As an alternative to satisfying Pauli's criterion, one can consider a finite dimensional quantum dial [130] (also known as a Larmor clock [131, 29]), a system which proceeds cyclically through a series of states at an even pace with respect to the parameter  $t$ . One finds that as the resolution of this clock increases, so too does its energy fluctuations, and therefore its disturbance on a system with which it interacts (for example the device measuring the time) [132]. Nonetheless, with an appropriate choice of initial state, this clock can approximate the kind satisfying Pauli's criterion [133].

In this regard, it is also worth noting the quantum speed limit to the time  $T_{orth}$  taken for a system to move between two orthogonal (and therefore perfectly distinguishable) pure states, given for time-independent  $H$  by [134]

$$T_{orth} \geq \pi \max \left\{ \frac{\hbar}{\langle H \rangle}, \frac{\hbar}{\sigma_H} \right\}. \quad (4.2)$$

We can then see this as a limit to the clock's resolving power. A pedagogical review of quantum speed limits can be found in [135].

### 4.2.3 Parameter estimation

Instead of trying to construct an operator which follows the parameter as closely as possible, one can take an observable with some known time-dependence, and to which a self-adjoint operator can be associated, and then use the Robertson relation to formulate a time-energy uncertainty principle in the manner of Mandelstam and Tamm [136]. This can be generalised beyond the self-adjointness of the intermediary observable by optimising over every possible Positive-Operator Valued Measure (POVM), invoking to the Cramér-Rao bound (see Section 4.4.2) to obtain a general time-energy uncertainty relation, valid for any closed quantum system [137]:

$$\sigma_{t_{est}} \sigma_H \geq \frac{1}{2} \quad (4.3)$$

---

<sup>2</sup>Such a clock is sometimes referred to as "ideal" but we use that term only in its relativistic sense (i.e. as in Section 4.1).

where  $t_{est}$  is an unbiased estimator of the elapsed parameter time  $t$ . The generality of this result suggests that, despite the parametric role of time in the standard formulation of quantum mechanics, it is subject to the same fundamental quantum indeterminacy as observables such as position. This is a suggestion rather than an implication since the existence of a general uncertainty principle alone isn't enough to imply a kind of temporal non-realism;<sup>3</sup> we cannot invoke the Kochen-Specker theorem, for example.

#### 4.2.4 Event-times

Rather than associating the possible states of a system with elapsed times, one can ask at which time a certain event occurred. For example, one can measure the time-of-arrival of a particle [139, 140], finding a limit to the accuracy which depends on the kinetic energy of the particle [141]. A review of event-time observables, as well as a partial catalogue of time-energy uncertainty relations and their shortcomings can be found [142].

#### 4.2.5 Atomic clocks

The term “quantum clock” is sometimes used synonymously with atomic clock. An atomic clock uses the energy difference between a pair of electronic states within an atom as a reference oscillator, to which a laser's frequency is tuned, and whose oscillations are then used to count time. In the modelling of atomic clocks, the concerns are primarily practical rather than fundamental (e.g. [143]); the behaviour of the atom(s) is modelled quantum mechanically as part of the process of determining that the laser is correctly tuned, and quantum sources of noise in the laser are considered. Time is considered as a classical parameter of the laser's oscillating phase. The latest generation of atomic clocks, which use optical-frequency transitions, are currently the state-of-the-art in timekeeping, both in terms of accuracy (the accord between the observed frequency of the reference oscillator and its theoretical value) and precision (the narrowness of the distribution of measurements - often called “stability” in the literature regarding atomic clocks). Current optical clocks have reached fractional instabilities and inaccuracies as low as  $10^{-18}$  [144, 145]. With this accuracy a clock would lose less than one second in 15 billion years (c.f. the age of the universe: 13.8 billion years), and with this precision a clock is sensitive to gravitational time-dilation over height differences of 2 cm on the surface of the Earth [30]. Given the rate of improvement of this technology (see Figure 1 of [31],

<sup>3</sup>By “non-realism” we mean that it is not an “element of physical reality” in the sense of the famous Einstein-Podolsky-Rosen (EPR) argument [138].

for example), one can anticipate an even greater sensitivity in the near future. The detection of a nuclear transition in thorium-229 [146], proposed as a new frequency standard [147], means that we may soon enter an era of “nuclear clocks”, surpassing that which is achievable with clocks based on electronic transitions. Considering this ever-increasing precision together with proposals to exploit quantum effects for superior timekeeping (e.g. [32, 33]), we see that it will become not only possible, but in fact necessary to consider gravity alongside quantum mechanics when discussing timekeeping. The non-triviality (from a relativistic perspective) of referring to the same time at different places will become manifest: “it appears that tomorrow’s super clocks will be so accurate that as far as life on Earth is concerned, the time that they keep will be too good to be true” [148]

#### 4.2.6 The quantum hourglass

A novel model, introduced in [149, 150] equates the keeping of time with the ability to produce a sequence of signals (i.e. ticks). This “quantum hourglass” approach is perhaps the most operationalist of those discussed here. While it makes use of the usual parametric time in the background, it does not treat it as a quantity of interest. In this formalism, one can relate the frequency of ticks (the resolution of a clock) to the power it consumes [149]. One can ask how many ticks can be produced in a well-defined order by phrasing timekeeping as a three-party “alternate ticks game” [150], where two parties are tasked with sending ticks to a referee in alternating order. As a consequence of the interactions between the components of the individual clock systems, they cannot maintain alternate ticks indefinitely, with the average number of alternating ticks achieved limited by the dimensionality of their Hilbert spaces. Comparing this to a classical stochastic system, one finds that the quantum version exhibits a quadratic increase in this scaling with dimension [151]. This clock has also been investigated in a thermodynamic context: requiring it to run autonomously reveals the necessary generation of entropy during its operation [152].

### 4.3 Relativistic quantum clocks

Maintaining an operationalist perspective, one can see that there are a number of conceptual issues which arise when combining general and quantum theory. One such issue is in understanding the limitations posed by quantum theory on the clocks and rods of general relativity, and how this in turn affects the information gathered by an observer<sup>4</sup>. Some progress has been made with this issue, for example [130], wherein

<sup>4</sup>We limit ourselves to the discussion of clocks, and the curious reader is referred to [153] for a review of possible limitations to spatial measurements.

the mass and mass uncertainty of a clock system are related to its accuracy and precision (neglecting spacetime curvature). In [154], using a gedankenexperiment, one such mass-time relation is rederived and combined with the “hoop conjecture” (a conjectured minimum size before gravitational collapse [44]), to argue that the product of a clock’s spatial and temporal uncertainty is bounded below by the product of the Planck length and the Planck time. Uncertainty between the frequency (i.e. energy) and emission time of a photon can be used to derive a limit to clock synchronisability equal to the Planck length (in natural units) [153]. Considering multiple quantum clocks, one finds that the reaction of the spacetime to their presence acts to limit the joint measurability of time along nearby worldlines [155].

A second, perhaps more difficult problem, is that of reconciling the definition of time via a pointlike trajectory in general relativity with the impossibility of such trajectories according to quantum mechanics (a result of the uncertainty principle between position and momentum). A third issue is the prediction that acceleration affects quantum states via the Unruh effect [156, 157] and the DCE [158], which in turn will affect clock rates [159]. Deviations from clock ideality have been predicted in experiments using muon decays to keep time [160, 161], in neutrino flavour-oscillation clocks [162], and in a twin-paradox scenario using Superconducting QUantum Interference Devices (SQUIDS) [116] (as we describe in Section 4.4.2). The notion of clock ideality has also been critiqued on philosophical grounds (see [163], Section 6.2.1). We must therefore reconsider whether it is always possible to measure and remove acceleration effects and recover an ideal clock. A fourth issue is that, given the locality of the equivalence principle (i.e. it only holds exactly along pointlike paths), it is unclear to what extent it applies to quantum objects, which do not follow pointlike trajectories.

Attempting to canonically quantise the general theory of relativity leads to the Wheeler-DeWitt equation [164], according to which the state of the universe vanishes under the action of the Hamiltonian. Explaining how time arises from this apparently “frozen” state is sometimes referred to as the problem of time. In-depth reviews of this problem (and others also given the same name), as well as some proposed solutions, can be found in [165, 11].

## 4.4 The quantum light clock

### 4.4.1 The model

We wish to investigate the issues described above, seeking to answer the following questions: what time does a quantum clock measure as it travels through space-

time, and what factors affect its precision? What are the fundamental limitations imposed by quantum theory on the measurement of time, and are these affected by the motion of the clock? To answer this, we cannot in general rely on the Schrödinger equation, as we must use a particular time parameter therein, which in turn requires the use of a particular classical trajectory. We now describe a quantum version of the light clock, introduced in [116], with which these questions have been explored in Minkowski spacetime. In Chapter 6 we will develop this model further and analyse a scenario in curved spacetime. This approach is semiclassical, and as such is peripheral to the problem(s) of time in quantum gravity. The mirrors of the clock are treated classically, having well-defined trajectories, but the electromagnetic field is quantised. The clock is associated to a classical observer, whose trajectory is determined by the clock's, and whose clock-time we define based on their measurement of the field. Here we consider only flat spacetime and  $1 + 1$  dimensions.

A massless scalar field is used to model the light inside the clock, and its mirrors are described by the boundary condition that the field vanishes, giving a discrete mode structure. Starting at rest in an inertial frame, with proper time coordinate  $t$ , the field is initialised in a coherent state of the lowest-energy mode (labelled 1, with frequency  $\omega_1$ ), whose form in the covariance matrix formalism is given in Equations (3.16). The mean phase  $\theta$  of the state, given in Equation (3.14), is then used to define the (mean) time of the clock as

$$\tilde{t}(\theta) := -\frac{\theta}{\omega_1} = -\frac{1}{\omega_1} \arctan\left(\frac{\langle p_1 \rangle}{\langle q_1 \rangle}\right), \quad (4.4)$$

where  $q_1$  and  $p_1$  are the quadrature operators (defined in Equations (3.4)) of mode 1. Note that we use a different sign convention to [116] so that the clock-time evolves in the forward direction.

Let us denote the initial displacement parameter of the clock's coherent state by  $\alpha_0 = |\alpha_0|e^{i\theta_0}$ . The clock's starting time is then  $\tilde{t}(\theta_0)$ . If the clock remains at rest in the inertial frame for some period of time  $\Delta t$ , then its phase evolves to  $\theta_0 + \Delta\theta$ , with  $\Delta\theta = -\omega_1\Delta t$ . In other words, the clock-time evolves by an amount  $\Delta\tilde{t} = \Delta t$ .

#### 4.4.2 Review of results

##### The twin paradox

In [116], considering a pair of these clocks, the famous twin paradox scenario (where one observer remains stationary while another completes a round-trip, measuring a smaller elapsed time than the stationary observer) was revisited. One clock plays the role of the stationary twin, while the other undergoes a round-trip trajectory

consisting of segments of constant<sup>5</sup> proper acceleration and inertial motion, interspersed with “free” evolution in the relevant inertial/accelerated frames. By composing the Bogoliubov transformations corresponding to changes between inertial and accelerated frames (and the free motion in between), one arrives at the total transformation of the accelerated twin’s field state. Applying the transformation of first moments given in (3.22), and Equations (3.23) and (3.24), to the expression for the mean phase, Equation (3.14), it was found that the mean phase  $\Delta\theta$  accrued by the accelerated clock satisfies

$$\tan \Delta\theta = -\frac{\Im(\alpha_{11} - \beta_{11})}{\Re(\alpha_{11} - \beta_{11})}, \quad (4.5)$$

where  $\alpha_{mn}$  and  $\beta_{mn}$  denote the Bogoliubov coefficients of the total transformation. The authors of [116] showed that this results in a difference in clock-times for the two observers which is distinct from the difference in their proper times, analysing the possibility of observing this effect in a SQUID.

### Precision-degradation

The model was also applied in [167] in order to analyse how the round-trip trajectory of the accelerated twin affects the precision of that twin’s phase measurements (i.e. the precision of the clock), framing this as a problem in quantum metrology. The field of quantum metrology developed in parallel to quantum information [168, 169], and is concerned with the application of quantum features, such as squeezing or entanglement, to improve the precision with which some quantity is measured. Say we seek to estimate a parameter  $\lambda$  by making  $M$  measurements. The variance  $\Delta\lambda_{est}$  of estimators of  $\lambda$  satisfy the quantum Cramér-Rao bound [168]

$$\Delta\lambda_{est} \geq \frac{1}{\sqrt{MH_\lambda}}, \quad (4.6)$$

where  $H_\lambda$  is the quantum Fisher information (QFI). One can therefore use the QFI to quantify the precision with which a parameter can be measured: a greater QFI implies a greater precision. We note, however, that the QFI is obtained by an unconstrained optimization over all POVMs [168], and as such gives the theoretical maximum precision, without any consideration of the feasibility of the measurement process required to achieve it. Let us denote the first and second moments of a Gaussian state of a single mode  $k$  by  $d^k$  and  $\sigma^k$  respectively (where the superscript  $k$  is a label, not an index or exponent). These comprise 6 real components, giving 5 degrees of freedom (since  $\sigma_{ij}^k = \sigma_{ji}^k$ ). We can then equivalently express the state

<sup>5</sup>constant in time, but spatially varying. The two mirrors experience different accelerations in accordance with the notion of “Born rigidity” [166].

in terms of the following parameters [170]: a (real) displacement  $\alpha$ , a (complex) squeezing  $\zeta = re^{i\phi}$ , the phase  $\theta$  and the purity  $P$ . These are related to the first and second moments by

$$\alpha = \sqrt{(d_1^k)^2 + (d_2^k)^2}, \quad (4.7a)$$

$$P = \frac{1}{4\sqrt{\det \sigma^k}}, \quad (4.7b)$$

$$r = \frac{1}{2} \operatorname{arctanh} \left( \frac{\sqrt{(\sigma_{11}^k - \sigma_{22}^k)^2 + (2\sigma_{12}^k)^2}}{\sigma_{11}^k + \sigma_{22}^k} \right), \quad (4.7c)$$

$$\tan(2\theta + \phi) = \frac{2\sigma_{12}^k}{\sigma_{11}^k - \sigma_{22}^k}, \quad (4.7d)$$

combined with the previous expression for the phase  $\theta$  (Equation (3.14)). The QFI for the phase is then given by [167]

$$H_\theta = 4\alpha^2 P [\cosh(2r) + \sinh(2r) \cos \phi] + \frac{4 \sinh^2(2r)}{1 + P^2}. \quad (4.8)$$

This allowed the authors of [116] to quantify the change in precision of the accelerated twin's clock, finding a decrease in the precision of the clock for squeezed vacuum and coherent pointer states. In the absence of motion, optimising  $H_\theta$  for a fixed mean energy (i.e. mean particle number), one finds that the squeezed vacuum state gives the greatest precision in phase estimation [170]. However, this state was found to be significantly more susceptible to degradation of precision due to the clock's motion.

### 4.4.3 Summary

Considering this clock model in light of the conflicts between relativity and quantum theory listed in Section 4.3, we note that:

- the clock is no longer a pointlike system;
- assuming the boundaries to be large enough that they may be approximated by classical mechanics, we can ascribe well-defined spacetime trajectories to the clock;
- the quantum uncertainty associated with the clock-time can be quantified via inequality 4.6, using the quantum Fisher information and the Cramér-Rao bound;

- we do not a priori assume the possibility of perfect correlation between arbitrarily many clocks - it is expected that the uncertainty associated with the phase estimation prohibits arbitrarily accurate synchronisation.

Given these qualitative differences, we wish to investigate quantitatively how the clock time along some trajectory differs from the proper time of a pointlike observer in more general scenarios. This requires the development of a formalism for describing the effect of motion over a curved background on the quantum state inside the cavity. The development of such a formalism is the subject of Chapter 5, and our progress regarding this clock model is detailed in Chapter 6.

## Part II

# Space-time curvature effects in quantum systems

## Chapter 5

# Boundary motion and the Dynamical Casimir Effect

### 5.1 Introduction

In general, the mode solutions to the field's equation of motion (Equation (2.16)) can be defined across a very large patch of a space (compared with, say, the spatial extent of some apparatus on earth). The particles associated with single-mode states are then correspondingly delocalised.<sup>1</sup> We wish to describe quantum systems moving through curved spacetime, which therefore requires a degree of localisation. One way to localise field states is to construct multi-mode creation operators such that field excitations are concentrated in the region of interest. We, on the other hand, wish to consider quantum systems contained within some apparatus, and to this end we consider the field to be confined by a potential. To simplify the problem, so that we don't need to consider the effect of the shape of the potential, or the leakage of the confined particles, we consider an infinite potential well. This corresponds to the condition that the field vanishes at some boundaries (an example of Dirichlet boundary conditions). A massless scalar field subject to these boundary conditions can be used to model the electromagnetic field in an optical cavity or the phonons of a BEC confined in a box trap. We will refer to the system (the field and the boundaries) as a cavity.

Given a quantum field thus localised, we then need a formalism for describing the effect of boundary motion on the field. This chapter describes our results in developing such a formalism; we derive the Bogoliubov coefficients corresponding to a

---

<sup>1</sup>Though we do not have an unproblematic operator to associate to particle position, the notion of localisation can be made more rigorous by, for example, considering the response of idealised particle detectors to the field (see e.g. [14, 171] and references therein).

finite period of motion through a stationary spacetime. The particle-creating aspect of the transformation of the field state is known to as the dynamical Casimir effect (DCE), though this is sometimes used to refer to the overall transformation of the field state. We begin with a brief overview of the DCE and the ways in which the field transformation can be calculated. In Section 5.3 we describe the quantisation of the field, localised as discussed above, before deriving the Bogoliubov transformation of the field modes due to a period of boundary motion in Section 5.4. As we explained in Section 2.2.5, this allow us to describe the corresponding transformation of any initial field state. We apply this to a well-known scenario in Section 5.5, finding a new effect due to spacetime curvature, as well as recovering earlier results. In Section 5.6 we consider how these results are modified if one considers a BEC instead of an optical cavity, and using some rather crude assumptions we find a potential amplification of the effect. We then summarise and discuss our results in Section 5.7

## 5.2 A brief overview of the DCE

The DCE arises due to non-adiabatic changes in the mode structure of a field, and therefore the eigenstates of its Hamiltonian after quantisation, which manifests as a change in the field's quantum state. Thus the vacuum state is transformed into a non-vacuum one, which we perceive as the generation of particles. The motion of a boundary [158] or another potential [172] constraining the field, or changes in material properties of a medium containing the field [173], all result in mode-structure changes, which in turn can give rise to this effect. Reviews of the DCE (in flat spacetime) can be found in [174, 175].

Physical implementations of the DCE include photons generated by accelerated mirrors [158] (specifically due to changes in acceleration [176, 177, 178]), phononic excitations induced by changes in the external potential holding a BEC [179], and photons generated by modulating the inductance of a SQUID [180]. The two latter implementations have been demonstrated experimentally [181, 182, 179].

Methods for calculating the DCE can be broadly separated into two categories (with some overlap). Hamiltonian methods such as those described in [183, 174, 184] allow, for example, the consideration of the finite refractive index of the mirrors [178, 185], and the resistive forces acting on them due to the created particles [175, 186]. On the other hand, one can consider the solution of the field equations subject to some externally imposed boundary trajectories, an approach in which we can employ QFT in curved spacetime, and which is therefore more suited to relativistic considerations. It is this latter approach that we adopt here. The first calculations

of the DCE were carried out in this manner, exploiting conformal transformations (which leave the field equation unchanged from its inertial-coordinate form) to some coordinates in which the boundaries are stationary [158, 187, 176]. This reveals the difficulty of maintaining a particle interpretation during the boundary motion (see the introductory discussion in [176]), a problem which is equally present for quantum fields in non-stationary spacetimes (as discussed in Section 2.2.3).

A distinct variant of this conformal approach is developed in [188], which takes a view “local” to an observer at the center of a cavity, who undergoes some time-dependent proper acceleration. The boundary trajectories are set such that they are at a constant distance in the instantaneous Rindler frame corresponding to the observer’s proper acceleration at a given moment in time. One can then calculate the effect of a finite period of acceleration on the quantum field inside the cavity, not with a single conformal coordinate transformation, but rather by integrating through a continuum of them.

For arbitrary boundary motion, it is not possible to find a conformal transformation between inertial coordinates and some coordinates in which the boundaries are stationary. Given trajectories for which such a transformation cannot be found, one can seek the solution to the field equation in terms of “instantaneous” mode solutions [183, 189], and then use some approximations particular to the given trajectories to solve the resulting infinite set of coupled differential equations. This can then be used to connect solutions before a finite period of motion to solutions afterwards - effectively a scattering problem. In Appendix B, it is shown for a restricted set of trajectories that adapting this method to curved spacetime gives results coinciding with those which we present in Section 5.4.

Using the framework of QFT in curved spacetime to examine the DCE allows considerations such as the analogy between the DCE and the radiation emitted by a collapsing star [190], or the effect of motion on a quantum clock in the twin paradox scenario, as discussed in Section 4.4.2. In the context of quantum cosmology, one can consider particle creation due to some expanding boundaries of the universe as a kind of DCE [191]. Boundary motion in a static curved spacetime was investigated in [192], considering a cavity with a single mirror moving briefly over a short distance, but a general description of the DCE in curved spacetime has remained an open problem. The following sections present our progress in this regard.

Before we describe our results, it is useful to clarify the distinction between the DCE and the Unruh effect (the thermal field experienced by an accelerating observer). Considering a single moving mirror, one can choose a trajectory such that it emits a thermal spectrum of particles as  $t \rightarrow \infty$  (see e.g. Section 2.5 of [193] for a pedagogical treatment). However, this trajectory is distinct from that of a uniformly-accelerating

observer. In fact, a uniformly-accelerating mirror does not radiate [176]. If we now consider two mirrors (i.e. a cavity), again uniform acceleration does not by itself result in a thermal state. Indeed, if the motion of a cavity's mirrors could alone reduce the purity of the field state contained therein, the Hamiltonian approach (and subsequent unitary evolution) used by a number of authors (e.g. [174]) would be invalid. However, if we allow the cavity to couple to the field external to it,<sup>2</sup> the cavity may act as an effective particle detector for the external field, and in this case the field inside the cavity will thermalise, as described in [157]. A short description of the relations between the Unruh effect, Hawking radiation and the DCE (and the limits of these relations) is given in Section IV.F of [14].

### 5.3 Stationary boundaries

We will work in  $1 + 1$  dimensions, though in Appendix C we show how the results in this chapter can be generalised to include more spatial dimensions. Consider a massless scalar field  $\Phi$  in a stationary spacetime. Every stationary  $1 + 1$ D spacetime is static, and it is always possible to find some coordinate system in which the metric is conformally flat [47], that is to say there exist some coordinates  $(t, x)$  such that  $g_{\mu\nu}(t, x) = w(t, x)\eta_{\mu\nu}$ , where  $\eta_{\mu\nu}$  is the Minkowski metric and the function  $w(t, x)$  is called the conformal factor. The stationary property of the spacetime implies that  $w(t, x) = w(x)$ , and therefore  $\partial_t$  is a timelike Killing vector. The Klein-Gordon equation (Equation (2.16)) then takes the same form as in an inertial coordinate frame in flat space:

$$(\partial_t^2 - \partial_x^2) \Phi = 0. \quad (5.1)$$

Denoting the positions of the boundaries in the  $x$ -coordinate by  $x_j$ , with  $j = 1, 2$ , we solve the field equation subject to the conditions  $\Phi(t, x = x_1) = \Phi(t, x = x_2) = 0$ , giving

$$\phi_m(t, x) = N_m e^{-i\omega_m t} \sin[\omega_m(x - x_1)] \quad (5.2)$$

and their complex conjugates, where  $N_m = 1/\sqrt{m\pi}$  is a normalization constant and  $\omega_m := m\pi/L$ , are the mode frequencies (with  $m = 1, 2, 3, \dots$  labeling the mode), and  $L = x_2 - x_1$  is the cavity length. The inner product between solutions (Equation (2.18)) becomes

$$(\varphi, \chi) = -i \int_{x_1}^{x_2} dx [\varphi(\partial_t \chi^*) - \chi^*(\partial_t \varphi)], \quad (5.3)$$

---

<sup>2</sup>Note that considering a non-perfectly-reflecting mirror can result in an effective coupling between the field inside and outside of the cavity.

and we can quantise the field following the procedure described in Section 2.2.3, giving a vacuum state  $|0\rangle$ , and the field operator

$$\Phi(t, x) = \sum_m \left[ a_m \phi_m(t, x) + a_m^\dagger \phi_m^*(t, x) \right]. \quad (5.4)$$

We will find it useful to express the time evolution of the field operator (recall that we use the Heisenberg picture) as a Bogoliubov transformation (see Section 2.2.5); an evolution by an amount  $\Delta t$  in the  $t$ -coordinate corresponds to the Bogoliubov coefficients  $\alpha_{mn} = e^{-i\omega_m \Delta t} \delta_{mn}$  and  $\beta_{mn} = 0$ .

Here we have quantised the field with respect to the timelike Killing vector  $\partial_t$ , and since the proper time of any observer at fixed  $x_0$  is  $\tau(t) = \sqrt{w(x_0)}t$ , this observer will agree with the separation into positive and negative-frequency modes according to  $\partial_t$ . It is therefore with respect to these observers that we define Hilbert space of the stationary cavity.

## 5.4 The effect of boundary motion

We now derive the Bogoliubov transformation corresponding to a finite period of boundary motion. To do this, we make the assumption that an infinitesimal time-step can be described as the combination of a displacement effect and pure phase-evolution of stationary mode solutions. This gives a picture analogous to the separation of a Hamiltonian into free and interacting terms  $H = H_0 + H_{int}$ , as we shall see. Hence, in the same vein as [188], a differential equation for the total transformation can be derived.

We will write Bogoliubov transformations in matrix form (i.e. Equation (2.43)). We define a matrix of frequencies  $\Omega := \text{diag}(\omega_1, \omega_2, \dots, -\omega_1, -\omega_2, \dots)$ . To make explicit the dependence on the boundary conditions, let us write this as  $\Omega(x_1, x_2)$  and the stationary mode solutions in Equation 5.2 as  $\phi_m(t, x; x_1, x_2)$ . The assumption described in the preceding paragraph is then expressed mathematically as

$$\begin{aligned} \phi_m(t + \delta t, x; x_1 + \delta x_1, x_2 + \delta x_2) = \\ \{ \exp [i\Omega(x_1 + \delta x_1, x_2 + \delta x_2)\delta t] S_\delta(\delta x_1, \delta x_2) \} \phi_m(t, x; x_1, x_2), \end{aligned} \quad (5.5)$$

where  $S_\delta(\delta x_1, \delta x_2)$  represents the transformation<sup>3</sup>

$$\phi_m(t, x; x_1, x_2) \rightarrow \phi_m(t, x; x_1 + \delta x_1, x_2 + \delta x_2). \quad (5.6)$$

---

<sup>3</sup>For this transformation, there is an ambiguity in the domain in which the inner products are to be taken. However, the Bogoliubov coefficients obtained for the different domains differ only at second order in the infinitesimals, and therefore vanish when we use them to obtain Equation (5.8).

If we now consider motion for some finite time  $t$ , and denote the corresponding transformation matrix by  $S(t)$ , then composing transformations gives

$$S(t + \delta t) = \exp [i\Omega(x_1 + \delta x_1, x_2 + \delta x_2)\delta t] S_\delta(\delta x_1, \delta x_2) S(t), \quad (5.7)$$

and then from the definition of the derivative, we have

$$\frac{dS}{dt} = \left[ i\Omega + M^{[1]} \frac{dx_1}{dt} + M^{[2]} \frac{dx_2}{dt} \right] S \quad (5.8)$$

with

$$M^{[j]} := \begin{pmatrix} A^{[j]} & B^{[j]} \\ B^{[j]*} & A^{[j]*} \end{pmatrix}, \quad (5.9a)$$

$$A_{mn}^{[j]} := \left( \frac{\partial \phi_m}{\partial x_j}, \phi_n \right), \quad B_{mn}^{[j]} := - \left( \frac{\partial \phi_m}{\partial x_j}, \phi_n^* \right), \quad (5.9b)$$

where  $j = 1, 2$  and square brackets indicate that the index labels a boundary (distinguishing it from mode indices, orders in a series expansion and exponents). The Lie algebra condition given in Equation 2.45 is equivalent here to the conditions  $A^{[j]} = -A^{[j]\dagger}$  and  $B^{[j]} = B^{[j]T}$ , which are indeed satisfied. We consider the motion to occur between  $t = 0$  and  $t = T$ , and we define

$$\Theta(t) := \int_0^t dt' \Omega(t'). \quad (5.10)$$

Seeking a solution of the form  $S(t) = e^{i\Theta(t)} \bar{S}(t)$  for some  $\bar{S}(t)$ , we find

$$S(T) = e^{i\Theta(T)} \mathcal{T} \exp \left[ \int_0^T dt \sum_{j=1}^2 e^{-i\Theta(t)} M^{[j]} e^{i\Theta(t)} \frac{dx_j}{dt} \right]. \quad (5.11)$$

where  $\mathcal{T} \exp$  denotes the time-ordered exponential.

Let us now assume that the coordinate velocities of the boundaries  $\frac{dx_j}{dt}$  are small (with respect to the speed of light) throughout the motion. We can use the Dyson series to express the time-ordered exponential in Equation (5.11) to second order in  $\frac{dx_j}{dt}$ . We write the resulting Bogoliubov coefficients as in Equation (2.46), i.e.

$\alpha_{mn} = \alpha_{mn}^{(0)} + \alpha_{mn}^{(1)} + \alpha_{mn}^{(2)}$  and  $\beta_{mn} = \beta_{mn}^{(1)} + \beta_{mn}^{(2)}$ , with

$$\alpha_{mn}^{(0)} = e^{i\bar{\omega}_m(T)} \delta_{mn} \quad (5.12a)$$

$$\alpha_{mn}^{(1)} = e^{i\bar{\omega}_m(T)} \sum_{j=1}^2 \int_0^T dt A_{mn}^{[j]} e^{-i[\bar{\omega}_m(t) - \bar{\omega}_n(t)]} \frac{dx_j}{dt} \quad (5.12b)$$

$$\alpha_{mn}^{(2)} = e^{i\bar{\omega}_m(T)} \sum_{j,k=1}^2 \int_0^T dt_2 \int_0^{t_2} dt_1 C_{mn}^{[jk]}(t_1, t_2) e^{-i[\bar{\omega}_m(t_2) - \bar{\omega}_n(t_1)]} \frac{dx_j}{dt_2} \frac{dx_k}{dt_1} \quad (5.12c)$$

$$\beta_{mn}^{(1)} = e^{i\bar{\omega}_m(T)} \sum_{j=1}^2 \int_0^T dt B_{mn}^{[j]} e^{-i[\bar{\omega}_m(t) + \bar{\omega}_n(t)]} \frac{dx_j}{dt} \quad (5.12d)$$

$$\beta_{mn}^{(2)} = e^{i\bar{\omega}_m(T)} \sum_{j,k=1}^2 \int_0^T dt_2 \int_0^{t_2} dt_1 D_{mn}^{[jk]}(t_1, t_2) e^{-i[\bar{\omega}_m(t_2) + \bar{\omega}_n(t_1)]} \frac{dx_j}{dt_2} \frac{dx_k}{dt_1}, \quad (5.12e)$$

where

$$\bar{\omega}_m(t) := \int_0^t dt' \omega_m(t') \quad (5.13a)$$

$$C_{mn}^{[jk]}(t_1, t_2) := \sum_p \left[ A_{mp}^{[j]} A_{pn}^{[k]} e^{i[\Theta_p(t_2) - \Theta_p(t_1)]} + B_{mp}^{[j]} B_{pn}^{[k]} e^{-i[\Theta_p(t_2) - \Theta_p(t_1)]} \right] \quad (5.13b)$$

$$D_{mn}^{[jk]}(t_1, t_2) := \sum_p \left[ A_{mp}^{[j]} B_{pn}^{[k]} e^{i[\Theta_p(t_2) - \Theta_p(t_1)]} + B_{mp}^{[j]} A_{pn}^{[k]} e^{-i[\Theta_p(t_2) - \Theta_p(t_1)]} \right]. \quad (5.13c)$$

In Appendix B, we check Equations 5.12 to first order by considering the subset of trajectories where the cavity length is a constant (in the conformally flat coordinates), in which case one can approximately solve the field equations to find the Bogoliubov coefficients without using the specific functional form of the trajectory.

One can see the role played by different terms in Equations 5.12. The term  $\alpha_{mn}^{(0)}$  gives the phase change in the absence of mode-mixing and particle creation effects, the first-order terms treat the mode-mixing ( $\alpha$ ) and particle creation ( $\beta$ ) effect of each boundary individually, and the second-order terms give these effects as a mixture of both boundaries' motions. The first and second-order terms play the role of the ‘‘interaction Hamiltonian’’ in the analogy mentioned above, and disappear in the limit of adiabatic (i.e. infinitely slow) motion. Integrating by parts (using the fact that the velocity is zero at  $t = 0$  and  $t = T$ ), one can see a correspondence between the first-order terms in Equations 5.12 above and Equations 6 in [188].

We exploit the simplicity of the Klein-Gordon equation in conformally flat coordinates, but trajectories in coordinates more natural to a given problem can be mapped to ones in the conformally flat coordinates. Furthermore, the temporal coordinate  $t$  is used as a bookkeeping coordinate, which can be related to the proper time of

an observer in the usual way. Both of these points are illustrated in the example in Section 5.5.

## 5.5 Example: an oscillating boundary in the presence of a massive body

We now consider a scenario where, in the presence of a stationary, spherically symmetric, massive body, one boundary is fixed while the other oscillates in the direction radial to the body. The DCE due to sinusoidal boundary oscillation in flat spacetime is a well-studied problem, e.g. [15, 194, 189], and this boundary trajectory was used to observe the DCE experimentally [181]. One finds a resonance in the creation of particles when the boundary oscillates at the sum-frequency of two modes. This resonance was examined in a weak gravitational field using a short-time approximation in [192]. Here, we use the results described in Section 5.4 to find expressions for the  $\beta_{mn}$  coefficients, revealing further particle-creation resonances due to the spacetime curvature.

We model the spacetime containing the massive body by the Schwarzschild spacetime described in Section 2.1.4. Recall that the line element was given by

$$ds^2 = -f(r)dt^2 + \frac{1}{f(r)}dr^2 + r^2d\Omega^2$$

with  $f(r) := 1 - r_S/r$ , where  $r_S = 2GM$  is the Schwarzschild radius of the body, and we defined the tortoise coordinate  $r_*(r) := r + r_S \ln \left| \frac{r}{r_S} - 1 \right|$ . Disregarding the angular coordinates, we can quantise the field in the way described in Section 5.3; Equations (5.2) and (5.4) hold, with  $x = r_*$ . The observers for whom this is the appropriate quantisation are then the shell observers described in Section 2.1.4, i.e. our results correspond to the experience of some stationary experimenter at a radial distance  $r_e$  with proper time  $\tau_e = \sqrt{f(r_e)}t$  (Equation (2.10)). The effect of the spacetime curvature on the spatial structure of the mode functions is illustrated in Figure 5.1.

We consider one boundary to be fixed at  $r_1 = r_0$ , and the other boundary at  $r_2(t) = (r_0 + L_0)[1 + \delta(t)]$  to move from  $t = 0$  to  $t = T$  such that there is a sinusoidal oscillation of the proper length, i.e.

$$L_p(t) = L_{p,0} + \tilde{A} \sin(\nu t). \quad (5.14)$$

with  $L_{p,0} = \int_{r_0}^{r_0+L_0} \frac{dr}{f(r)}$ . For simplicity of presentation, it is assumed the boundary returns to its initial position at  $t = T$ , i.e.  $\nu T = p\pi$  for some  $p \in \mathbb{N}$ . Assuming

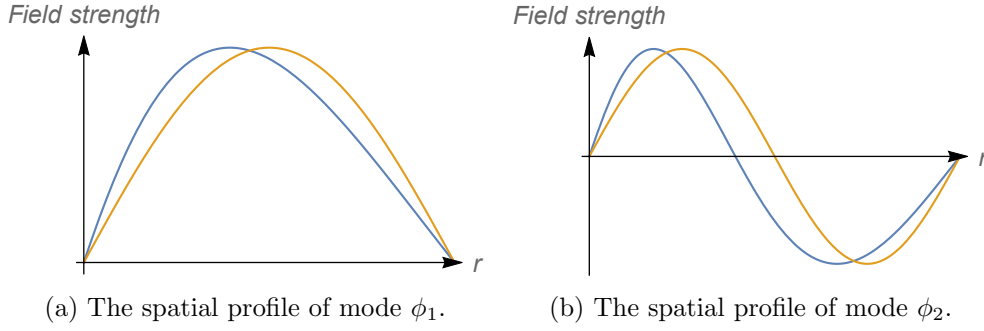


Figure 5.1: A cartoon of  $\sin[\omega_m(r_*(r) - r_*(r_1))]$  for  $m = 1$  and  $m = 2$ , in the case of no (orange) and strong (blue) curvature (as quantified by  $r_S$ ). This illustrates how the curvature “pulls” the modes towards the gravitating body in the Schwarzschild  $r$ -coordinate.

the oscillation amplitude to be much smaller than the distance to the centre of the gravitating body, one finds

$$r_2(t) = r_0 + L_0 + A \sin(\nu t) \quad \text{with} \quad A = \frac{\sqrt{f(r_0 + L_0)}}{\sqrt{f(r_0 + L_0)} + \frac{r_s}{2(r_0 + L_0)}} \tilde{A}, \quad (5.15)$$

to first order in  $\delta(t)$ . We further assume  $\varepsilon := A/L_0 \ll 1$  and  $\varepsilon \gg r_S/r$ , which are easily satisfied in experiments at the Earth’s surface. We will work to first order in  $r_S/r$  and second order in  $\varepsilon$ . For reference, in SQUID-based DCE experiments one can achieve a fractional change of the (effective) length as large as  $\sim 0.1$  [195, 181], and at the surface of the Earth, we have  $r_S/r \sim 10^{-9}$ .

The  $\beta_{mn}$  quantify particle creation, as exemplified by Equation (2.41). To find these coefficients, we use Equations (5.12), giving

$$\beta_{mn} = e^{i\omega_n T} \varepsilon \nu \sqrt{\omega_m \omega_n} \frac{f(r_0)}{f(r_0 + L_0)} \left\{ i \frac{(-1)^p - e^{i(\omega_m + \omega_n)T}}{(\omega_m + \omega_n)^2 - \nu^2} + \frac{A r_S}{(r_0 + L_0)^2} \frac{\nu}{\omega_m + \omega_n} \frac{e^{i(\omega_m + \omega_n)T} - 1}{\left(\frac{\omega_m + \omega_n}{2}\right)^2 - \nu^2} \right\}, \quad (5.16)$$

where the  $\{\omega_m\}$  are the unperturbed mode frequencies. The first term in the braces in Equation (5.16) persists in the limit of zero curvature (i.e.  $r_S \rightarrow 0$ ), and exhibits the familiar resonance for a driving frequency of  $\nu = \omega_m + \omega_n$ . The second term gives a novel contribution due to curvature, with its own resonance at the subharmonic  $\nu = \frac{1}{2}(\omega_m + \omega_n)$ ,<sup>4</sup> though this is strongly suppressed by the factor of  $A r_S / (r_0 + L_0)^2$ . Including more terms of  $\varepsilon$  and  $r_S/r$  in our approximation, one finds

<sup>4</sup>To avoid a potential confusion, we emphasize that this half-wavelength resonance is distinct from the fact that, when driving the mirror at  $\nu = \omega_m + \omega_n$ , one obtains a peak in the *output spectrum* of an initially-empty cavity at  $\nu/2$  (or the nearest frequencies to that, if  $m + n$  is odd).

further subharmonic resonances, each one increasingly suppressed, and all vanishing in the limit of zero curvature. These are the result of the nonlinear relationship between the proper length and the length in the tortoise coordinate  $r_*$ . Stated in more physical terms, the length relevant to the experimenter, the proper length, differs nontrivially from the appropriate notion of length for a massless particle (sometimes called the “radar length” [119]), and this difference depends on the curvature of the spacetime, quantified in this case by  $r_S$ . A single-frequency sinusoidal modulation of the proper length corresponds to a complex motion in the conformally-flat length. This complex motion can be seen as a weighted sum of sinusoids with different frequencies (i.e. a Fourier series), and each of these terms gives rise to a new resonance. Conversely, one could imagine the experimenter contriving a complex modulation of the proper length such that the motion in the  $r_*$ -coordinate is exactly sinusoidal, in which case only the standard resonance would remain.

Taking a driving frequency resonant with the first term, i.e.  $\nu = \omega_q + \omega_r$  for some  $q$  and  $r$ , and then considering the regime  $\nu T \gg 1$ , one obtains

$$|\beta_{mn}|^2 = \frac{1}{4} \left( 1 - 2 \frac{L_0 r_s}{r_0^2} \right) mn \left( \varepsilon \frac{f(r_0)\pi}{L_0} T \right)^2 \delta_{m+n, q+r}. \quad (5.17)$$

We thus find a curvature-induced reduction in particle number, as noted in [192], and we recover Equation (4.5) of [189] in the flat-spacetime limit. This reduction is in line with the physical interpretation of the novel resonances given above.

If we now drive the boundary at the novel resonance,  $\nu = \frac{1}{2}(\omega_q + \omega_r)$  for some  $q$  and  $r$ , the coefficient for which the curvature-dependent contribution is largest is

$$\beta_{qr} = i e^{i\omega_q T} \varepsilon \frac{\sqrt{qr} f(r_0)^2}{f(r_0 + L_0)} \left[ -\frac{2}{3} \frac{1 - (-1)^p}{f(r_0)(q+r)} + \varepsilon \frac{\pi}{8} \frac{r_S T}{f(r_0 + L_0)(r_0 + L_0)^2} \right]. \quad (5.18)$$

From Equation (5.18), one can see that it is in principle possible to conduct an experiment for long enough that the curvature-dependent contribution dominates, since in the  $\beta_{mn}$  for modes other than  $q$  and  $r$  (Equation (5.16)), the value of  $T$  only serves to set the phases. Taking the Schwarzschild radius of the Earth, and considering the parameters used in the SQUID setup of [116] at the surface, one finds that the observation of this resonance would take an astronomically long time. Instead of a photonic DCE, we can consider phononic excitations of a BEC, which modifies the metric that we must use (see Appendix A of [55]). There are cases where relativistic effects too small to detect with an optical cavity may be brought into an observable regime with a BEC setup [196, 55], and by preparing a suitable probe state and measuring its transformation due to the motion, one might be able to profit from the increased sensitivity afforded by quantum metrology [25, 26]. In

Section 5.6 we discuss the potential of this platform to observe the novel resonance.

## 5.6 Curved-spacetime DCE in BEC systems

As noted in Section 5.2, modulating the trapping potential of a BEC affects the mode structure of the phonons, giving rise to a DCE. This has been implemented in [179], for example, where correlated phonon pairs are produced by sinusoidal modulation the trap potential.

In [54], by modelling a BEC in a fully relativistic manner, and using a slight modification of the usual mean-field description,<sup>5</sup> it was shown that under certain conditions (see Section 5, particularly Equations 62, of [54]) the phonon field obeys the Klein-Gordon equation with an effective metric that includes contributions from the properties of the bulk fluid:

$$\mathbf{g}_{\mu\nu} = \rho \frac{c}{c_s} \left[ g_{\mu\nu} + \left( 1 - \frac{c_s^2}{c^2} \right) \frac{v_\mu v_\nu}{c^2} \right] \quad (5.19)$$

where  $\rho$ ,  $c_s$  and  $v^\mu$  are related respectively to the density, speed of sound and phase gradient of the mean field (see [54] for detailed definitions). While the derivation of the effective metric in [54] considered only a flat background spacetime, it was shown in Appendix A of [55] that the result also holds for a curved background. The same metric was also derived in [197] for perturbations of a classical fluid. Assuming the background metric  $g_{\mu\nu}$  to be flat, one can control the properties of the BEC so that the effective metric  $\mathbf{g}_{\mu\nu}$  simulates a particular spacetime (see [198, 199] for general discussions, and [200] for an example). Turning these proposals around, in [27] it was suggested that one could instead use a BEC to detect changes in the background spacetime. By an appropriate coordinate transformation, we can see moving boundaries in a static spacetime as stationary boundaries in a dynamical spacetime. Combining these two ideas leads us to the question of whether or not such a BEC setup will allow us to detect the curved-spacetime contribution to the DCE.

We can follow the procedure described above, particularly Sections 5.3 and 5.4, the only necessary modification being that we must find coordinates that are conformally flat with respect to the effective metric  $\mathbf{g}_{\mu\nu}$ , which depends on the properties of the BEC. As a first step, let us consider a 1+1D Schwarzschild spacetime, as in Section 5.5, containing a BEC which is static, so that  $c_s$  and  $\rho$  are constant and  $v^\mu = (c/\sqrt{f(r)}, 0)$ . With these conditions, we find that the effective metric gives the

<sup>5</sup>The density of the BEC is described as quantum perturbations (i.e. phonons) around a classical mean field (the ‘‘bulk’’)

following spacetime interval (in the usual Schwarzschild coordinates):

$$ds^2 = \rho \left[ -\frac{c_s}{c} f(r) dt^2 + \frac{c}{c_s} \frac{1}{f(r)} dr^2 \right] \quad (5.20)$$

and therefore our conformally flat coordinates in this case are given by  $x(r) = \frac{c}{c_s} \left[ r + r_s \ln \left( \frac{r}{r_s} - 1 \right) \right]$ , i.e. the usual tortoise coordinate scaled by a factor of  $\frac{c}{c_s}$ . Considering typical values for the speed of sound to run from  $\sim 1 \text{ mm s}^{-1}$  [201] to  $\sim 1 \text{ cm s}^{-1}$  [179], we have  $\frac{c}{c_s}$  ranging from  $\sim 10^{10}$  to  $\sim 10^{11}$ . If we now return to the oscillating-boundary example given in Section 5.5, we see that small oscillations in the Schwarzschild coordinate  $r$  are greatly amplified in our new conformally flat coordinate  $x$ . We therefore find an example where, as in the proposals in [196, 55], a relativistic effect too small to detect with an optical cavity might be brought into an observable regime with a BEC setup.

## 5.7 Conclusion and Discussion

We have given a simple method allowing the calculation of the DCE in a cavity due to motion in curved spacetime by effectively separating the timescales of cavity motion and field-state evolution. As well as giving some general formulas for the Bogoliubov transformation of the field state, we have considered the experimental scenario used to observe the DCE [181], now using the Schwarzschild spacetime, and found a novel resonance in particle creation as a result of the curvature. This is a consequence of the distinction between the radar length and the proper length of the cavity, whose inequality is in turn a consequence of the spacetime curvature. This illustrates that when discussing the notion of an object's length in a given frame in curved spacetime, one must specify by what measure the length is to be determined. We briefly discussed the possibility of amplifying this effect using a BEC. The results described in this chapter underpin the following ones. We now note some limitations of our approach, and some possible extensions.

By prescribing the boundary trajectories, we ignore the backreaction (and therefore resistive force) on the mirrors due to particle creation. In light of the additional curvature-dependent terms in the example above, we see that this backreaction will be affected by the presence of gravity, and therefore alter the “quantum friction” [175, 202] resisting the acceleration of an object through spacetime. Another limitation is our assumption of perfectly-reflecting boundaries, which implies that the purity of the field state inside the cavity is unaffected by the motion. Relaxing this assumption would allow a consideration of coupling between intra-cavity modes and global ones, and the resulting loss of purity of the former. One could then

investigate the decoherence induced by non-inertial motion, including the effect of gravity.

It would be of interest to see if our approach can be modified to consider asymptotically static motion of a single boundary through curved space. This would require the procedure followed in Sections 5.3 and 5.4 to be adapted for the continuous-spectrum case. One could then compare trajectories in curved spacetime with known flat-spacetime results such as those described in [203] in order to investigate how the curvature affects those results.

Finally, we note that our analysis of the BEC implementation was a sketch for the purpose of showing the possible benefit of using such a platform, and that the subject deserves a much fuller treatment, with serious attention to experimental details. To go beyond the rough analysis presented above, there are a number of tasks. The first is to check that the assumption of constant density and speed of sound is feasible, and if not, to find more realistic spatiotemporal profiles, and see how this affects the resulting metric. Furthermore, the changes in the potential which produce the effect can induce a non-negligible modulation of the bulk properties (as in [204]), and we must account for this in our analysis. This might be done by treating all of the extra metric terms induced by such modulations as temporary “source terms” in the Klein-Gordon equation. Preliminary calculations suggest this to be a feasible approach, and it remains to see to what extent these terms would affect the measurability of the curved-spacetime contribution to the DCE.

## Chapter 6

# Quantum and classical effects in a falling light-clock

### 6.1 Introduction

In this chapter we further develop the clock model described in Section 4.4 and use the results of Chapter 5 to consider an example where gravity plays a role. As discussed in Section 4.4, this is a quantum version of the light clock, commonly attributed to Einstein, whose “ticks” are the propagation of light back and forth between two mirrors. We recall that the clock consists of a particular mode of a localized quantum field; the boundaries confining the field define the spatial extent of the clock, and the clock time is given by the phase of a Gaussian state. This gives a clock that can undergo classical relativistic trajectories, but whose dynamics are described by QFT in curved spacetime. The former property means that we can compare this to an ideal clock (in the sense described in Section 4.1) by considering a classical observer attached to the cavity, while the latter property allows us to consider the effect of the spacetime curvature on the whole extent of the quantum field. Since our aim is to investigate the interplay of quantum mechanics and relativity, we must be careful to distinguish between classical nonideality of the clock, and nonideality arising from quantum effects. We further recall that we adopt the principle of operationalism. As an aside to the reader sceptical of the appropriateness of this clock model, we compare it with an atomic clock (Section 4.2.5), where time is kept by phase estimation of the coherent state emitted by a laser whose cavity is adjusted to match a chosen resonance of the reference atom.

In the work reviewed in Section 4.4.2, the use of uniformly accelerated (Rindler) reference frames determined the evolution of the clock length. This results in a number of desirable properties, such as Born rigidity (a lack of relativistic stresses on the

clock support system), constant radar distance (the distance as measured by timing classical light pulses), and constant proper distance. In curved spacetime, however, these properties cannot in general be satisfied concurrently. Einstein described the general theory of relativity as follows: “all our well-substantiated space-time propositions amount to the determination of space-time coincidences. [...] The introduction of a system of co-ordinates serves no other purpose than an easy description of totality of such coincidences [205]”. Notions of length in the theory are then only well-defined in as far as they can be described in these terms. As we already saw in the example given in Section 5.5, the inequivalence of different notions of length in curved spacetime can have novel consequences. We must therefore take care to specify the physical situation according to which the clock is moved, and in particular how this acts individually upon the two mirrors.

The clock model is developed in Section 6.2, showing the state-independence of the clock time for Gaussian states, and the separation of the clock time into classical and quantum contributions, and describing some of the issues in attempting to generalise the model to curved spacetime. Section 6.3 presents the falling-clock scenario, comparing classical clock effects with ideal pointlike observers, and presenting numerical investigations into quantum effects on the clock time. We also briefly consider how changes in the strength of the gravitational field affect the clock readings. Our results, their limitations, and their possible consequences are discussed in Section 6.4.

## 6.2 Classical and quantum effects on the clock time

Here, as in Section 4.4, we use a state of the first mode of the cavity ( $m = 1$ ) to set the clock, and we use  $q$  and  $p$  to represent the quadrature operators (defined in Equations (3.4)) of this mode. The phase  $\theta$  a Gaussian state was given in Equation (3.14):  $\tan \theta = \langle p \rangle / \langle q \rangle$ . There is a freedom in how the quadrature operators are defined, reflecting the relational nature of the phase; multiplying  $a_1$  by an arbitrary reference phase acts to shift  $\theta$  by that amount. We can set  $\theta = 0$ , for example, by choosing this reference phase such that  $\langle p \rangle = 0$ .

Let the clock be initialised in an arbitrary (Gaussian) initial state with first moments  $\langle x \rangle_0$  and  $\langle p \rangle_0$ . After a Bogoliubov transformation of the first moments according to Equation (3.25a), the phase of the clock satisfies

$$\tan \theta = \frac{-\text{Im}(\alpha_{11} - \beta_{11}) \langle x \rangle_0 + \text{Re}(\alpha_{11} + \beta_{11}) \langle p \rangle_0}{\text{Re}(\alpha_{11} - \beta_{11}) \langle x \rangle_0 + \text{Im}(\alpha_{11} + \beta_{11}) \langle p \rangle_0}. \quad (6.1)$$

If we define the quadrature operators with a reference phase such that the clock is initialised at zero (i.e.  $\langle p \rangle_0 = 0$ ), then the final phase no longer depends on the

initial state, but only on the Bogoliubov coefficients, which in turn depend on the mode solutions to the field equation and the motion of the boundaries. The time as measured by the clock is then uniquely determined by the background spacetime metric and the clock motion. Consequently, the results described in [116] hold for all Gaussian states, not only the coherent state used therein.

We consider two clocks, with their phases both initialised at zero. The reference clock, labelled  $A$ , remains at rest (with respect to the stationary spacetime), and the other clock, labelled  $B$ , undergoes a finite period of motion. A classical observer is associated with each clock, following one of the clock-mirrors along its trajectory. We will examine how the readings of clocks  $A$  and  $B$  differ, and contrast this with the difference in the proper time of the corresponding classical observers. As in Chapter 5, we use coordinates in which the metric is conformally flat, denoted by  $(t, x)$ , as bookkeeping coordinates, and assume the motion of clock  $B$  to take place in the interval  $0 < t < T$ . The trajectories of the two mirrors of clock  $B$  are denoted  $x_1(t)$  and  $x_2(t)$  (where  $x_1(t) < x_2(t)$ ), and the instantaneous frequency (with respect to  $t$ ) of mode  $m$  of this clock is therefore  $\omega_m(t) = m\pi/[x_2(t) - x_1(t)]$ . Assuming the two clocks to initially have the same length (in the  $x$ -coordinate), the mode frequencies of the stationary clock,  $A$ , are then  $\omega_m^A := \omega_m(0)$ , and its field state transforms according to the Bogoliubov coefficients  $\alpha_{mn}^A = \exp[i\omega_m^A T] \delta_{mn}$  and  $\beta_{mn}^A = 0$ , giving a phase of  $\theta_A = -\omega_1^A T$ . The minus sign is a consequence of the definition of positive-frequency modes as those with phases that evolve in the negative direction with increasing time [47].

We then need to determine the Bogoliubov coefficients  $\alpha_{mn}^B$  and  $\beta_{mn}^B$  for clock  $B$ 's transformation. The separation of  $\Phi$  into well-defined positive and negative-frequency modes as described in Section 2.2.3 is not possible for general boundary motion [176], so we use the results of Chapter 5, specifically Equations (5.12), and from there determine the evolution of the clock phase using Equation (6.1). We work to second order in the velocities  $dx_j/dt$ , and define  $\theta_B^{Cl} := -\int_0^T dt' \omega_1(t')$  (i.e. the phase accrued by a classical oscillator with a time-dependent frequency), and further define  $\bar{\alpha}_{mn} := e^{im\theta_B^{Cl}} \alpha_{mn}^B$  and  $\bar{\beta}_{mn} := e^{im\theta_B^{Cl}} \beta_{mn}^B$ . Then from Equations (5.12) we see that the coefficients can be written

$$\alpha_{mn}^B = e^{-im\theta_B^{Cl}} \left[ \delta_{mn} + \bar{\alpha}_{mn}^{(1)} + \bar{\alpha}_{mn}^{(2)} \right] \quad (6.2a)$$

$$\beta_{mn}^B = e^{-im\theta_B^{Cl}} \left[ \bar{\beta}_{mn}^{(1)} + \bar{\beta}_{mn}^{(2)} \right]. \quad (6.2b)$$

From Equation (6.1) (with  $\langle p \rangle_0 = 0$ ), we can write the phase of clock  $B$  as

$$\theta_B = \theta_B^{Cl} + \theta_B^{Qu} \quad (6.3)$$

with

$$\begin{aligned} \theta_B^{Qu} := & - \left[ \text{Im} \left( \bar{\alpha}_{11}^{(1)} - \bar{\beta}_{11}^{(1)} \right) + \text{Im} \left( \bar{\alpha}_{11}^{(2)} - \bar{\beta}_{11}^{(2)} \right) \right] \\ & + \text{Re} \left( \bar{\alpha}_{11}^{(1)} - \bar{\beta}_{11}^{(1)} \right) \text{Im} \left( \bar{\alpha}_{11}^{(1)} - \bar{\beta}_{11}^{(1)} \right). \end{aligned} \quad (6.4)$$

Equation (6.3) thus gives the separation of clock  $B$ 's phase into a classical part  $\theta_B^{Cl}$ , and a quantum part  $\theta_B^{Qu}$ , the latter arising due to the transformation of  $B$ 's quantum state as a consequence of the clock's motion. In the following sections, we explore these two effects with a specific example.

From the above, one can find the phase accrued by both clocks in an amount of bookkeeping time  $T$ . In the work discussed in Section 4.4, one could simply convert phases to a quantities with dimensions of time by dividing by the frequency of the clock mode,<sup>1</sup> i.e. Equation (4.4), this frequency being the same (to within the approximation used) for both clocks [116]. In curved spacetime however, matters are more complicated. Generally, the frequency of clock  $B$ 's reference mode will vary with respect to the bookkeeping time  $t$ , and therefore with respect to clock  $A$ , throughout the motion. For an observer carrying clock  $B$  to determine how this frequency varies, they would need to know the trajectories of the clock's boundaries, as well as the value of  $T$ , which is not in keeping with the principle of operationalism. To speak of the local reading of each clock, we must therefore use the phase, without converting it to a time. We could choose to use the timescale set by the frequency of the reference clock  $A$  to write these readings as quantities with dimensions of time:

$$\tilde{t}_A(\theta) := -\frac{N_A}{\omega_1^A} \theta, \quad (6.5)$$

where  $N_A$  is the lapse function (see Equation (2.3)) scaling  $\omega_1^A$  in accordance with the gravitational time dilation experienced by observer  $A$ . This must however be done with the caveat that  $\tilde{t}(\theta)$  is the time that observer  $A$  associates with the phase  $\theta$ . Clock  $A$ 's time  $\tilde{t}_A(\theta_A)$  is by construction equal to the proper time  $\tau_A$  of it's associated observer. Equation (6.5) is then one way to generalise Equation (4.4), with the important caveat above. In any case, since it is linear in  $\theta$ , taking ratios of  $\tilde{t}_A(\theta)$  for different phases is the same as taking ratios of the phases themselves.

To differentiate the difference in clock reading (i.e. phase) of clocks  $A$  and  $B$ , from the difference in proper times of their corresponding observers, we refer to the former as the ‘‘phase discrepancy’’ between the clocks.

---

<sup>1</sup>as is done in the measurement of time by atomic clocks

## 6.3 A falling quantum clock

### 6.3.1 The scenario

We now present a numerical investigation of the difference in clock times for the clocks introduced in Section 6.2. In particular, we wish to examine to its magnitude in a parameter regime which could feasibly be attained on the Earth. We consider a scenario where clock  $A$  is kept fixed 110m above the Earth's surface and clock  $B$  falls freely from that height to the surface, comparing the fall-time as measured by the two clocks. The choice of height is based on the size of the Bremen Drop Tower at the Center of Applied Space Technology and Microgravity (ZARM) [206]. We model the spacetime around the Earth using the Schwarzschild metric introduced in Section 2.1.4, with Schwarzschild coordinates  $(t, r)$ , and as in Section 5.5 we arrive at the conformally flat coordinates by taking  $x = r_*$ , where  $r_*$  is the tortoise coordinate. The Schwarzschild radius was defined by  $r_S := 2GM$ , where  $M$  is the mass of the Earth (except where stated otherwise). For each clock, we take their corresponding observer to follow the lower mirror (the one with smaller  $r$ ). Observer  $A$ , at position  $r_A$ , is a shell observer experiencing the proper time  $\tau_A = \sqrt{f(r_A)}T$  during the motion, i.e. the lapse function is  $N_A = \sqrt{f(r_A)}$ . The mirrors of clock  $B$  follow drip trajectories determined by Equations (2.12-2.14), to be solved with  $r_0 = r_A$  for the lower mirror and  $r_0 = r_A + L_0$  for the upper one, where  $L_0$  is the initial clock size. We take  $L_0 = 1$  m, except where stated otherwise. The proper time of the classical observer associated with clock  $B$  is given by Equation (2.13).

### 6.3.2 Classical clocks and proper times

In this section we examine the classical part of the phase discrepancy between clocks  $A$  and  $B$ , comparing this with the proper times of the corresponding pointlike observers. First, we can gain some insight by solving for the mirror trajectories perturbatively in  $r_S/r_A$  and  $L_0/r_A$ , from which we find (to second order in these quantities)

$$\frac{\theta_B^{Cl}}{\theta_A} = 1 + \frac{1}{2} \left\{ \frac{a_A L_0}{c^2} - \frac{1}{3} \frac{r_S}{r_A} + \left( \frac{r_S}{r_A} \right)^2 \left[ \frac{1}{3} + \frac{1}{10} \left( \frac{cT}{r_A} \right)^2 \right] \right\} \left( \frac{cT}{r_A} \right)^2 \quad (6.6)$$

where  $a_A$  is the proper acceleration felt by observer  $A$  (Equation (2.11), with  $r_0 = r_A$ ). The extent to which this quantity is not equal to unity then quantifies the classical phase discrepancy between the two clocks. The component proportional to  $a_A L_0 / 2c^2$  is reminiscent of the case of an accelerating light clock in flat spacetime (see Exercise 3.10 in [119]), though here it is the stationary clock which undergoes proper acceleration. In the scenario we consider here,  $a_A / c^2 \sim 10^{-16} \text{ m}^{-1}$ , while

$r_S/r_A \sim 10^{-9}$ , and therefore Equation (6.6) tells us that the classical discrepancy is extremely insensitive to changes in length in this regime.

We now compare the classical phase discrepancy with the usual relativistic time dilation between the observers  $A$  and  $B$ . Specifically, we compare the fractional differences defined by

$$\mathcal{F}_{\text{point}} := \frac{\tau_B - \tau_A}{\tau_A} \quad \text{and} \quad \mathcal{F}_{\text{ext}} := \frac{\theta_B^{Cl} - \theta_A}{\theta_A}. \quad (6.7)$$

The evolution of these quantities during the fall is given in Figure 6.1. We can see that the finite extent of the clock acts to increase the magnitude of the difference in clock readings compared to the ideal case, and that this effect is of considerable magnitude. While this is given in terms of the bookkeeping coordinate  $t$ , we recall that this coordinate is simply the proper time of observer  $A$  scaled by  $\sqrt{f(r_A)}$ .

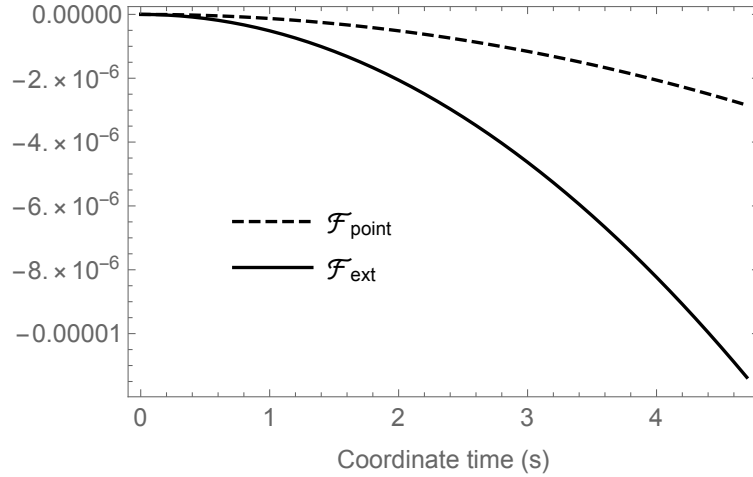


Figure 6.1: The fractional difference between the readings of dropped and stationary clocks in the case of pointlike, ideal clocks (dashed line), and classical light clocks (solid line), as a function of  $t$ . Their negative values indicate that the dropped clocks experience less time passing than the stationary ones. Curves shown for  $L_0 = 1$  m and a fall of 110 m to the surface of the Earth.

### 6.3.3 The quantum contribution to the phase discrepancy

The total fractional difference in phases between the clocks is

$$\frac{\theta_B - \theta_A}{\theta_A} = \mathcal{F}_{\text{ext}} + \frac{\theta_B^{Qu}}{\theta_A}, \quad (6.8)$$

and therefore  $\theta_B^{Qu}/\theta_A$  quantifies the quantum contribution to the fractional phase discrepancy. The behaviour of this quantity during the fall is shown in Figure 6.2a.

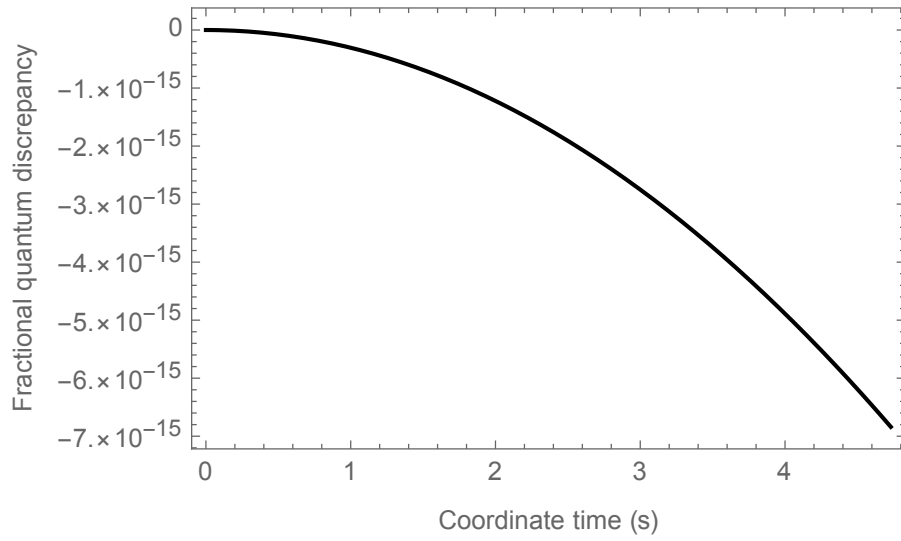
There we see that the motion-induced change in the quantum state acts to increase the phase discrepancy. For this quantum part we cannot find a closed-form expression like the one in Equation (6.6), but numerically we find the same insensitivity to clock size. Specifically, considering initial lengths from  $0.1 \mu\text{m}$  to  $10 \text{ m}$  (in the  $r$ -coordinate), we find that the curve in Figure 6.2a does not noticeably change. Examining this effect on a much smaller scale reveals an oscillatory behaviour (Figure 6.2b). These oscillations occur at the frequency of the clock mode and therefore are affected by changes in clock size, in contrast with the secular behaviour in Figure 6.2a. Specifically, they increase in frequency but also decrease in amplitude as we consider smaller clocks. Figure 6.2b illustrates this behaviour for two different values of initial length, finding oscillations of amplitude  $\sim 10^{-19}$  for initial lengths on the order of  $1 \text{ m}$ .

### 6.3.4 Curvature dependence

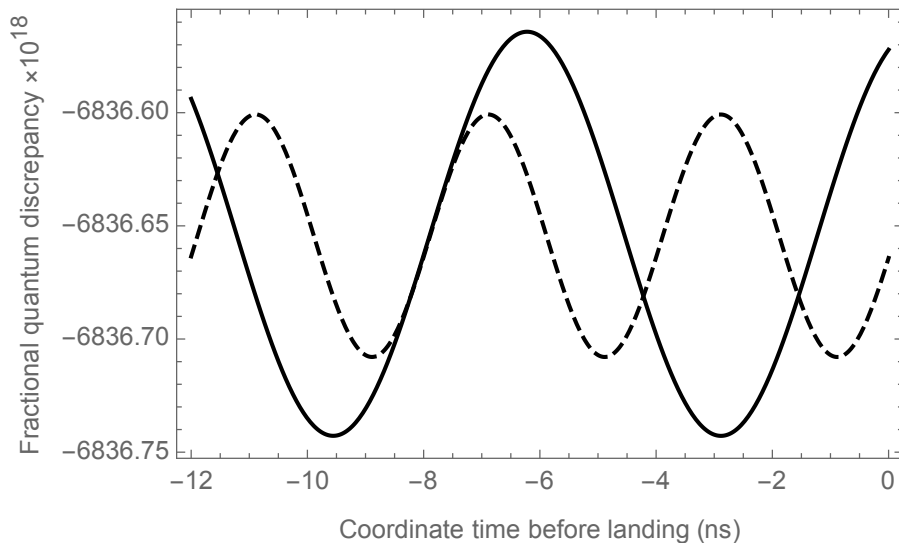
Though we have been primarily interested in the parameter regime corresponding to Earth-based experiments, it is interesting to consider how our results change with the curvature (as quantified by  $r_S$ ). We consider the range  $0 < r_S < 100$ , while continuing to use the same  $r_A$  as before (i.e. fixed at  $110 \text{ m}$  higher than the radius of the Earth). The results are shown in Figure 6.3. The overall fall time decreases with increasing curvature, an effect which wins out over tidal forces to decrease the magnitude of  $\mathcal{F}_{\text{ext}}$ . This approximate linearity of this decrease in the regime considered here is shown by the red curve in Figure 6.3. This behaviour is not surprising, given Equation (6.6). Perhaps more surprising is the seemingly linear increase in the magnitude of the fractional quantum effect  $\theta_B^{Qu}/\theta_A$  (the blue curve in Figure 6.3).

## 6.4 Summary and discussion

We have presented a model of a quantum relativistic light clock which moves in a stationary spacetime. It was shown for gaussian field states that the mean phase shift (and therefore mean clock time) of such a clock does not depend on the initial state, only the transformation applied to that state, which itself depends only on the spacetime and the motion, as is the case for an ideal classical clock. Assuming low-velocities (with respect to relevant coordinates), we found that the phase of a clock after a period of motion separates into the sum of a classical part, incorporating the changing frequency (i.e. photon round-trip time) of the clock, and a quantum part, arising from the transformation of the quantum state due to the motion. We then presented a numerical investigation of a scenario where one clock is held at a



(a) Secular variation for  $L_0 = 1$  m, though the behaviour on this scale is effectively length-independent (see text).



(b) Small-scale oscillations (magnified by  $10^{18}$ ) towards the end of clock  $B$ 's fall, shown for  $L_0 = 1$  m (solid line) and  $L_0 = 0.6$  m (dashed line).

Figure 6.2: The overall (a) and small-time-scale (b) quantum contribution (i.e.  $\theta_B^{Qu}/\theta_A$ ) to the fractional phase discrepancy between the clocks during a fall of 110 m to the surface of the Earth. This contribution acts to increase the difference in phase between the two clocks. For comparison,  $\mathcal{F}_{\text{ext}} \approx -10^{-5}$  at the end of the motion.

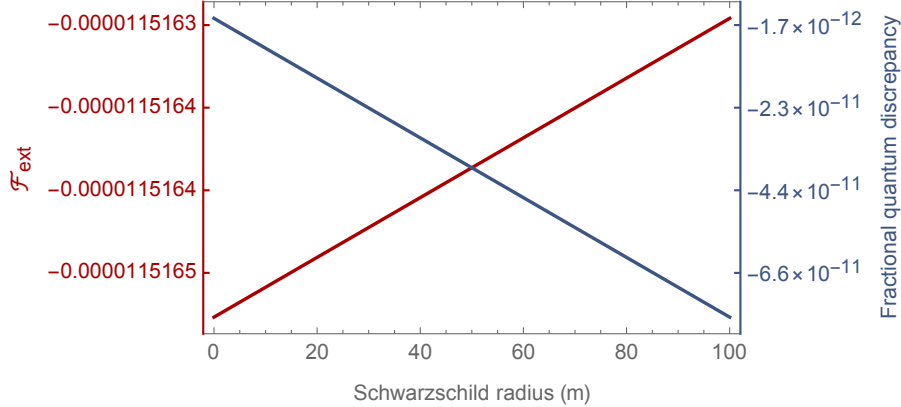


Figure 6.3: The approximately linear behaviour of the fractional classical ( $\mathcal{F}_{\text{ext}}$ , red) and quantum ( $\theta_B^{Cl}/\theta_A$ , blue) contributions to the difference in phase between  $A$  and  $B$ , as a function of the spacetime curvature (i.e. Schwarzschild radius), after a fall of 110 m to the surface of the Earth. Note that, since these phase differences are negative, the rising (falling) curve is decreasing (increasing) in magnitude. For comparison, the Schwarzschild radius of the Earth is  $r_S \sim 1$  cm.

constant height above the surface of the Earth (whose gravitational field we model using the Schwarzschild metric) the other is dropped to the surface. First examining the classical part of the discrepancy between the phases of the two clocks, we argued that it is effectively independent of the clock size in this scenario. Comparing this discrepancy with the time dilation experienced between two corresponding classical observers, we found that the former is greater in magnitude. The quantum contribution acted to further delay the dropped clock, an effect which our numerical investigation found to be similarly insensitive to clock size. However, considering this quantum effect on a smaller time-scale, one finds a slight oscillatory behaviour which does depend on clock size, increasing in frequency and decreasing in amplitude as the initial size of the clock decreases. Finally, considering how the results change if we study a scenario with a stronger or weaker spacetime curvature, we found that, for a fixed drop-height, the classical and quantum effects respectively decrease and increase in magnitude with increasing curvature, raising the possibility of a regime in which quantum effects dominate.

While the quantum effect on the clock phase is small in a terrestrial drop-tower experiment, being on the order of  $10^{-15}$  times the stationary clock's phase (Figure 6.2a), it is not insignificant, particularly in light of the ability of modern atomic clocks (and therefore laser cavities) to achieve frequency stabilities on the order of 1 part in  $10^{18}$  [207]. However, an attempt to observe the effect would face serious difficulties, not least the preservation of quantum coherence during the motion, as well as the short integration time afforded by the fall. Furthermore, an experimental setup would likely require that the two mirrors be fixed to a support, meaning that

one must consider the effect of the support’s rigidity on the classical contribution [4], and investigate to what extent the effect is modified.

The oscillating aspect of the quantum effect distinguishes it qualitatively from the classical one, raising a number of interesting questions from an operationalist perspective. A local time reference constructed via the moving clock would exhibit a many-to-one relationship with respect to the stationary one, and allow for the possibility that the order of events separated by a timelike interval be different for observers  $A$  and  $B$ , in contrast with the usual causal structure of relativity. That quantum mechanics may give rise to new causal structures is discussed in e.g. [208], though our approach is limited by the fact that clock readings are defined via the expectation values of quantum states, prohibiting coherent temporal (and therefore causal) superpositions.

Another interpretation of the oscillating aspect is as the breakdown of clock  $B$ ’s utility as a time reference, and hence the emergence of a minimum meaningful time-scale due to the motion. This is distinct from the usual notion of quantum uncertainty resulting from the variation in the measurements performed on quantum states. The decrease in amplitude of the oscillations with decreasing clock size could then be interpreted as an increase in the resolution of the moving clock as the frequency (i.e. energy) of the clock mode increases.

One could, as in the classical case, argue that clock  $B$ ’s deviation from ideality is an artifact, and can be subtracted by measuring the trajectory of its mirrors. This is not without its conceptual issues, as quantum theory demands that there be some uncertainty associated with this measurement, hindering an agent’s efforts to perform this “recalibration”. This would be particularly problematic if the uncertainty associated with the recalibration is of non-negligible magnitude compared to the quantum effect on the clock time. We cannot analyse this within the current formalism however, which treats the clock mirrors as classical objects. Furthermore, it seems likely that the effects predicted here are not fundamental (i.e. clock-independent). One might then argue that the presence of these effects is a consequence of having used the “wrong” system as a clock. Such an argument should be followed by specifying the “right” system to use as a clock - even atomic frequency references exhibit classical deviations from ideality when subjected to tidal forces (see [44], p.396).

There are a number of other limitations to our approach. We have considered only Gaussian field states in  $1 + 1$  dimensions, neglecting polarisation. We have not considered the process by which the phase, and therefore clock time, is measured. There is necessarily some uncertainty associated with this, which will depend upon the clock’s quantum state, as discussed in Section 4.4.2. We have likewise not considered the problem of comparing the phases of two spatially separated systems

in a curved background, which is accompanied by its own operational issues, such as perhaps requiring observers to have accurate knowledge of the spacetime metric, and of each system's position. Moreover, the phase is periodic, and so in order to use the clock as a time reference, a system for counting the oscillations must be included. The requirement that this bipartite system function continuously leads to a number of quantum and thermodynamic considerations (see e.g. [149, 152]). While consideration of any of these aspects may numerically affect the results above, it seems very unlikely that any of them will be able to restore ideality to the clock.

## Chapter 7

# Entanglement generation and degradation in curved spacetime

### 7.1 Introduction

In this chapter we present our work regarding the generation and degradation of entanglement between modes of a relativistic quantum field. The work discussed in Section 3.4 concerned entanglement between global (or at least highly delocalised) field modes. This raises the question of how to interpret the operational meaning of the entanglement, particularly in light of the causal issues arising when one considers ideal measurements of the field [209, 210]. One solution is to couple the field to idealised pointlike systems, such as Unruh-DeWitt detectors, as in the entanglement harvesting procedure mentioned in Section 3.4 (though these models can have their own issues with causality [211]). Another solution is to consider the field to be confined to some region, as in an optical cavity, and as we have done in Chapters 5 and 6. The idea of using a relativistic field thus localised as a device for quantum information protocols was introduced in [212]. This was further developed in [213], where it was shown that a method for establishing entangled states between separate cavities [214] can be applied between observers quantising the field according to different timelike Killing vectors, specifically those corresponding to inertial and uniformly accelerated observers. The entanglement obtained is reduced, unless one can adjust the cavity length in accordance with the acceleration.

Since the boundaries of the cavity shield the field inside from the causal horizon associated with non-inertial motion, the field state evolves according to a local unitary transformation, preserving its purity. This contrasts with the case of global field modes discussed above. However, if we are only able to access a subset of modes, then we have an effective loss of purity. An example of such a restriction is the

case where the field is to be probed by an atom whose only non-negligible coupling is to a single mode. In this context, entanglement degradation due to non-uniform motion has been analysed for scalar [20] and spinor [215] fields, considering an entangled pair of systems where one undergoes finite segments of uniform acceleration, finding that the resulting degradation varies periodically with the duration of these segments.

One can also consider entanglement within a single cavity. For example, the vacuum state of a cavity exhibits entanglement between spatial portions [216], just as in the discussion of vacuum entanglement in Section 3.4. A finite period of uniform acceleration generates entanglement between pairs of modes of a scalar or spinor field in a cavity [19] (as well as genuine multipartite entanglement across modes [23]). This effect, like the degradation mentioned above, is periodic in the duration of acceleration. The initial-state dependence of the generated entanglement changes with the nature of the field: for charged fermions, the Pauli exclusion principle and charge conservation prohibit the generation of entanglement between initially populated modes [19], and entanglement generation can be enhanced for a scalar field by starting with a single-mode squeezed state [217].

The studies in entanglement generation and degradation in a cavity described above were limited to finite periods of uniform acceleration in Minkowski spacetime due to the difficulty in describing the effect of arbitrary boundary motion in arbitrary spacetimes, as discussed in Section 5.2. The generalisation to time-dependent proper accelerations in Minkowski spacetime given in [188] allowed the authors to study entanglement generation for periodic acceleration, finding a resonance in entanglement generation similar to the resonance in the DCE due to a single oscillating boundary (i.e. the flat-spacetime limit of the example in Section 5.5). The work we presented in Chapter 5 lets us consider wider set of boundary motions and include curved spacetimes, as we do in the following.

We examine the generation and degradation of entanglement in a number of scenarios. As in Section 6.3, the scenarios we consider will involve a drop to the surface of the Earth from a height of 110 m, based on the apparatus of the drop tower at ZARM. This apparatus was used in the first experimental investigation into the effect of gravitational motion on entangled states [43]. We again use the Schwarzschild metric, a massless scalar field, and obtain the Bogoliubov coefficients corresponding to the fall via Equations (5.12), though here we need to compute more than just off-diagonal coefficients (in contrast with Chapter 6). We again use the Schwarzschild time coordinate  $t$  as a bookkeeping coordinate, which we recall is related to the proper time of some stationary experimenter by Equation (2.10). For simplicity, we again take the initial length of each cavity to be 1 m (in the  $r$ -coordinate); choos-

ing other values ranging from  $10^{-6}$  m to 1 m affects the numerical results below, but does not change their order of magnitude (except where stated otherwise), nor change any of their qualitative features.

Note that localising the field to the inside of a cavity does not entirely solve the issue of causality mentioned above; projective measurements within a cavity of any finite size can still violate causality. To avoid this, transformations of the field must be “ultralocal” [218], e.g. products of unitary transformations perfectly localised at spacetime points on a spacelike hypersurface. To model the process of measuring the field, one can consider a pointlike detector coupling locally to the relevant field mode(s) (as in the Jaynes-Cummings model). In that case causality is preserved as long as we restrict ourselves to the consideration of timescales significantly larger than the time required for light to cross the cavity [210], as is the case here. We will not explicitly model the detection procedure, and as such our results should be treated as an idealised case, ignoring effects arising from the process of detection.

We first numerically investigate the entanglement generated between pairs of modes of a single cavity, initially in the vacuum state, and dropped to the Earth (Section 7.2), before considering the degradation of entanglement between one mode in a stationary cavity, and one mode in a dropped cavity (Section 7.3). In those cases we use the negativity, defined in Equation (3.2), as a measure of entanglement. Then in Section 7.4 we derive a general expression for the change in entanglement fidelity, defined in Equation (3.3), after a perturbative Bogoliubov transformation. This is followed by some numerical results regarding the reduction in entanglement fidelity after a single cavity, initially containing a two-mode entangled state, is dropped. The scenarios considered in Sections 7.2 and 7.3, and the use of the negativity as an entanglement measure, allow us to make contact with previous theoretical work, and greatly simplifies the calculations. On the other hand, the scenario and quantifier of entanglement (the entanglement fidelity) considered in Section 7.4 more closely resembles the experiment mentioned above [43].

## 7.2 Scenario 1: generation of entanglement in a single dropped box

We consider a single cavity, initially in the vacuum state  $|0\rangle$ . In this state, the negativity between any pair of modes is of course zero. After a Bogoliubov transformation of the form given in Equation (2.46), the vacuum state transforms according to Equation (2.48), and the negativity between the modes  $m$  and  $n$  (after tracing

out all others, and with  $m \neq n$ ) is given to lowest order by [217]

$$\mathcal{N}_{\text{vac}} = \left| \beta_{mn}^{(1)} \right|. \quad (7.1)$$

Subjecting the cavity to the fall described above, Equation (5.12d) gives

$$\mathcal{N}_{\text{vac}} = \frac{\sqrt{mn}}{(m+n)L_{*,0}} \left| \int_0^T dt e^{-i[\bar{\omega}_m(t) + \bar{\omega}_n(t)]} \left[ (-1)^{m+n} \frac{dr_{*,1}}{dt} - \frac{dr_{*,2}}{dt} \right] \right|, \quad (7.2)$$

where  $r_{*,j}$  is the trajectory of mirror  $j$  in the Schwarzschild tortoise coordinate used in previous chapters, and  $L_{*,0}$  is the initial length in this coordinate. For a cavity undergoing some period of acceleration in flat space, if modes  $m$  and  $n$  are of the same parity (i.e. if  $m+n$  is even), then  $\beta_{mn}^{(1)} = 0$  (see e.g. [188]) and therefore  $\mathcal{N}_{\text{vac}} = 0$  to first order. From Equation (7.2) we see that this is not the case here, a consequence of the tidal force between the two boundaries, giving rise to a non-zero difference in tortoise-coordinate velocities throughout the fall. This case is the only example in the present chapter where a change in the initial length appreciably changes the result.

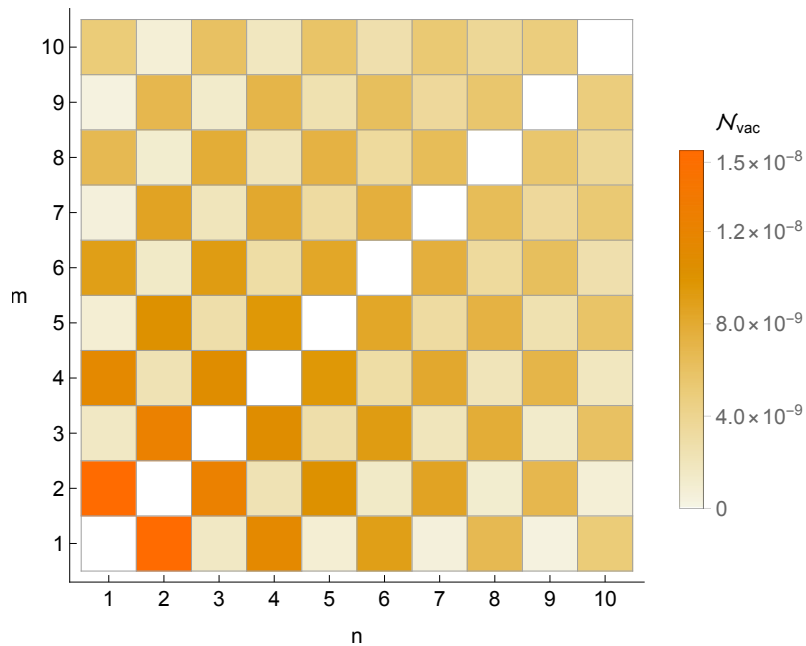


Figure 7.1: The negativity between modes in a single cavity, initially in the vacuum state, after a fall of 110 m to the surface of the Earth.

The negativity after the fall is shown in Figure 7.1 for a selection of values of  $m$  and  $n$ . There we see that, while entanglement is generated between same-parity modes, it is significantly less than between modes of different parity. In tandem with that, we see a tendency for more entanglement to be generated between lower modes,

and between nearby modes. This behaviour can be understood from the form of Equation (7.2); the prefactor acts to suppress entanglement generation for modes which are not near to each other, and increase entanglement generation for higher, nearby modes, but the latter is counteracted by the exponential term in the integral, which oscillates quickly with respect to the velocities, and does so with increasing frequency as  $m$  and  $n$  are increased, reducing the value of the integral<sup>1</sup>.

As an aside we note that, given Equation (7.1) and the results of Section 5.5, an oscillating trajectory of one or more mirrors will produce resonances in the generated entanglement in a similar manner to those pointed out in [188], but now manifesting the novel resonances due to spacetime curvature described in Section 5.5.

## 7.3 Scenario 2: degradation of entanglement between separated partners

### 7.3.1 Setup

In this second scenario, we consider an entangled state between mode  $m$  in one cavity and  $n$  in another. The cavity containing mode  $m$  is subjected to the fall described in Section 7.1, and the modes corresponding to that cavity therefore undergo a Bogoliubov transformation. We examine entanglement degradation given two different initial entangled states: a Bell state (Section 7.3.2) and a two-mode squeezed vacuum state (Section 7.3.3). First, following [217], we will find it useful to define

$$f_m^\alpha := \frac{1}{2} \sum_{p \neq m} |\alpha_{pm}^{(1)}|^2 \quad \text{and} \quad f_m^\beta := \frac{1}{2} \sum_{p \neq m} |\beta_{pm}^{(1)}|^2, \quad (7.3)$$

which are to be calculated using Equations (5.12b) and (5.12d) respectively.

### 7.3.2 Negativity for an initial Bell state

We defined the Bell states in Equation (3.21). In particular, we choose the state  $|\Phi^+\rangle = (1/\sqrt{2})(|0_m 0_n\rangle + |1_m 1_n\rangle)$ . As noted in Section 3.3, this state has negativity  $\mathcal{N}_{\text{Bell}} = 1/2$ . The state after the perturbative Bogoliubov transformation can be found by writing  $|\Phi^+\rangle$  in terms of raising operators acting on the vacuum state, and then using Equations (2.38) and (2.48). After transforming the state of the cavity with which the mode  $m$  is associated, the negativity is given to lowest order by [20]

$$\mathcal{N}_{\text{Bell}} = \frac{1}{2} - \mathcal{N}_{\text{Bell}}^{(2)} \quad (7.4)$$

<sup>1</sup>cf. the justification of the ‘‘stationary phase approximation’’ [219].

with

$$\mathcal{N}_{\text{Bell}}^{(2)} := f_m^\alpha + 2f_m^\beta. \quad (7.5)$$

In [20], a comparable scenario to the one we consider here was investigated; instead of a dropped cavity, the authors considered one which undergoes a finite stretch of acceleration, finding that  $\mathcal{N}_{\text{Bell}}^{(2)}$  varies periodically in the duration of this stretch. In our case, the mode-dependence of this quantity, and its evolution throughout the fall for a given  $m$ , are shown in Figures 7.2 and 7.3 respectively.

### 7.3.3 Negativity for an initial two-mode squeezed vacuum states

We described the two-mode squeezed vacuum state with a real squeezing parameter  $\zeta$  in Equations (3.17), giving both its density matrix and its representation in the covariance matrix formalism. The covariance-matrix representation of Bogoliubov transformations was given in Section 3.2.4. Transforming the part of the state associated with the falling cavity, one finds that the covariance matrix for the state of both cavities transforms as

$$\begin{pmatrix} \cosh(2\zeta)\mathbb{1}_2 & \sinh(2\zeta)\sigma_z \\ \sinh(2\zeta)\sigma_z & \cosh(2\zeta)\mathbb{1}_2 \end{pmatrix} \rightarrow \begin{pmatrix} \Gamma_m & C \\ C & \Gamma_n \end{pmatrix} \quad (7.6)$$

where

$$\Gamma_m = \cosh(2\zeta)\mathcal{M}_{mm}\mathcal{M}_{mm}^T + \sum_{p \neq m} \mathcal{M}_{mp}\mathcal{M}_{mp}^T, \quad (7.7)$$

and with  $\Gamma_n = \cosh(2\zeta)\mathbb{1}_2$  and  $C = \sinh(2\zeta)\sigma_z\mathcal{M}_{mm}^T$ . We recall that  $\sigma_z$  is the third Pauli matrix, and that the matrices  $\mathcal{M}_{pq}$  were defined in Equation (3.24). As noted in Section 3.3, the negativity of the initial state is  $\mathcal{N}_{\text{TMSV}} = (1/2)(e^{2|\zeta|} - 1)$ . Equation (3.29) then can be used to calculate the negativity after the transformation, giving (to lowest order) [65]

$$\mathcal{N}_{\text{TMSV}} = \frac{1}{2}(e^{2|\zeta|} - 1) - \mathcal{N}_{\text{TMSV}}^{(2)} \quad (7.8)$$

with

$$\mathcal{N}_{\text{TMSV}}^{(2)} := e^{2|\zeta|} \left[ \frac{1}{2}(e^{2|\zeta|} - 1)(f_m^\alpha + f_m^\beta) + f_m^\beta \right]. \quad (7.9)$$

As with the Bell state, for a finite-duration period of acceleration in flat spacetime,  $\mathcal{N}_{\text{TMSV}}^{(2)}$  exhibits an oscillatory behaviour, (as can be inferred from Figures 7.2 and 7.3 of [65]). For the present case, considering some example values of  $|\zeta|$ , the mode-dependence of  $\mathcal{N}_{\text{TMSV}}^{(2)}$ , and its evolution throughout the fall for a given  $m$ , are shown in Figures 7.2 and 7.3 respectively.

### 7.3.4 Results and discussion

As we saw in Sections 7.3.2 and 7.3.3, the entanglement degradation, as quantified by  $\mathcal{N}_{\text{Bell}}^{(2)}$  and  $\mathcal{N}_{\text{TMSV}}^{(2)}$  (which we will collectively refer to as  $\mathcal{N}^{(2)}$ ) is independent of the mode  $n$  of the stationary cavity. It seems likely that causality requires this to be the case, though the negativity is not an observable per se.<sup>2</sup> Figure 7.2 shows how, for the initial states described above,  $\mathcal{N}^{(2)}$  increases with the mode number  $m$  of the dropped cavity's state. Figure 7.3 shows the monotonic increase of  $\mathcal{N}^{(2)}$  as the cavity falls.

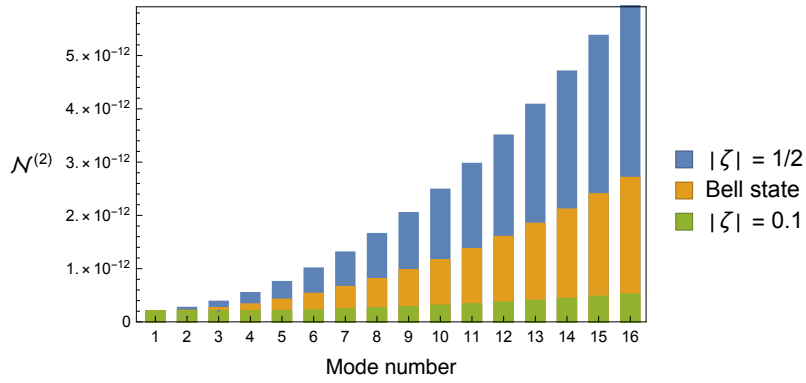


Figure 7.2: Entanglement degradation, as quantified by  $\mathcal{N}^{(2)}$  as a function of the mode number  $m$  of the dropped cavity's initial state. This is shown for an initial Bell state  $|\Phi^+\rangle$  (orange), as well as for initial two-mode squeezed vacuum states with a squeezing parameter of magnitude 1/2 (blue) and 1/10 (green).

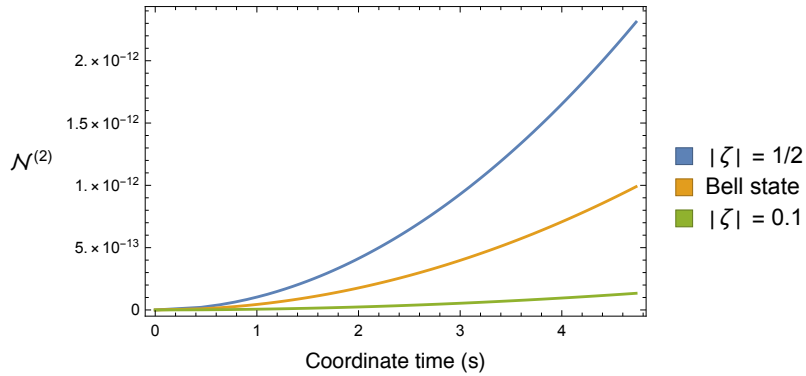


Figure 7.3: The evolution of the entanglement degradation throughout the fall (in terms of the Schwarzschild time coordinate  $t$ ) for an initial Bell state  $|\Phi^+\rangle$  (orange), as well as for initial two-mode squeezed vacuum states with a squeezing parameter of magnitude 1/2 (blue) and 1/10 (green), with  $m = 10$  in all cases.

<sup>2</sup>If this  $n$ -independence weren't true, one could imagine the the holder of the stationary cavity, arbitrarily far away, performing some local operation which is detected via the increase/decrease in entanglement degradation in the dropped cavity.

In the regime considered here, no oscillations of  $\mathcal{N}^{(2)}$  were apparent at any scale, though we cannot rule them out in a different parameter regime. The monotonic increase in negativity seen in Figure 7.3 contrasts with the oscillatory behaviour found in the flat-spacetime scenario mentioned above. One similarity, however, is the increased sensitivity of the state to degradation for higher  $m$  (see Figures 7.2 and 7.3 of [65], noting that  $f_m^\alpha \gg f_m^\beta$ ) which can be seen for the present case in Figure 7.2.

The oscillating term in the integrand of  $\beta_{mn}^{(1)}$  has a higher frequency than the one for  $\alpha_{mn}^{(1)}$  (see Equations (5.12)). Consequently, for comparatively slowly-varying velocities, the magnitude of former is generally smaller than that of the latter. Indeed, in the regime considered here,  $f_m^\beta$  is between 1 and 5 orders of magnitude smaller than  $f_m^\alpha$ . The entanglement degradation is therefore largely determined by  $f_m^\alpha$ . If we choose the squeezing parameter such that the initial negativity of the two-mode squeezed state is the same as for the Bell state, i.e.  $\zeta = \log \sqrt{2}$ , then  $\mathcal{N}_{\text{TMSV}}^{(1)} = \mathcal{N}_{\text{Bell}}^{(1)} + f_m^\beta$ , and the behaviour of  $\mathcal{N}_{\text{TMSV}}^{(1)}$  is then very similar to that of  $\mathcal{N}_{\text{Bell}}^{(1)}$ . For the large-scale behaviour shown in Figures 7.2 and 7.3, one can therefore equally take the results for the Bell state (orange) to be for a two-mode squeezed state with  $\zeta = \log \sqrt{2}$ .

The results show that the degradation of entanglement in this scenario is orders of magnitude smaller than the generation of entanglement from the vacuum between pairs of modes in a single cavity (Scenario 1, Figure 7.1), though both effects occur on an extremely small scale. To understand the relation between the two effects, consider the following. Let us write the Hilbert space of the field states in the dropped cavity as  $\mathcal{H}_m \otimes \mathcal{H}_R$ , where  $\mathcal{H}_m$  corresponds to mode  $m$ , and  $\mathcal{H}_R$  to all other modes. Denoting the Hilbert space corresponding to mode  $n$  in the stationary cavity as  $\mathcal{H}_n$ , we can write the unitary evolution of the field in both cavities between  $t = 0$  and  $t = T$  as  $U_n \otimes U_{mR}$ , where  $U_{mR}$  acts on  $\mathcal{H}_m \otimes \mathcal{H}_R$ . Note that  $U_{mR}$  was the transformation that generated entanglement in Scenario 1. Given the separable form of the transformation, the entanglement between the spaces  $\mathcal{H}_n$  and  $\mathcal{H}_m \otimes \mathcal{H}_R$  cannot change, and therefore the reduction of entanglement between  $m$  and  $n$  must be compensated by the generation of entanglement between mode  $m$  and modes  $R$ .

While this has some of the flavour of results regarding the monogamy of entanglement, the fact that there is no maximally-entangled state in a continuous-variable system prevents us from reasoning based on monogamy alone. In particular, since there is no upper bound to the entanglement between  $\mathcal{H}_m$  and any other system, it is always possible to generate entanglement between  $\mathcal{H}_m$  and  $\mathcal{H}_R$  without affecting the entanglement between  $\mathcal{H}_m$  and  $\mathcal{H}_n$ .

## 7.4 Scenario 3: change in entanglement fidelity within a single apparatus

### 7.4.1 Setup

In this final scenario we investigate how mode-mixing and particle creation affect change the entanglement fidelity when a single cavity, containing a Bell state of modes  $m$  and  $n$ , is made to fall from the drop tower. This is necessarily a second-order effect [220]. We could proceed by calculating the perturbative Bogoliubov transformations of each Bell state up to that order, normalising them,<sup>3</sup> and then finding the entanglement fidelity via Equation (3.3). We can instead considerably simplify this lengthy procedure by the considerations in the following section.

### 7.4.2 Perturbative transformation of the entanglement fidelity

First, working to second order, let us write a perturbed but unnormalised field state  $|\tilde{\psi}\rangle$  as

$$|\tilde{\psi}\rangle = |\psi^{(0)}\rangle + |\psi^{(1)}\rangle + |\psi^{(2)}\rangle \quad (7.10)$$

where  $|\psi^{(j)}\rangle$  denotes that a term is of  $j^{\text{th}}$ -order in the expansion parameter. The term  $|\psi^{(0)}\rangle$  is normalised, being the state which results from the straightforward time evolution of a stationary cavity, i.e. the target state. Equation (3.3) then gives the entanglement fidelity with respect to the target state as

$$F_{\psi^{(0)}} = N^2 \left| \langle \psi^{(0)} | \tilde{\psi} \rangle \right|^2 \quad (7.11)$$

where  $N$  is a real number normalising  $N|\tilde{\psi}\rangle$ . Introducing the notation

$$\psi_{jk} := \langle \psi^{(j)} | \psi^{(k)} \rangle, \quad (7.12)$$

we can then expand  $N^2$  to second order:

$$N^2 := \langle \tilde{\psi} | \tilde{\psi} \rangle^{-1} = 1 - \psi_{01} + \psi_{10} + \psi_{11} + \psi_{02} + \psi_{20} + (\psi_{01} + \psi_{10})^2 \quad (7.13)$$

and consequently, Equation (7.11) gives

$$F_{\psi^{(0)}} = 1 + |\psi_{01}|^2 - \psi_{11}. \quad (7.14)$$

---

<sup>3</sup>This is made necessary by the perturbative nature of the transformation - see e.g. [220].

In the following, we will write this as

$$F_X = 1 - F_X^{(2)}, \quad (7.15)$$

with  $F_X^{(2)} := -|\psi_{01}|^2 + \psi_{11}$  and where  $X = \Phi^+, \Phi^-, \Psi^+, \Psi^-$  will label the initial Bell state (which in turn determines the  $\psi_{jk}$ ). The  $F_X^{(2)}$  then quantify the decrease in entanglement fidelity, much as  $\mathcal{N}^{(2)}$  did for the negativity. From Equation (7.15) we see that we only need to calculate the transformed states to first order, and that we do not need to normalise them. We now consider the correlated states,  $|\Phi^+\rangle$  and  $|\Phi^-\rangle$ , and the anticorrelated states,  $|\Psi^+\rangle$  and  $|\Psi^-\rangle$  separately.

### 7.4.3 Correlated states

Let us first consider the correlated Bell states  $|\Phi^+\rangle$  and  $|\Phi^-\rangle$ . Recalling the notation introduced in Equations (2.46) in light of Equations (5.12), we see that in our case  $G_m = e^{i\bar{\omega}_m(T)}$ , where  $\bar{\omega}_m(T)$  was defined in Equation (5.13a). Using Equation (7.15) to calculate the entanglement fidelity after the transformation, we obtain

$$F_{\Phi^+}^{(2)} = -\Im \left( G_n \beta_{nm}^{(1)*} \right)^2 - \Re \left[ \sum_p \left( \beta_{pm}^{(1)} \alpha_{pn}^{(1)*} + \beta_{pn}^{(1)*} \alpha_{pm}^{(1)} \right) \right] \\ + \frac{1}{2} \left[ \sum_{p,q} \left| \beta_{pq}^{(1)} \right|^2 + \left| \beta_{mn}^{(1)} \right|^2 + \sum_p \left( \left| \alpha_{pm}^{(1)} \right|^2 + \left| \alpha_{pn}^{(1)} \right|^2 \right) \right] \quad (7.16a)$$

$$F_{\Phi^-}^{(2)} = -\Re \left( G_n \beta_{nm}^{(1)*} \right)^2 + \Re \left[ \sum_p \left( \beta_{pm}^{(1)} \alpha_{pn}^{(1)*} + \beta_{pn}^{(1)*} \alpha_{pm}^{(1)} \right) \right] \\ + \frac{1}{2} \left[ \sum_{p,q} \left| \beta_{pq}^{(1)} \right|^2 + \left| \beta_{mn}^{(1)} \right|^2 + \sum_p \left( \left| \alpha_{pm}^{(1)} \right|^2 + \left| \alpha_{pn}^{(1)} \right|^2 \right) \right], \quad (7.16b)$$

where we have made use of the perturbative form of the Bogoliubov identities given in Equations (2.47). Equations (7.16) are symmetric in  $m$  and  $n$ , a consequence of Equation (2.47c).

Given the roles of the coefficients  $\alpha_{pq}$  and  $\beta_{pq}$  in determining mode-mixing and changes in particle number respectively, we can interpret the physical origin of some of the terms in Equations (7.16a). The first term in each equation arises due to the generation of pairs of particles in modes  $m$  and  $n$  but with a different phase to that of  $|1_m 1_n\rangle$  in the target state. The sum over the magnitudes of the  $\beta_{pq}^{(1)}$  coefficients describes the generation of particle population from the vacuum across all modes of the field, and the final term results from the transfer of population out of modes  $m$  and  $n$  due to mode-mixing.

#### 7.4.4 Anticorrelated states

We now consider the anticorrelated Bell states  $|\Psi^+\rangle$  and  $|\Psi^-\rangle$ . We find the reduction in entanglement fidelity for these initial states in the same manner as in Section 7.4.3, giving

$$F_{\Psi^+}^{(2)} = -\Im \left( G_n \alpha_{mn}^{(1)*} \right)^2 + \Re \left( \sum_p \beta_{pm}^{(1)} \beta_{pn}^{(1)*} \right) + \frac{1}{2} \left( \sum_{p,q} |\beta_{pq}^{(1)}|^2 + \sum_p |\alpha_{pm}^{(1)} + \alpha_{pn}^{(1)}|^2 \right) \quad (7.17a)$$

$$F_{\Psi^-}^{(2)} = -\Im \left( G_n \alpha_{mn}^{(1)*} \right)^2 - \Re \left( \sum_p \beta_{pm}^{(1)} \beta_{pn}^{(1)*} \right) + \frac{1}{2} \left( \sum_{p,q} |\beta_{pq}^{(1)}|^2 + \sum_p |\alpha_{pm}^{(1)} - \alpha_{pn}^{(1)}|^2 \right) \quad (7.17b)$$

where we have again made use of Equations (2.47). As for the correlated states, these expressions are symmetric in  $m$  and  $n$ , a consequence of Equation (2.47b).

As for the correlated states, we can interpret the physical origin of some of the terms appearing in Equations (7.17). The first term in each equation describes the exchange of population between modes  $m$  and  $n$ , but in such a way that the relative phase of  $|0_m 1_n\rangle$  and  $|0_n 1_m\rangle$  may be modified. Again, the sum over the magnitudes of the  $\beta_{pq}^{(1)}$  coefficients describes the generation of particle population from the vacuum across all modes of the field, and the final term results from the transfer of population out of modes  $m$  and  $n$  due to mode-mixing.

#### 7.4.5 Results and discussion

The reduction in entanglement fidelity after the fall is shown in Figure 7.4 for each initial state, and for a range of modes  $m$  and  $n$ . As in Section 7.3, we see broadly an increase in the extent of the effect with increasing mode, though now the result of course depends on  $n$  as well as  $m$ , since both modes belong to the dropped cavity. We also see a difference in behaviour between the correlated states and the anticorrelated ones. The reduction in entanglement fidelity for the correlated states (Figures 7.4a and 7.4b) simply increases strictly as either  $m$  or  $n$  is increased. For the anticorrelated states however (Figures 7.4c and 7.4d), the mode-dependence is more complicated. For the initial state  $|\Psi^-\rangle$  (Figure 7.4d), we see a valley around  $m = n$ , and a monotonic increase away from that valley (as long as  $m + n$  does not decrease). For the initial state  $|\Psi^+\rangle$  (Figure 7.4c), we see the same valley, but

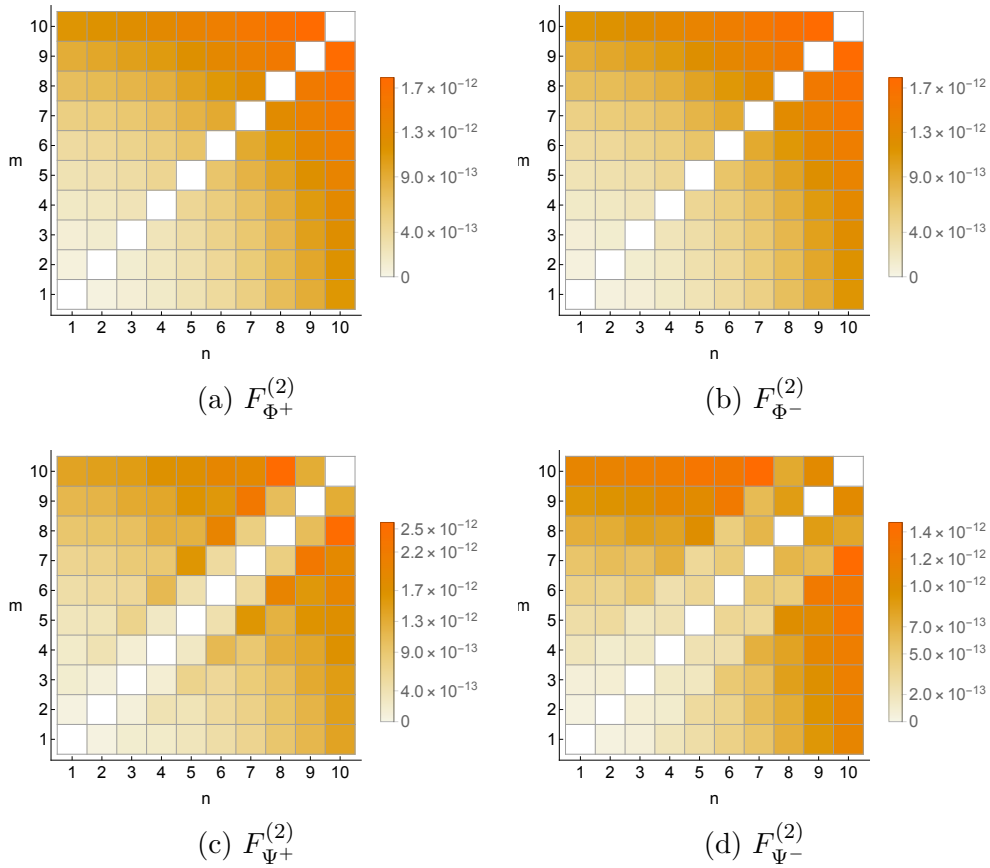


Figure 7.4: Mode dependence of the reduction in entanglement fidelity after the fall for the four initial states.

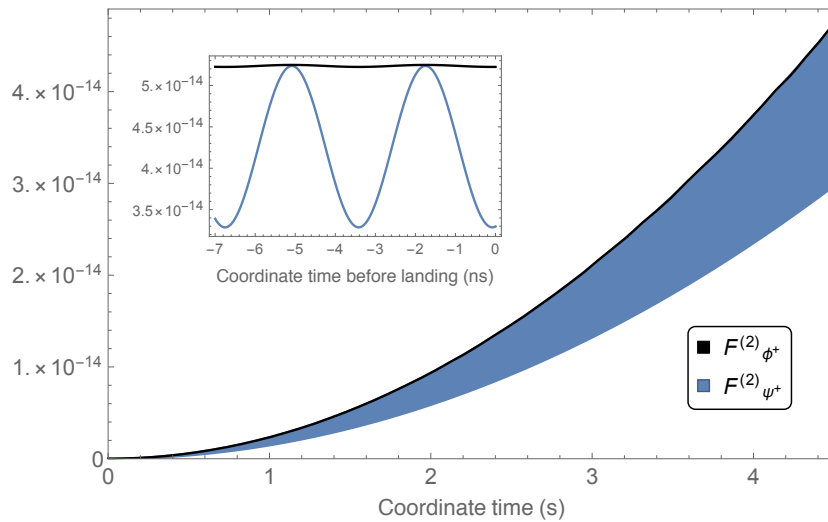


Figure 7.5: The evolution of  $F_{\Phi^+}^{(2)}$  (black) and  $F_{\Psi^+}^{(2)}$  (blue) throughout the fall, with  $m = 1$  and  $n = 2$ . The inset shows the small-scale oscillations of these quantities, which for  $F_{\Psi^+}^{(2)}$  are of a sufficient amplitude and frequency to give the blue curve the appearance of a band.

followed immediately by a sharp ridge where  $m$  and  $n$  differ by 2, which then slowly decreases as we move away from the central valley.

Figure 7.5 gives the behaviour of  $F_{\Phi^+}^{(2)}$  and  $F_{\Psi^+}^{(2)}$  throughout the fall for  $m = 1$  and  $n = 1$ . We see large-amplitude oscillations of  $F_{\Psi^+}^{(2)}$ , and significantly smaller oscillations of  $F_{\Phi^+}^{(2)}$ . This can be explained by the fact that for  $F_{\Psi^+}^{(2)}$  the amplitude of the oscillations is determined by the magnitude of  $\alpha_{mn}^{(1)}$  (from the first term in Equation (7.17a)), while for  $F_{\Phi^+}^{(2)}$  they are determined by the magnitude of  $\beta_{mn}^{(1)}$  (from the first term in Equation (7.16a)), and as we discussed in Section 7.3.4, the former is generally significantly larger than the latter (for slowly varying velocities). We also see that  $F_{\Phi^+}^{(2)}$  is strictly larger than  $F_{\Psi^+}^{(2)}$  throughout the fall.

Recent experiments have sought to detect any changes in entanglement fidelity in a drop-tower scenario similar to the one described here [43]. In that experiment, entangled photon pairs were produced in a  $|\Psi^-\rangle$ -type state with respect to horizontal and vertical polarisation states, travelling in optical fibres during a fall of 1.4 s. A reduction in fidelity greater than 1.08% was ruled out by the experiment, and there is (to our knowledge) no theoretical prediction regarding a reduction in fidelity for this experimental setup. For comparison, the reduction predicted here is on the order of  $10^{-12}\%$  for a fall of approximately 4.5 s, though our model deals with particle-number states of a cavity, not photon-polarisation states in an optical fibre, and our results are therefore of limited applicability. It would be of interest to develop a model to predict the outcome of such an experiment, and see if the prediction varies significantly in magnitude from the results we present here.

## 7.5 Conclusion

We have examined three scenarios involving motion-induced changes in entanglement as a result of a cavity being dropped from a certain height. In the first scenario, we considered the generation of entangled particles in pairs of modes in a single cavity. The results contrast with the case of uniform acceleration in flat space-time in that entanglement can be generated to first order between modes of the same parity, a consequence of the tidal forces experienced by the cavity, though this effect is strongly suppressed compared to entanglement generation between modes with differing parities. We found that more entanglement is generated for modes with a lower frequency, and between neighbouring modes.

The second scenario regarded the degradation of entanglement shared between two cavities when one remains stationary and the other is dropped. We found that when the initial state is either a two-mode squeezed state or a Bell state, the coarse behaviour of the entanglement degradation is determined by mode-mixing effects. As

a consequence, the behaviour of the degradation for a two-mode squeezed vacuum behaves as a scaled version of the Bell state, with the scaling determined by the squeezing parameter. In contrast with the flat-spacetime scenario mentioned above, we found no oscillations in the degradation over time, though we did find an increase in the degradation with increasing mode number (of the dropped cavity's initial state), in accordance with those results.

In the third scenario, we studied the change in entanglement fidelity when a cavity, two of whose modes are prepared in a Bell state, is dropped. We found general expressions for the reduction in entanglement fidelity after a perturbative Bogoliubov transformation (Equations (2.46)), and presented numerical investigations into how this reduction depended on the chosen mode and initial state. We found a non-trivial mode dependence, with some similarities to the study of the decrease in negativity, and some differences. Here, unlike for the reduction in negativity, we found an oscillatory behaviour over time, being significantly stronger for a particular initial state.

## Part III

# Conclusion, appendices and bibliography

# Chapter 8

## Conclusion

### 8.1 Summary

We set out to find novel effects in quantum systems as a result of spacetime curvature, focussing on the measurement of time and changes in entanglement content. In order to describe a spatially-localised system while fully incorporating general relativity, we considered a quantum field confined by boundaries, embedded in a curved spacetime. We used a massless scalar field to model the electromagnetic field (ignoring polarisation), which we described using QFT in curved spacetime. A key issue that then arises is the necessity for a timelike Killing vector with which to associate a quantisation of the field. This leaves open the problem of how to describe the evolution of the field state when the system undergoes some arbitrary motion. We gave a partial solution to this problem, namely a method for calculating the Bogoliubov transformation (and therefore the transformation of the field state) connecting the cavity modes before the motion with those after it. This requires that the motion be finite in duration with respect to a stationary spacetime. We worked in  $1+1\text{D}$ , but an extension to  $3+1\text{D}$  was given in Appendix C. The resulting equations were solved perturbatively, assuming the velocity (in the conformally flat coordinates) to be proportional to some small parameter.

The results described above gave a way to calculate the DCE in curved spacetime. Applying this to the case where a single boundary oscillates, we found that the presence of spacetime curvature results in novel particle creation resonances, and recovered some previous results regarding the known resonance. The novel resonances provide an example of how our intuitive, flat-spacetime understanding of length can correspond in curved spacetime to different notions depending on the context. We also briefly considered the application of our approach to phonon states of a BEC, sketching an argument for the potential amplification of the effect. We used the

Schwarzschild spacetime to model the Earth's gravitational field, and continued to do so in the subsequent chapters.

We reviewed a quantum model of the light clock in an earlier chapter, described using Gaussian state quantum mechanics, the relevant elements of which were also reviewed. Developing this model further, we found that the deviation between the times of two such clocks separates into a classical effect resulting from the changing frequency, and an effect arising from the motion-induced change of the state of the quantum field. We showed for Gaussian states that this does not depend on the clock's initial state, only the transformation applied to it, which is in turn determined by the spacetime and the clock's path through it. Employing the results of the preceding chapter to calculate the transformation of the field state, we considered a situation where a clock falls to the Earth from a droptower, comparing it to one remaining fixed. Examining the classical and quantum effects separately, we found that the former was greater in magnitude than the discrepancy between two comparable, ideal, classical observers, resulting in other words in a greater time dilation. The quantum effect acted to further increase this difference, though it was unsurprisingly many orders of magnitude smaller than the classical one. Examining this on a small scale, we found oscillations in the clock time, depending on the size (and therefore fundamental frequency) of the clock. Stepping outside of our restriction that we consider Earth-based experiments for a moment, we found that when increasing the spacetime curvature while keeping all other parameters fixed, the classical effect diminished in magnitude while the quantum one grew.

Moving on to our discussion of entanglement, we gave a numerical investigation of three scenarios, each making use of the same droptower setup as above. First was the generation of entanglement between pairs of modes in a single dropped cavity. While non-inertial motion in flat spacetime does not create entanglement between pairs of modes with the same parity, the tidal force in our scenario does cause some entanglement to be generated between these modes. The entanglement generated between mode pairs of different parity was nonetheless significantly higher. Superimposed on this effect was a decrease in entanglement generation with increasing frequency-difference between modes and a greater generation for lower-frequency modes. In the second scenario we considered entanglement distributed between two systems, one of which is made to fall. Considering a Bell state and a two-mode squeezed vacuum state, we found that the behaviour of the entanglement degradation for the squeezed state is effectively a scaled version of the behaviour for the Bell state, a consequence of the dominance of the mode-mixing aspect of the state transformation over the particle-creating one. The degradation increased with increasing mode number of the initial state in the dropped cavity. We saw no oscillations in the degradation on the scale considered, unlike previous studies in flat spacetime.

In the two scenarios described above we used the negativity to quantify the generation/degradation of entanglement. This measure has the benefit of being comparatively easy to calculate, but cannot be easily measured. For this reason, we used the entanglement fidelity to quantify the effect in the third scenario, inspired by a related experiment [43]. We first derived a general expression for the reduction in entanglement fidelity as a consequence of a perturbative Bogoliubov transformation. Applying this to Bell states within a single cavity, we found that the reduction exhibited an interesting state-dependence, as evidenced by our numerical study. We found the landscape of mode-dependence to be a little more complex for the anticorrelated states. Likewise, the time-evolution of the fidelity differed between the correlated and the anticorrelated states, with the latter exhibiting large-scale oscillations.

## 8.2 Taking things further

There are a number of limitations to the results described above. It would be of interest, for example, to see the role played by a non-zero spin. A reconsideration of the scenario where we investigated the change in entanglement fidelity in a dropped box (Section 7.4), now including polarisation, would make the results more relevant to the actual experiment being carried out [43]. Other aspects which could modify the results are the presence of mass, and a consideration of all  $3 + 1$  (known) dimensions.

The method described in Chapter 5 relied upon the assumption that the system is effectively stationary on the timescale of the mode frequencies (Equation (5.5)). However, we have not quantified the limits of this assumption, for example by using a multiple scale analysis, leaving open the risk of extending the method beyond its regime of validity. This issue has recently been solved in [221], where the method in Chapter 5 is generalised and made more rigorous, extending it to the case of a finite period of “slow” spacetime dynamics.

The use of an optical cavity, while simplifying our analysis, is not a particularly practical experimental platform on which to test the effect of large-scale motion through curved spacetime. A more detailed analysis of the BEC implementation discussed in Section 5.6 would be of value, carefully analysing how the spacetime and the motion affect the behaviour of the bulk. In this regard, we note that the first space-based BEC experiments have now begun [222]. Since the majority of laboratory-scale quantum systems are described non-relativistically, often via a Hamiltonian operator, it may be of use to the research community to find a common language between these descriptions and the Bogoliubov transformations often used in relativistic quantum information. To this end, Appendix D gives a recipe for

translating perturbative Bogoliubov transformations into unitary operators to first order. To apply this to the work described so far, it must be extended to at least second order.

Perhaps the most important development of our work would be a better understanding of the specific role of curvature in the results we have presented. For a pointlike observer, Einstein's equivalence principle allows us to equate free-fall with flat spacetime. However, for a system with some finite extent, tidal forces will reveal the curvature of the spacetime. Likewise, one can equate a pointlike object at rest in a gravitational field with one undergoing some proper acceleration in flat spacetime, and one finds again that this equivalence breaks down for a system with finite extent. This is illustrated in [223], for example, where it is shown that a reference frame at rest in a uniform gravitational field is not equivalent to a uniformly accelerating one. Given these considerations, one might find a comparable flat-spacetime scenario to the droptower trajectories used here by starting in a reference frame with a certain proper acceleration, undergoing a period of inertial motion, and then ending in another accelerated reference frame. By choosing the appropriate parameters for the initial and final accelerations, as well as the duration of inertial motion, one might compare that scenario with the results presented in Chapters 6 and 7. Of particular interest is the question of whether there exist qualitative differences between the cases of curved and flat spacetime (as in the novel resonance predicted in Chapter 5), rather than merely quantitative differences, a question to which we so far have no answer.

# Bibliography

- [1] P. Ginsparg. Kenneth g. wilson: Renormalized after-dinner anecdotes. *Journal of Statistical Physics*, 157(4-5):610–624, 2014. 5
- [2] M. P. E. Lock and I. Fuentes. Dynamical casimir effect in curved spacetime. *New Journal of Physics*, 19(7):073005, 2017. 7
- [3] M. P. E. Lock and I. Fuentes. Relativistic quantum clocks. In *Time in Physics*, pages 51–68. Springer, 2017. 7
- [4] D. Rätzel, F. Schneiter, D. Braun, T. Bravo, R. Howl, M. P. E. Lock, and I. Fuentes. Frequency spectrum of an optical resonator in a curved spacetime. *New Journal of Physics*, 20(5):053046, 2018. 7, 84
- [5] M. P. Lock and I. Fuentes. Quantum and classical effects in light-clock falling in schwarzschild geometry. *arXiv preprint arXiv:1901.08000*, 2019. 7
- [6] M. P. E. Lock and I. Fuentes. Generation and degradation of entanglement in a drop-tower. In preparation. 7
- [7] R. M. Gingrich and C. Adami. Quantum entanglement of moving bodies. *Physical Review Letters*, 89(27):270402, 2002. 16
- [8] P. M. Alsing and I. Fuentes. Observer-dependent entanglement. *Classical and Quantum Gravity*, 29(22):224001, 2012. 16, 17, 48
- [9] S. J. Summers and R. Werner. The vacuum violates bell’s inequalities. *Physics Letters A*, 110(5):257–259, 1985. 16, 47
- [10] R. Bousso. The holographic principle. *Reviews of Modern Physics*, 74(3):825, 2002. 16, 48
- [11] C. J. Isham. Canonical quantum gravity and the problem of time. In *Integrable systems, quantum groups, and quantum field theories*, pages 157–287. Springer, 1993. 16, 56

- [12] D. N. Page and W. K. Wootters. Evolution without evolution: Dynamics described by stationary observables. *Physical Review D*, 27(12):2885, 1983. 16
- [13] W. K. Wootters. time replaced by quantum correlations. *International journal of theoretical physics*, 23(8):701–711, 1984. 16
- [14] L. C. B. Crispino, A. Higuchi, and G. E. A. Matsas. The unruh effect and its applications. *Reviews of Modern Physics*, 80(3):787, 2008. 17, 26, 27, 48, 62, 65
- [15] V. V. Dodonov. Photon creation and excitation of a detector in a cavity with a resonantly vibrating wall. *Physics Letters A*, 207(3):126–132, 1995. 17, 69
- [16] J. L. Ball, I. Fuentes-Schuller, and F. P. Schuller. Entanglement in an expanding spacetime. *Physics Letters A*, 359(6):550–554, 2006. 17, 49
- [17] I. Fuentes, R. B. Mann, E. Martín-Martínez, and S. Moradi. Entanglement of dirac fields in an expanding spacetime. *Physical Review D*, 82(4):045030, 2010. 17, 49
- [18] I. Fuentes-Schuller and R. B. Mann. Alice falls into a black hole: entanglement in noninertial frames. *Physical review letters*, 95(12):120404, 2005. 17, 49
- [19] N. Friis, D. E. Bruschi, J. Louko, and I. Fuentes. Motion generates entanglement. *Physical Review D*, 85(8):081701, 2012. 17, 87
- [20] D. E. Bruschi, I. Fuentes, and J. Louko. Voyage to alpha centauri: Entanglement degradation of cavity modes due to motion. *Physical Review D*, 85(6):061701, 2012. 17, 87, 90, 91
- [21] G. Adesso, I. Fuentes-Schuller, and M. Ericsson. Continuous-variable entanglement sharing in noninertial frames. *Physical Review A*, 76(6):062112, 2007. 17
- [22] N. Friis, A. R. Lee, K. Truong, C. Sabín, E. Solano, G. Johansson, and I. Fuentes. Relativistic quantum teleportation with superconducting circuits. *Physical review letters*, 110(11):113602, 2013. 17
- [23] N. Friis, M. Huber, I. Fuentes, and D. E. Bruschi. Quantum gates and multipartite entanglement resonances realized by nonuniform cavity motion. *Physical Review D*, 86(10):105003, 2012. 17, 87
- [24] D. E. Bruschi, A. Dragan, A. R. Lee, I. Fuentes, and J. Louko. Relativistic motion generates quantum gates and entanglement resonances. *Physical review letters*, 111(9):090504, 2013. 17

- [25] M. Ahmadi, D. E. Bruschi, and I. Fuentes. Quantum metrology for relativistic quantum fields. *Physical Review D*, 89(6):065028, 2014. 17, 46, 71
- [26] M. Ahmadi, D. E. Bruschi, C. Sabín, G. Adesso, and I. Fuentes. Relativistic quantum metrology: Exploiting relativity to improve quantum measurement technologies. *Scientific reports*, 4, 2014. 17, 46, 71
- [27] C. Sabín, D. E. Bruschi, M. Ahmadi, and I. Fuentes. Phonon creation by gravitational waves. *New Journal of Physics*, 16(8):085003, 2014. 17, 72
- [28] P. W. Bridgman. *The logic of modern physics*. Macmillan New York, 1927. 17, 50, 51
- [29] A. Peres. *Quantum theory: concepts and methods*, volume 57. Springer Science & Business Media, 2006. 17, 53
- [30] T. L. Nicholson. *A new record in atomic clock performance*. PhD thesis, University of Colorado, 2015. 18, 54
- [31] N. Poli, C. W. Oates, P. Gill, and G. M. Tino. Optical atomic clocks. *Rivista del Nuovo Cimento*, 36:555–624, 2013. 18, 54
- [32] P. Kómár, E. M. Kessler, M. Bishof, L. Jiang, A. S. Sørensen, J. Ye, and M. D. Lukin. A quantum network of clocks. *Nature physics*, 10(8):582587, 2014. 18, 55
- [33] O. Hosten, N. J. Engelsen, R. Krishnakumar, and M. A. Kasevich. Measurement noise 100 times lower than the quantum-projection limit using entangled atoms. *Nature*, 2016. 18, 55
- [34] A. W. Harrow and A. Montanaro. Quantum computational supremacy. *Nature*, 549(7671):203, 2017. 18
- [35] D. E. Bruschi, A. Datta, R. Ursin, T. C. Ralph, and I. Fuentes. Quantum estimation of the schwarzschild spacetime parameters of the earth. *Physical Review D*, 90(12):124001, 2014. 18
- [36] A. Dragan, I. Fuentes, and J. Louko. Quantum accelerometer: Distinguishing inertial bob from his accelerated twin rob by a local measurement. *Physical Review D*, 83(8):085020, 2011. 18
- [37] R. Howl, L. Hackermüller, D. E. Bruschi, and I. Fuentes. Gravity in the quantum lab. *Advances in Physics: X*, 3(1):1383184, 2018. 18

- [38] J. Yin, Y. Cao, Y.-H. Li, J.-G. Ren, S.-K. Liao, L. Zhang, W.-Q. Cai, W.-Y. Liu, B. Li, H. Dai, et al. Satellite-to-ground entanglement-based quantum key distribution. *Physical review letters*, 119(20):200501, 2017. 18
- [39] A. Derevianko and M. Pospelov. Hunting for topological dark matter with atomic clocks. *Nature Physics*, 10(12):933–936, 2014. 18
- [40] M. D. Gabriel and M. P. Haugan. Testing the einstein equivalence principle: Atomic clocks and local lorentz invariance. *Physical Review D*, 41(10):2943, 1990. 18
- [41] P. C. Davies. Quantum mechanics and the equivalence principle. *Classical and Quantum Gravity*, 21(11):2761, 2004. 18
- [42] S. Reynaud, C. Salomon, and P. Wolf. Testing general relativity with atomic clocks. *Space science reviews*, 148(1-4):233–247, 2009. 18
- [43] M. Fink, A. Rodriguez-Aramendia, J. Handsteiner, A. Ziarkash, F. Steinlechner, T. Scheidl, I. Fuentes, J. Pienaar, T. C. Ralph, and R. Ursin. Experimental test of photonic entanglement in accelerated reference frames. *Nature Communications*, 8:15304, 2017. 19, 48, 87, 88, 98, 103
- [44] C. W. Misner, K. S. Thorne, and J. A. Wheeler. *Gravitation*. Macmillan, 1973. 20, 51, 52, 56, 84
- [45] R. M. Wald. *General relativity*. University of Chicago press, 2010. 20, 32
- [46] J. Preskill. Lecture notes: “quantum field theory in curved spacetime” (1990). <http://www.theory.caltech.edu/~preskill/notes.html>. Accessed: 06-09-2018. 20
- [47] N. D. Birrell and P. C. W. Davies. *Quantum fields in curved space*. Cambridge university press, 1984. 20, 26, 31, 65, 77
- [48] L. Parker and D. Toms. *Quantum field theory in curved spacetime: quantized fields and gravity*. Cambridge University Press, 2009. 20
- [49] R. M. Wald. *Quantum field theory in curved spacetime and black hole thermodynamics*. University of Chicago Press, 1994. 20
- [50] S. S. Schweber. *QED and the men who made it: Dyson, Feynman, Schwinger, and Tomonaga*. Princeton University Press, 1994. 24
- [51] M. E. Peskin. *An introduction to quantum field theory*. CRC Press, 2018. 24

- [52] P. A. M. Dirac. The fundamental equations of quantum mechanics. *Proc. R. Soc. Lond. A*, 109(752):642–653, 1925. 25
- [53] N. Friis, A. R. Lee, and J. Louko. Scalar, spinor, and photon fields under relativistic cavity motion. *Physical Review D*, 88(6):064028, 2013. 25
- [54] S. Fagnocchi, S. Finazzi, S. Liberati, M. Kormos, and A. Trombettoni. Relativistic bose–einstein condensates: a new system for analogue models of gravity. *New Journal of Physics*, 12(9):095012, 2010. 25, 72
- [55] D. E. Bruschi, C. Sabín, A. White, V. Baccetti, D. K. Oi, and I. Fuentes. Testing the effects of gravity and motion on quantum entanglement in space-based experiments. *New Journal of Physics*, 16(5):053041, 2014. 25, 71, 72, 73
- [56] H. Bruus and K. Flensberg. *Many-body quantum theory in condensed matter physics: an introduction*. Oxford university press, 2004. 27
- [57] A. Ashtekar and A. Magnon. Quantum fields in curved space-times. *Proc. R. Soc. Lond. A*, 346(1646):375–394, 1975. 30
- [58] S. Takagi. Vacuum noise and stress induced by uniform accelerationhawking-unruh effect in rindler manifold of arbitrary dimension. *Progress of Theoretical Physics Supplement*, 88:1–142, 1986. 30
- [59] R. M. Wald. The history and present status of quantum field theory in curved spacetime. In *Einstein and the Changing Worldviews of Physics*, pages 317–331. Springer, 2012. 31
- [60] S. W. Hawking. Particle creation by black holes. *Communications in mathematical physics*, 43(3):199–220, 1975. 31, 48, 49
- [61] L. Parker. Particle creation in expanding universes. *Physical Review Letters*, 21(8):562, 1968. 31
- [62] C. Weedbrook, S. Pirandola, R. García-Patrón, N. J. Cerf, T. C. Ralph, J. H. Shapiro, and S. Lloyd. Gaussian quantum information. *Reviews of Modern Physics*, 84(2):621, 2012. 33, 41, 42, 45
- [63] Arvind, B. Dutta, N. Mukunda, and R. Simon. The real symplectic groups in quantum mechanics and optics. *Pramana*, 45(6):471–497, 1995. 35
- [64] I. D. Tveritinov. Several remarks on the representation of the infinite-dimensional symplectic group and on the construction of the metaplectic group. *Mathematical Notes*, 75(5-6):805–818, 2004. 35

- [65] N. Friis. *Cavity mode entanglement in relativistic quantum information*. PhD thesis, University of Nottingham, 2013. arXiv:1311.3536. 35, 91, 93
- [66] R. Horodecki, P. Horodecki, M. Horodecki, and K. Horodecki. Quantum entanglement. *Reviews of modern physics*, 81(2):865, 2009. 37, 38
- [67] M. B. Plenio and S. Virmani. An introduction to entanglement measures. *Quantum Information & Computation*, 7(1):1–51, 2007. 37, 38
- [68] G. Adesso, S. Ragy, and A. R. Lee. Continuous variable quantum information: Gaussian states and beyond. *Open Systems & Information Dynamics*, 21(01n02):1440001, 2014. 37, 41
- [69] Aristotle. Metaphysics, book viii. <http://classics.mit.edu/Aristotle/metaphysics.8.viii.html>. Accessed: 06-09-2018. 38
- [70] J. S. Bell. Bertlmann’s socks and the nature of reality. *Le Journal de Physique Colloques*, 42(C2):C2–41, 1981. 38
- [71] J. G. Richens, J. H. Selby, and S. W. Al-Safi. Entanglement is necessary for emergent classicality in all physical theories. *Physical review letters*, 119(8):080503, 2017. 38
- [72] M. A. Nielsen. Conditions for a class of entanglement transformations. *Physical Review Letters*, 83(2):436, 1999. 38
- [73] J. Gray, L. Banci, A. Bayat, and S. Bose. Measuring entanglement negativity. *arXiv preprint arXiv:1709.04923*, 2017. 39
- [74] J. Laurat, G. Keller, J. A. Oliveira-Huguenin, C. Fabre, T. Coudreau, A. Serafini, G. Adesso, and F. Illuminati. Entanglement of two-mode gaussian states: characterization and experimental production and manipulation. *Journal of Optics B: Quantum and Semiclassical Optics*, 7(12):S577, 2005. 39, 44
- [75] G. Vidal and R. F. Werner. Computable measure of entanglement. *Physical Review A*, 65(3):032314, 2002. 39
- [76] B. Schumacher. Sending entanglement through noisy quantum channels. *Physical Review A*, 54(4):2614, 1996. 39
- [77] B. B. Blinov, D. L. Moehring, L. M. Duan, and C. Monroe. Observation of entanglement between a single trapped atom and a single photon. *Nature*, 428(6979):153, 2004. 39
- [78] S. L. Braunstein and P. Van Loock. Quantum information with continuous variables. *Reviews of Modern Physics*, 77(2):513, 2005. 40, 41

- [79] U. Leonhardt. *Measuring the quantum state of light*, volume 22. Cambridge university press, 1997. 40
- [80] T. L. Curtright and C. K. Zachos. Quantum mechanics in phase space. *Asia Pacific Physics Newsletter*, 1(01):37–46, 2012. 41
- [81] A. Kenfack and K. Życzkowski. Negativity of the wigner function as an indicator of non-classicality. *Journal of Optics B: Quantum and Semiclassical Optics*, 6(10):396, 2004. 41
- [82] E. F. Galvao. Discrete wigner functions and quantum computational speedup. *Physical Review A*, 71(4):042302, 2005. 41
- [83] A. Serafini. Multimode uncertainty relations and separability of continuous variable states. *Physical review letters*, 96(11):110402, 2006. 41
- [84] R. L. Hudson. When is the wigner quasi-probability density non-negative? *Reports on Mathematical Physics*, 6(2):249–252, 1974. 42
- [85] G. Grynberg, A. Aspect, and C. Fabre. *Introduction to quantum optics: from the semi-classical approach to quantized light*. Cambridge university press, 2010. 43
- [86] J. Goold, M. Huber, A. Riera, L. del Rio, and P. Skrzypczyk. The role of quantum information in thermodynamicsa topical review. *Journal of Physics A: Mathematical and Theoretical*, 49(14):143001, 2016. 44
- [87] M. A. Nielsen and I. L. Chuang. *Quantum Computation and Quantum Information: 10th Anniversary Edition*. Cambridge University Press, 2010. 45
- [88] M. W. Mitchell, J. S. Lundeen, and A. M. Steinberg. Super-resolving phase measurements with a multiphoton entangled state. *Nature*, 429(6988):161, 2004. 45
- [89] D. Braun, P. Jian, O. Pinel, and N. Treps. Precision measurements with photon-subtracted or photon-added gaussian states. *Physical Review A*, 90(1):013821, 2014. 45
- [90] M. A. de Gosson. *Symplectic geometry and quantum mechanics*, volume 166. Springer Science & Business Media, 2006. 46
- [91] G. Adesso and F. Illuminati. Entanglement in continuous-variable systems: recent advances and current perspectives. *Journal of Physics A: Mathematical and Theoretical*, 40(28):7821, 2007. 46, 47

- [92] Č. Brukner, M. S. Kim, J.-W. Pan, and A. Zeilinger. Correspondence between continuous-variable and discrete quantum systems of arbitrary dimensions. *Physical Review A*, 68(6):062105, 2003. 47
- [93] R. Simon. Peres-horodecki separability criterion for continuous variable systems. *Physical Review Letters*, 84(12):2726, 2000. 47
- [94] S. J. Summers. Bells inequalities and quantum field theory. In *Quantum Probability and Applications V*, pages 393–413. Springer, 1990. 47
- [95] B. Reznik. Entanglement from the vacuum. *Foundations of Physics*, 33(1):167–176, 2003. 48
- [96] E. Martin-Martinez and N. C. Menicucci. Entanglement in curved spacetimes and cosmology. *Classical and Quantum Gravity*, 31(21):214001, 2014. 48
- [97] H. Reeh and S. Schlieder. Bemerkungen zur unitäräquivalenz von lorentz-invarianten feldern. *Il Nuovo Cimento (1955-1965)*, 22(5):1051–1068, 1961. 48
- [98] H. Casini and M. Huerta. Entanglement entropy in free quantum field theory. *Journal of Physics A: Mathematical and Theoretical*, 42(50):504007, 2009. 48
- [99] H. Casini. Geometric entropy, area and strong subadditivity. *Classical and Quantum Gravity*, 21(9):2351, 2004. 48
- [100] H. Casini and M. Huerta. A c-theorem for entanglement entropy. *Journal of Physics A: Mathematical and Theoretical*, 40(25):7031, 2007. 48
- [101] M. Srednicki. Entropy and area. *Physical Review Letters*, 71(5):666, 1993. 48
- [102] J. Eisert, M. Cramer, and M. B. Plenio. Colloquium: Area laws for the entanglement entropy. *Reviews of Modern Physics*, 82(1):277, 2010. 48
- [103] J. D. Bekenstein. Black holes and entropy. *Physical Review D*, 7(8):2333, 1973. 48
- [104] L. Bombelli, R. K. Koul, J. Lee, and R. D. Sorkin. Quantum source of entropy for black holes. *Physical Review D*, 34(2):373, 1986. 48
- [105] C. Cao, S. M. Carroll, and S. Michalakis. Space from hilbert space: Recovering geometry from bulk entanglement. *Physical Review D*, 95(2):024031, 2017. 48
- [106] M. Van Raamsdonk. Building up spacetime with quantum entanglement. *General Relativity and Gravitation*, 42(10):2323–2329, 2010. 48

- [107] C. M. Will. The confrontation between general relativity and experiment. *Living reviews in relativity*, 9(1):3, 2006. 48
- [108] W. Israel. Thermo-field dynamics of black holes. *Physics Letters A*, 57(2):107–110, 1976. 48
- [109] C. Rovelli and M. Smerlak. Unruh effect without trans-horizon entanglement. *Physical Review D*, 85(12):124055, 2012. 48
- [110] P. M. Alsing, I. Fuentes-Schuller, R. B. Mann, and T. E. Tessier. Entanglement of dirac fields in noninertial frames. *Physical Review A*, 74(3):032326, 2006. 49
- [111] G. Adesso and I. Fuentes-Schuller. Correlation loss and multipartite entanglement across a black hole horizon. *Quantum Information and Computation*, 9(7&8):0657–0665, 2009. 49
- [112] E. Martín-Martínez, L. J. Garay, and J. León. Unveiling quantum entanglement degradation near a schwarzschild black hole. *Physical review D*, 82(6):064006, 2010. 49
- [113] E. Martín-Martínez, L. J. Garay, and J. León. Quantum entanglement produced in the formation of a black hole. *Physical Review D*, 82(6):064028, 2010. 49
- [114] R. Schützhold and W. G. Unruh. Quantum correlations across the black hole horizon. *Physical Review D*, 81(12):124033, 2010. 49
- [115] A. Almheiri, D. Marolf, J. Polchinski, and J. Sully. Black holes: complementarity or firewalls? *Journal of High Energy Physics*, 2013(2):62, 2013. 49
- [116] J. Lindkvist, C. Sabín, I. Fuentes, A. Dragan, I.-M. Svensson, P. Delsing, and G. Johansson. Twin paradox with macroscopic clocks in superconducting circuits. *Physical Review A*, 90(5):052113, 2014. 50, 56, 57, 58, 59, 71, 77, 78
- [117] A. Peres. Unperformed experiments have no results. *American Journal of Physics*, 46(7):745–747, 1978. 50
- [118] A. Einstein. Zur elektrodynamik bewegter körper. *Annalen der physik*, 322(10):891–921, 1905. 50
- [119] W. Rindler. *Relativity: special, general, and cosmological*. Oxford University Press on Demand, 2006. 51, 71, 79

- [120] R. U. SEXTL and H. K. URBANTKE. *Relativity, groups, particles: special relativity and relativistic symmetry in field and particle physics*. Springer-Verlag Wien, 2001. 51
- [121] A. EINSTEIN. On the influence of gravitation on the propagation of light. *Annalen der Physik*, 35(898-908):906, 1911. 51
- [122] R. V. POUND and G. A. REBKA JR. Apparent weight of photons. *Physical Review Letters*, 4(7):337, 1960. 51
- [123] J. WEST. A light clock satisfying the clock hypothesis of special relativity. *European journal of physics*, 28(4):693, 2007. 51
- [124] S. C. FLETCHER. Light clocks and the clock hypothesis. *Foundations of Physics*, 43(11):1369–1383, 2013. 51
- [125] H. P. ROBERTSON. The uncertainty principle. *Physical Review*, 34(1):163, 1929. 52
- [126] W. PAULI. Die allgemeinen prinzipien der wellenmechanik. *Handbuch der Physik*, 5:1–168, 1958. 52
- [127] J. C. GARRISON and J. WONG. Canonically conjugate pairs, uncertainty relations, and phase operators. *Journal of Mathematical Physics*, 11(8):2242–2249, 1970. 52
- [128] M. SRINIVAS and R. VIJAYALAKSHMI. The time of occurrence in quantum mechanics. *Pramana*, 16(3):173–199, 1981. 52
- [129] A. S. L. MALABARBA, A. J. SHORT, and P. KAMMERLANDER. Clock-driven quantum thermal engines. *New Journal of Physics*, 17(4):045027, 2015. 53
- [130] H. SALECKER and E. P. WIGNER. Quantum limitations of the measurement of space-time distances. *Physical Review*, 109(2):571, 1958. 53, 55
- [131] J. P. FALCK and E. H. HAUGE. Larmor clock reexamined. *Physical Review B*, 38(5):3287, 1988. 53
- [132] A. PERES. Measurement of time by quantum clocks. *Am. J. Phys*, 48(7):552, 1980. 53
- [133] M. P. WOODS, R. SILVA, and J. OPPENHEIM. Autonomous quantum machines and finite sized clocks. *arXiv preprint arXiv:1607.04591*, 2016. 53
- [134] L. B. LEVITIN and T. TOFFOLI. Fundamental limit on the rate of quantum dynamics: the unified bound is tight. *Physical review letters*, 103(16):160502, 2009. 53

- [135] S. Deffner and S. Campbell. Quantum speed limits: from heisenbergs uncertainty principle to optimal quantum control. *Journal of Physics A: Mathematical and Theoretical*, 50(45):453001, 2017. 53
- [136] L. Mandelstam and I. Tamm. The uncertainty relation between energy and time in non-relativistic quantum mechanics. *J. Phys. USSR*, 9(4):249–254, 1945. 53
- [137] S. L. Braunstein, C. M. Caves, and G. J. Milburn. Generalized uncertainty relations: Theory, examples, and lorentz invariance. *Annals of Physics*, 247(1):135 – 173, 1996. 53
- [138] A. Einstein, B. Podolsky, and N. Rosen. Can quantum-mechanical description of physical reality be considered complete? *Physical review*, 47(10):777, 1935. 54
- [139] J. G. Muga, R. Sala, and J. P. Palao. The time of arrival concept in quantum mechanics. *Superlattices and microstructures*, 23(3-4):833–842, 1998. 54
- [140] J. J. Halliwell, J. Evaeus, J. London, and Y. Malik. A self-adjoint arrival time operator inspired by measurement models. *Physics Letters A*, 379(39):2445–2451, 2015. 54
- [141] Y. Aharonov, J. Oppenheim, S. Popescu, B. Reznik, and W. G. Unruh. Measurement of time of arrival in quantum mechanics. *Physical Review A*, 57(6):4130, 1998. 54
- [142] P. Busch. The time–energy uncertainty relation. In *Time in quantum mechanics*, pages 73–105. Springer, 2008. 54
- [143] C. Grebing, A. Al-Masoudi, S. Dörscher, S. Häfner, V. Gerginov, S. Weyers, B. Lipphardt, F. Riehle, U. Sterr, and C. Lisdat. Realization of a timescale with an accurate optical lattice clock. *Optica*, 3(6):563–569, 2016. 54
- [144] B. J. Bloom, T. L. Nicholson, J. R. Williams, S. L. Campbell, M. Bishof, X. Zhang, W. Zhang, S. L. Bromley, and J. Ye. An optical lattice clock with accuracy and stability at the 10<sup>-18</sup> level. *Nature*, 2014. 54
- [145] I. Ushijima, M. Takamoto, M. Das, T. Ohkubo, and H. Katori. Cryogenic optical lattice clocks. *Nature Photonics*, 9(3):185, 2015. 54
- [146] L. von der Wense, B. Seiferle, M. Laatiaoui, J. B. Neumayr, H.-J. Maier, H.-F. Wirth, C. Mokry, J. Runke, K. Eberhardt, C. E. Düllmann, et al. Direct detection of the 229th nuclear clock transition. *Nature*, 533(7601):47–51, 2016. 55

- [147] C. J. Campbell, A. G. Radnaev, A. Kuzmich, V. A. Dzuba, V. V. Flambaum, and A. Derevianko. Single-ion nuclear clock for metrology at the 19th decimal place. *Physical review letters*, 108(12):120802, 2012. 55
- [148] D. Kleppner. Time too good to be true. *Physics Today*, 59(3):10, 2006. 55
- [149] P. Erker. The quantum hourglass: approaching time measurement with quantum information theory. Master’s thesis, ETH Zürich, 2014. 55, 85
- [150] S. Ranković, Y.-C. Liang, and R. Renner. Quantum clocks and their synchronisation—the alternate ticks game. *arXiv preprint arXiv:1506.01373*, 2015. 55
- [151] M. P. Woods, R. Silva, G. Pütz, S. Stupar, and R. Renner. Quantum clocks are more accurate than classical ones. *arXiv preprint arXiv:1806.00491*, 2018. 55
- [152] P. Erker, M. T. Mitchison, R. Silva, M. P. Woods, N. Brunner, and M. Huber. Autonomous quantum clocks: does thermodynamics limit our ability to measure time? *Physical Review X*, 7(3):031022, 2017. 55, 85
- [153] S. Hossenfelder. Minimal length scale scenarios for quantum gravity. *Living Rev. Relativity*, 16(2):90, 2013. 55, 56
- [154] L. Burderi, T. Di Salvo, and R. Iaria. Quantum clock: A critical discussion on spacetime. *Physical Review D*, 93(6):064017, 2016. 56
- [155] E. Castro Ruiz, F. Giacomini, and Č. Brukner. Entanglement of quantum clocks through gravity. *Proceedings of the National Academy of Sciences*, 114(12):E2303–E2309, 2017. 56
- [156] S. A. Fulling. Nonuniqueness of canonical field quantization in riemannian space-time. *Physical Review D*, 7(10):2850, 1973. 56
- [157] W. G. Unruh. Notes on black-hole evaporation. *Physical Review D*, 14(4):870, 1976. 56, 65
- [158] G. T. Moore. Quantum theory of the electromagnetic field in a variable-length one-dimensional cavity. *Journal of Mathematical Physics*, 11(9):2679–2691, 1970. 56, 63, 64
- [159] K. Lorek, J. Louko, and A. Dragan. Ideal clocks a convenient fiction. *Classical and Quantum Gravity*, 32(17):175003, 2015. 56
- [160] A. M. Eisele. On the behaviour of an accelerated clock. *Helvetica Physica Acta*, 60:1024–1037, 1987. 56

- [161] R. Pierini, K. Turzyński, and A. Dragan. Can a charged decaying particle serve as an ideal clock in the presence of a magnetic field? *Physical Review D*, 97(4):045006, 2018. 56
- [162] E. Knox. Flavour-oscillation clocks and the geometricity of general relativity. *The British Journal for the Philosophy of Science*, 61(2):433–452, 2010. 56
- [163] H. R. Brown and H. R. Brown. *Physical relativity: Space-time structure from a dynamical perspective*. Oxford University Press on Demand, 2005. 56
- [164] B. S. DeWitt. Quantum theory of gravity. i. the canonical theory. *Physical Review*, 160(5):1113, 1967. 56
- [165] E. Anderson. Problem of time in quantum gravity. *Annalen der Physik*, 524(12):757–786, 2012. 56
- [166] M. Born. The theory of the rigid electron in the kinematics of the principle of relativity. *Annalen der Physik*, 335:1–56, 1909. 58
- [167] J. Lindkvist, C. Sabín, G. Johansson, and I. Fuentes. Motion and gravity effects in the precision of quantum clocks. *Scientific reports*, 5, 2015. 58, 59
- [168] V. Giovannetti, S. Lloyd, and L. Maccone. Advances in quantum metrology. *Nature Photonics*, 5(4):222–229, 2011. 58
- [169] H. M. Wiseman and G. J. Milburn. *Quantum measurement and control*. Cambridge University Press, 2009. 58
- [170] O. Pinel, P. Jian, N. Treps, C. Fabre, and D. Braun. Quantum parameter estimation using general single-mode gaussian states. *Physical Review A*, 88(4):040102, 2013. 59
- [171] A. R. Lee. *Localised systems in relativistic quantum information*. PhD thesis, University of Nottingham, 2013. arXiv preprint arXiv:1309.4419. 62
- [172] T. Fujii, S. Matsuo, N. Hatakenaka, S. Kurihara, and A. Zeilinger. Quantum circuit analog of the dynamical casimir effect. *Physical Review B*, 84(17):174521, 2011. 63
- [173] V. V. Dodonov, A. B. Klimov, and D. E. Nikonov. Quantum phenomena in nonstationary media. *Physical Review A*, 47(5):4422, 1993. 63
- [174] V. V. Dodonov. Current status of the dynamical casimir effect. *Physica Scripta*, 82(3):038105, 2010. 63, 65

- [175] D. A. R. Dalvit, P. A. M. Neto, and F. D. Mazzitelli. Fluctuations, dissipation and the dynamical casimir effect. In *Casimir Physics*, pages 419–457. Springer, 2011. 63, 73
- [176] S. A. Fulling and P. C. W. Davies. Radiation from a moving mirror in two dimensional space-time: conformal anomaly. In *Proceedings of the Royal Society of London A: Mathematical, Physical and Engineering Sciences*, volume 348, pages 393–414. The Royal Society, 1976. 63, 64, 65, 77
- [177] L. H. Ford and A. Vilenkin. Quantum radiation by moving mirrors. *Physical Review D*, 25(10):2569, 1982. 63
- [178] G. Barton and C. Eberlein. On quantum radiation from a moving body with finite refractive index. *Annals of Physics*, 227(2):222–274, 1993. 63
- [179] J.-C. Jaskula, G. B. Partridge, M. Bonneau, R. Lopes, J. Ruaudel, D. Boiron, and C. I. Westbrook. Acoustic analog to the dynamical casimir effect in a bose-einstein condensate. *Physical Review Letters*, 109(22):220401, 2012. 63, 72, 73
- [180] J. R. Johansson, G. Johansson, C. M. Wilson, and F. Nori. Dynamical casimir effect in a superconducting coplanar waveguide. *Physical review letters*, 103(14):147003, 2009. 63
- [181] C. M. Wilson, G. Johansson, A. Pourkabirian, M. Simoen, J. R. Johansson, T. Duty, F. Nori, and P. Delsing. Observation of the dynamical casimir effect in a superconducting circuit. *Nature*, 479(7373):376–379, 2011. 63, 69, 70, 73
- [182] P. Lähteenmäki, G. S. Paraoanu, J. Hassel, and P. J. Hakonen. Dynamical casimir effect in a josephson metamaterial. *Proceedings of the National Academy of Sciences*, 110(11):4234–4238, 2013. 63
- [183] M. Razavy and J. Terning. Quantum radiation in a one-dimensional cavity with moving boundaries. *Physical Review D*, 31(2):307, 1985. 63, 64
- [184] J. Haro and E. Elizalde. Physically sound hamiltonian formulation of the dynamical casimir effect. *Physical Review D*, 76(6):065001, 2007. 63
- [185] G. Barton and C. A. North. Peculiarities of quantum radiation in three dimensions from moving mirrors with high refractive index. *Annals of Physics*, 252(1):72–114, 1996. 63
- [186] M. T. Jaekel and S. Reynaud. Motional casimir force. *Journal de Physique I*, 2(2):149–165, 1992. 63

- [187] P. Candelas and D. Deutsch. On the vacuum stress induced by uniform acceleration or supporting the ether. In *Proceedings of the Royal Society of London A: Mathematical, Physical and Engineering Sciences*, volume 354, pages 79–99. The Royal Society, 1977. 64
- [188] D. E. Bruschi, J. Louko, D. Faccio, and I. Fuentes. Mode-mixing quantum gates and entanglement without particle creation in periodically accelerated cavities. *New Journal of Physics*, 15(7):073052, 2013. 64, 66, 68, 87, 89, 90
- [189] J.-Y. Ji, H.-H. Jung, J.-W. Park, and K.-S. Soh. Production of photons by the parametric resonance in the dynamical casimir effect. *Physical Review A*, 56(6):4440, 1997. 64, 69, 71
- [190] P. C. W. Davies and S. A. Fulling. Radiation from moving mirrors and from black holes. In *Proceedings of the Royal Society of London A: Mathematical, Physical and Engineering Sciences*, volume 356, pages 237–257. The Royal Society, 1977. 64
- [191] I. Brevik, K. A. Milton, S. D. Odintsov, and K. E. Osetrin. Dynamical casimir effect and quantum cosmology. *Physical Review D*, 62(6):064005, 2000. 64
- [192] L. C. Céleri, F. Pascoal, and M. H. Y. Moussa. Action of the gravitational field on the dynamical casimir effect. *Classical and Quantum Gravity*, 26(10):105014, 2009. 64, 69, 71
- [193] R. Brout, S. Massar, R. Parentani, and P. Spindel. A primer for black hole quantum physics. *Physics Reports*, 260(6):329–446, 1995. 64
- [194] A. Lambrecht, M.-T. Jaekel, and S. Reynaud. Motion induced radiation from a vibrating cavity. *Physical review letters*, 77(4):615, 1996. 69
- [195] J. R. Johansson, G. Johansson, C. M. Wilson, and F. Nori. Dynamical casimir effect in superconducting microwave circuits. *Physical Review A*, 82(5):052509, 2010. 70
- [196] C. Sabín, D. E. Bruschi, M. Ahmadi, and I. Fuentes. Phonon creation by gravitational waves. *New Journal of Physics*, 16(8):085003, 2014. 71, 73
- [197] M. Visser and C. Molina-París. Acoustic geometry for general relativistic barotropic irrotational fluid flow. *New Journal of Physics*, 12(9):095014, 2010. 72
- [198] C. Barcelo, S. Liberati, and M. Visser. Analogue gravity from bose-einstein condensates. *Classical and Quantum Gravity*, 18(6):1137, 2001. 72

- [199] C. Barceló, S. Liberati, M. Visser, et al. Analogue gravity. *Living Rev. Rel*, 8(12):214, 2005. 72
- [200] J. Steinhauer. Observation of quantum hawking radiation and its entanglement in an analogue black hole. *Nature Physics*, 12(10):959, 2016. 72
- [201] J. Joseph, B. Clancy, L. Luo, J. Kinast, A. Turlapov, and J. E. Thomas. Measurement of sound velocity in a fermi gas near a feshbach resonance. *Physical review letters*, 98(17):170401, 2007. 73
- [202] P. C. W. Davies. Quantum vacuum friction. *Journal of Optics B: Quantum and Semiclassical Optics*, 7(3):S40, 2005. 73
- [203] M. R. R. Good, P. R. Anderson, and C. R. Evans. Time dependence of particle creation from accelerating mirrors. *Physical Review D*, 88(2):025023, 2013. 74
- [204] S. Robertson, F. Michel, and R. Parentani. Controlling and observing nonseparability of phonons created in time-dependent 1d atomic bose condensates. *Physical Review D*, 95(6):065020, 2017. 74
- [205] A. Einstein. Die grundlage der allgemeinen relativitätstheorie. *Annalen der Physik*, 354(7):769–822, 1916. English translation: The Principle of Relativity: Original Papers (1920), University of Calcutta press. 76
- [206] Bremen Drop Tower, ZARM. <https://www.zarm.uni-bremen.de/en/drop-tower/general-information.html>. Accessed: 2018-03-09. 79
- [207] N. Hinkley, J. A. Sherman, N. B. Phillips, M. Schioppo, N. D. Lemke, K. Beloy, M. Pizzocaro, C. W. Oates, and A. D. Ludlow. An atomic clock with 10–18 instability. *Science*, 341(6151):1215–1218, 2013. 83
- [208] O. Oreshkov, F. Costa, and Č. Brukner. Quantum correlations with no causal order. *Nature communications*, 3:1092, 2012. 84
- [209] R. D. Sorkin. Impossible measurements on quantum fields. In *Directions in general relativity: Proceedings of the 1993 International Symposium, Maryland*, volume 2, pages 293–305, 1993. 86
- [210] D. M. T. Benincasa, L. Borsten, M. Buck, and F. Dowker. Quantum information processing and relativistic quantum fields. *Classical and Quantum Gravity*, 31(7):075007, 2014. 86, 88
- [211] E. Martín-Martínez. Causality issues of particle detector models in qft and quantum optics. *Physical Review D*, 92(10):104019, 2015. 86

- [212] P. M. Alsing and G. J. Milburn. Teleportation with a uniformly accelerated partner. *Physical review letters*, 91(18):180404, 2003. 86
- [213] T. G. Downes, I. Fuentes, and T. C. Ralph. Entangling moving cavities in noninertial frames. *Physical review letters*, 106(21):210502, 2011. 86
- [214] D. E. Browne and M. B. Plenio. Robust generation of entanglement between two cavities mediated by short interactions with an atom. *Physical Review A*, 67(1):012325, 2003. 86
- [215] N. Friis, A. R. Lee, D. E. Bruschi, and J. Louko. Kinematic entanglement degradation of fermionic cavity modes. *Physical Review D*, 85(2):025012, 2012. 87
- [216] E. G. Brown, M. del Rey, H. Westman, J. León, and A. Dragan. What does it mean for half of an empty cavity to be full? *Physical Review D*, 91(1):016005, 2015. 87
- [217] N. Friis and I. Fuentes. Entanglement generation in relativistic quantum fields. *Journal of Modern Optics*, 60(1):22–27, 2013. 87, 89, 90
- [218] F. Dowker. Useless qubits in” relativistic quantum information”. *arXiv preprint arXiv:1111.2308*, 2011. 88
- [219] D. Hilbert. *Methods of mathematical physics*. CUP Archive, 2004. 90
- [220] N. Friis, M. Skotiniotis, I. Fuentes, and W. Dür. Heisenberg scaling in gaussian quantum metrology. *Physical Review A*, 92(2):022106, 2015. 94
- [221] L. C. Barbado, A. L. Baez-Camargo, and I. Fuentes. General method for computing the evolution of a quantum scalar field in curved spacetime. applications to small perturbations and cosmology. *arXiv preprint arXiv:1811.10507*, 2018. 103
- [222] E. Gibney. Universe’s coolest lab set to open up quantum world. *Nature*, 557(7704):151, 2018. 103
- [223] E. A. Desloge. Nonequivalence of a uniformly accelerating reference frame and a frame at rest in a uniform gravitational field. *American Journal of Physics*, 57(12):1121–1125, 1989. 104
- [224] C. Yuce and Z. Ozcakmakli. The dynamical casimir effect for two oscillating mirrors in 3d. *Journal of Physics A: Mathematical and Theoretical*, 41(26):265401, 2008. 124

# Appendix A

## Notation and abbreviations

Tables A.1 and A.2 respectively list the abbreviations and some of the notation used in the text.

<b>Abbreviation</b>	<b>Meaning</b>
BEC	Bose-Einstein Condensate
DCE	Dynamical Casimir Effect
EPR	Einstein-Podolsky-Rosen
POVM	Positive-Operator-Valued Measure
PPT	Positive Partial Trace
QFT	Quantum Field Theory
SQUID	Superconducting QUantum Interference Device
ZARM	Zentrum für Angewandte Raumfahrttechnologie und Mikrogravitation (Center of Applied Space Technology and Microgravity)

Table A.1: A list of the abbreviations used in the text.

Notation	Meaning
$\oplus$	the direct sum
$\otimes$	the tensor product
$A^{\otimes n}$	the tensor product of $A$ with itself, $n$ times
$\{\dots\}$	a set of objects
$\langle A \rangle$	the expectation value of $A$ with respect to some quantum state
$\det A$	the determinant of $A$
$\text{tr} A$	the trace of $A$
$A^T$	the transpose of $A$
$A^{TB}$	the partial transpose of $A$ with respect to the subspace $B$
$A^*$	the complex conjugate of $A$
$A^\dagger$	the Hermitian conjugate of $A$ ; $A^\dagger := A^{T*}$
$A^{(j)}$	the part of $A$ which is $j^{\text{th}}$ -order in some small quantity
$A^{[j]}$	denotes that $A$ corresponds to boundary $j$
$\Re(a), \Im(a)$	the real and imaginary parts of $a$ , respectively
$\partial_\mu$	partial derivative with respect to coordinate $x^\mu$
$\partial_y$	partial derivative with respect to quantity $y$
$\nabla_\mu$	covariant derivative
$\delta_{ij}, \delta_j^i$	Kronecker delta, equal to 1 if $i = j$ , and 0 otherwise)
$\mathbf{x}$	a spatial vector with components $x^k$ , with $k = 1, 2, 3$
$\mathcal{T}\text{exp}$	the time-ordered exponential

Table A.2: A list of the abbreviations used in the text.

## Appendix B

# The Bogoliubov transformation for constant-length motion

In this appendix, we present a test the validity of the results given in Chapter 5. Specifically, for the subset of boundary trajectories such that the distance between the boundaries is constant (in the conformally-flat coordinates), we give an alternative way to find the Bogoliubov transformation resulting from the motion, and show to first order that it coincides with the results of Chapter 5.

We adopt the notation and definitions of Chapter 5, and we further define

$$A := A^{[1]} + A^{[2]} \tag{B.1a}$$

$$B := B^{[1]} + B^{[2]}, \tag{B.1b}$$

where  $A^{[j]}$  and  $B^{[j]}$  (with  $j = 1, 2$ ) were defined in Equations (5.9b). For constant  $L$ , we have  $\frac{dx_1}{dt} = \frac{dx_2}{dt}$ , and then Equations (5.12) give, to first order

$$\alpha_{mn} = e^{i\omega_m T} \left[ \delta_{mn} + A_{mn} \int_0^T dt e^{-i(\omega_m - \omega_n)t} \frac{dx_1}{dt} \right] \tag{B.2a}$$

$$\beta_{mn} = e^{i\omega_m T} B_{mn} \int_0^T dt e^{-i(\omega_m + \omega_n)t} \frac{dx_1}{dt}. \tag{B.2b}$$

We will now show another way to derive Equations (B.2), starting from the equation of motion for the field (Equation (5.1)), which we recall here:

$$(\partial_t^2 - \partial_x^2) \Phi = 0. \tag{B.3}$$

In the same manner as [224], we move to new coordinates  $(t, q)$  with  $q(t, x) :=$

$x - x_1(t)$ , and thus

$$\partial_t^2 - \partial_x^2 \rightarrow \partial_t^2 + (\dot{q}^2 - 1) \partial_q^2 + \ddot{q} \partial_q + 2\dot{q} \partial_q \partial_t \quad (\text{B.4})$$

where a dot denotes the derivative with respect to  $t$ . To incorporate the low-velocity assumption, i.e.  $|\dot{q}| \ll 1$ , we assume that we can write  $\dot{q}(t) = \eta \dot{y}(t)$  for some  $y(t)$  and  $\eta \ll 1$ . To first order in  $\eta$ , Equation (B.3) is then

$$[\partial_t^2 - \partial_q^2 + \ddot{q} \partial_q + 2\dot{q} \partial_q \partial_t] \Phi(t, q) = 0 \quad (\text{B.5})$$

with the (now time-independent) boundary conditions  $\Phi(t, 0) = \Phi(t, L) = 0$ . We seek solutions  $\varphi_m(t, q)$  to Equation B.5 in terms of the spatial part of the stationary-cavity solutions given in Equation (5.2):

$$\varphi_m(t, q) = \sum_p Q_{mp}(t) N_p \sin(\omega_p q) \quad (\text{B.6})$$

For a cavity which is stationary for  $t \leq 0$  and  $t \geq T$ , we have the conditions

$$\varphi_m(t \leq 0, q) = N_m e^{-i\omega_m t} \sin(\omega_m q) \quad (\text{B.7a})$$

$$\varphi_m(t \geq T, q) = \sum_p \left\{ N_p \left( \tilde{\alpha}_{mp} e^{-i\omega_p t} + \tilde{\beta}_{mp} e^{i\omega_p t} \right) \sin(\omega_p q) \right\}, \quad (\text{B.7b})$$

i.e.

$$Q_{mn}(t \leq 0) = e^{-i\omega_m t} \delta_{mn} \quad (\text{B.8a})$$

$$Q_{mn}(t \geq T) = \tilde{\alpha}_{mn} e^{-i\omega_n t} + \tilde{\beta}_{mn} e^{i\omega_n t}, \quad (\text{B.8b})$$

where  $\tilde{\alpha}_{mn}$  and  $\tilde{\beta}_{mn}$  are the Bogoliubov coefficients encoding how the post-motion solutions can be written in terms of the pre-motion ones. We now insert the general solution (Equation (B.6)) into Equation (B.5) and obtain an infinite set of coupled differential equations for the  $Q_{mn}(t)$ . To do this, we use the following identities

$$\int_0^L dq N_m \sin(\omega_m q) N_n \sin(\omega_n q) = \frac{\delta_{mn}}{2\omega_n} \quad (\text{B.9a})$$

$$\int_0^L dq N_m \cos(\omega_m q) N_n \sin(\omega_n q) = g_{mn} \quad (\text{B.9b})$$

where

$$g_{mn} := \begin{cases} 0 & \text{for } m = n \\ \frac{\sqrt{mn} [1 - (-1)^{m+n}]}{(m+n)(m-n)\pi} & \text{for } m \neq n. \end{cases} \quad (\text{B.10})$$

We thus obtain

$$\ddot{Q}_{mn} + \omega_n^2 Q_{mn} = 2\omega_n \sum_p \left( 2\dot{q} \dot{Q}_{mp} + \ddot{q} Q_{mp} \right) g_{pn} \quad (\text{B.11})$$

Seeking solutions up to first order in  $\eta$ , we write  $Q_{mn} = Q_{mn}^{(0)} + \eta Q_{mn}^{(1)}$ , and hence obtain equations for the zero and first-order parts:

$$\ddot{Q}_{mn}^{(0)} + \omega_n^2 Q_{mn}^{(0)} = 0 \quad (\text{B.12a})$$

$$\ddot{Q}_{mn}^{(1)} + \omega_n^2 Q_{mn}^{(1)} = 2\omega_n \sum_p \left( 2\dot{y} \dot{Q}_{mp}^{(0)} + \ddot{y} Q_{mp}^{(0)} \right) g_{pn}. \quad (\text{B.12b})$$

The condition given in Equation (B.8a) then becomes

$$Q_{mn}^{(0)}(t \leq 0) = e^{-i\omega_m t} \delta_{mn} \quad \text{and} \quad Q_{mn}^{(1)}(t \leq 0) = 0. \quad (\text{B.13})$$

Assuming continuity of  $Q_{mn}(t)$  and  $\dot{Q}_{mn}(t)$  at  $t = 0$ , we solve Equations (B.12) subject to the conditions (B.13), giving

$$Q_{mn}^{(0)}(t) = e^{-i\omega_m t} \delta_{mn} \quad (\text{B.14a})$$

$$Q_{mn}^{(1)}(t) = g_{mn} \int_0^t ds \left[ (\omega_m + \omega_n) e^{-i(\omega_m - \omega_n)s} e^{-i\omega_n T} - (\omega_m - \omega_n) e^{-i(\omega_m + \omega_n)s} e^{i\omega_n T} \right] \dot{y}(s). \quad (\text{B.14b})$$

Now, comparing the definitions of  $A_{mn}$  and  $B_{mn}$  (Equations (B.1)), with that of  $g_{mn}$  (Equation (B.10)), we find that  $g_{mn} = -\frac{A_{mn}}{\omega_m + \omega_n}$  and  $g_{mn} = \frac{B_{mn}}{\omega_m - \omega_n}$ , and hence

$$Q_{mn}^{(0)}(t) = e^{-i\omega_m t} \delta_{mn} \quad (\text{B.15a})$$

$$Q_{mn}^{(1)}(t) = - \int_0^t ds \left[ A_{mn} e^{-i(\omega_m - \omega_n)s} e^{-i\omega_n T} + B_{mn} e^{-i(\omega_m + \omega_n)s} e^{i\omega_n T} \right] \dot{y}(s). \quad (\text{B.15b})$$

We obtain the Bogoliubov coefficients by using the condition given in Equation (B.8b) and continuity at  $t = T$ :

$$\tilde{\alpha}_{mn} = \delta_{mn} + A_{mn} \int_0^T dt e^{-i(\omega_m - \omega_n)t} \dot{x}_1(t) \quad (\text{B.16a})$$

$$\tilde{\beta}_{mn} = B_{mn} \int_0^T dt e^{-i(\omega_m + \omega_n)t} \dot{x}_1(t). \quad (\text{B.16b})$$

These correspond to the transformation from the pre-motion mode solutions to the post-motion solutions, where both sets of solutions are evaluated at  $t = T$ . To transform from pre-motion solutions evaluated at  $t = 0$  to post-motion solutions evaluated at  $t = T$ , we “undo” the phase evolution of the pre-motion solutions from

$t = 0$  to  $t = T$ , giving the coefficients:

$$\alpha_{mn} = e^{i\omega_m T} \left[ \delta_{mn} + A_{mn} \int_0^T dt e^{-i(\omega_m - \omega_n)t} \dot{x}_1(t) \right] \quad (\text{B.17a})$$

$$\beta_{mn} = e^{i\omega_m T} B_{mn} \int_0^T dt e^{-i(\omega_m + \omega_n)t} \dot{x}_1(t), \quad (\text{B.17b})$$

which are exactly Equations (B.2). The two methods therefore coincide.

## Appendix C

# The Bogoliubov transformation for boundary motion in a static 3+1D spacetime

The results presented in Section 5.4 can be straightforwardly generalised to a static spacetime with 3 + 1D. Considering such a spacetime, there exist some coordinates  $(t, \mathbf{x})$  (where  $\mathbf{x}$  has components  $x^k$  with  $k = 1, 2, 3$ ) such that the Klein-Gordon equation (Equation (2.16), with zero mass) is separable, i.e. one can seek solutions in the form  $\phi_m(t, \mathbf{x}) = T_m(t)X_m(\mathbf{x})$  (where the label  $m$  is no longer a single number). In this case,  $\partial_t$  is a timelike Killing vector, and (ignoring normalisation) we have  $T_m(t) = e^{-i\omega_m t}$  for some  $\omega_m$ . As in Section 5.4, we write the solutions as  $\phi_m(t, \mathbf{x}; \mathbf{x}_1, \mathbf{x}_2)$ , where  $\mathbf{x}_1$  and  $\mathbf{x}_2$  now denote the boundary positions in  $D$  spatial dimensions, and we can now follow exactly the same procedure as before, with  $S_\delta$  now comprised of inner products between  $\phi_m(t, \mathbf{x}; \mathbf{x}_1, \mathbf{x}_2)$  and  $\phi_m(t, \mathbf{x}; \mathbf{x}_1 + \delta\mathbf{x}_1, \mathbf{x}_2 + \delta\mathbf{x}_2)$ . The total transformation then satisfies the multi-dimensional generalisation of Equation (5.8):

$$\frac{dS}{dt} = \left[ i\Omega + M_k^{[1]} \frac{dx_1^k}{dt} + M_k^{[2]} \frac{dx_2^k}{dt} \right] S \quad (\text{C.1})$$

where the sum over  $k$  is implicit, and

$$M_k^{[j]} = \begin{bmatrix} A_k^{[j]} & B_k^{[j]} \\ B_k^{[j]*} & A_k^{[j]*} \end{bmatrix}, \quad (\text{C.2a})$$

$$\left( A_k^{[j]} \right)_{mn} := \left( \frac{\partial \phi_m}{\partial x_j^k}, \phi_n \right), \quad \left( B_k^{[j]} \right)_{mn} := - \left( \frac{\partial \phi_m}{\partial x_j^k}, \phi_n^* \right), \quad (\text{C.2b})$$

with  $j = 1, 2$ .

## Appendix D

# Unitary form of perturbative Bogoliubov transformations

In this Appendix we give a recipe for translating from perturbative Bogoliubov transformations of mode solutions to unitary transformation of field states (up to first order). We recall that the Bogoliubov coefficients are written perturbatively as (Equations (2.46))

$$\alpha_{mn} = G_m \delta_{mn} + \alpha_{mn}^{(1)} \quad (\text{D.1a})$$

$$\beta_{mn} = \beta_{mn}^{(1)} \quad (\text{D.1b})$$

with  $|G_m|^2 = 1$ . Let us write  $G_m = e^{i\theta_m}$  for some  $\theta_m \in \mathbb{R}$ . We note that every unitary transformation  $U$  can be written in terms of a generating Hermitian matrix  $H$  as  $U = e^{-iH}$ . Now, since the transformation which we seek is Gaussian, this matrix is at-most-quadratic in the ladder operators (see Section 3.2), and we can therefore write

$$H = -\frac{1}{2} \sum_{mn} \left( X_{mn} a_m^\dagger a_n + X_{mn}^* a_m a_n^\dagger + Y_{mn} a_m^\dagger a_n^\dagger + Y_{mn}^* a_m a_n \right) \quad (\text{D.2})$$

for some  $X = X^\dagger$  and  $Y = Y^T$ . Now, if we write the generator perturbatively as  $H = H_{(0)} + H_{(1)}$ , i.e.  $X = X^{(0)} + X^{(1)}$  and  $Y = Y^{(0)} + Y^{(1)}$ , then to reproduce the zero-order effect of Equations (D.1), we must have  $X_{mn}^{(0)} = -\delta_{mn}\theta_m$  and  $Y^{(0)} = 0$ . Now, from the definition of the exponential, we have

$$U = \sum_{k=0}^{\infty} \frac{(-i)^k}{k!} (H_{(0)} + H_{(1)})^k. \quad (\text{D.3})$$

It will be useful to introduce the following notation. We write  $\lfloor x \rfloor_k$ , with  $x \in \mathbb{N}$ , to represent the operator composed of product of  $k$  operators, each being either  $H_{(0)}$  or  $H_{(1)}$ , such that the subscripts of this product give the  $k$ -bit representation of the number  $x$ . For example, the 4-bit representation of the number 5 is 0101, and therefore  $\lfloor 5 \rfloor_4 \equiv H_{(0)}H_{(1)}H_{(0)}H_{(1)}$ . We leave  $\lfloor x \rfloor_k$  undefined in the case where  $x > 2^k - 1$  (i.e.  $x$  is too large to be represented with  $k$  bits). Using this notation, we have the relation

$$(H_{(0)} + H_{(1)})^k = \sum_{x=0}^{2^k-1} \lfloor x \rfloor_k, \quad (\text{D.4})$$

which can easily be proven by induction. Now, the order of a term represented by  $\lfloor x \rfloor_k$  is given by the Hamming weight (i.e. the number of 1's) of the binary representation of  $x$ . Therefore, since we work to first order, a term  $\lfloor x \rfloor_k$  is only non-negligible if  $x = 0$  (i.e. there term is zero-order) or if  $x = 2^j$  for some  $j \in \mathbb{N}$ . Consequently, combining Equations (D.3) and (D.4), to first order we have

$$\begin{aligned} U &= \sum_{k=0}^{\infty} \frac{(-iH_{(0)})^k}{k!} + \sum_{k=1}^{\infty} \frac{(-i)^k}{k!} \sum_{j=0}^{k-1} \frac{(-i)^j}{k!} \lfloor 2^j \rfloor_k \\ &= e^{-iH_{(0)}} + \sum_{k=1}^{\infty} \frac{(-i)^k}{k!} \sum_{j=0}^{k-1} H_{(0)}^{(k-1-j)} H_{(1)} H_{(0)}^j. \end{aligned} \quad (\text{D.5})$$

Now, for two arbitrary operators  $O_1$  and  $O_2$ , we have the relation

$$[O_1^k, O_2] = \sum_{j=0}^{k-1} O_1^{(k-1-j)} [O_1^j, O_2] O_1^j, \quad (\text{D.6})$$

which can also be proven by induction. Comparing Equation (D.6) with the last sum in (D.5), we seek some operator  $B$  such that

$$H_{(1)} = [H_{(0)}, B]. \quad (\text{D.7})$$

Such an operator is given by

$$\begin{aligned} B &= -\frac{1}{2} \sum_{mn} \left( \frac{X_{mn}^{(1)}}{\theta_m - \theta_n} a_m^\dagger a_n - \frac{X_{mn}^{(1)*}}{\theta_m - \theta_n} a_m a_n^\dagger \right. \\ &\quad \left. + \frac{Y_{mn}^{(1)}}{\theta_m + \theta_n} a_m^\dagger a_n^\dagger - \frac{Y_{mn}^{(1)*}}{\theta_m + \theta_n} a_m a_n \right). \end{aligned} \quad (\text{D.8})$$

Combining Equations (D.5-D.7), we then have

$$\begin{aligned} U &= e^{-iH(0)} + \sum_{k=1}^{\infty} \frac{(-i)^k}{k!} [H_{(0)}^k, B] \\ &= e^{-iH(0)} + [e^{-iH(0)}, B]. \end{aligned} \quad (\text{D.9})$$

The properties of  $X$  and  $Y$  imply that  $B^\dagger = -B$ , ensuring that  $U^\dagger U = \mathbf{1}$  (to first order).

Now, it remains only to express  $X^{(1)}$  and  $Y^{(1)}$  in terms of the Bogoliubov coefficients in Equation (D.1). To do this, we equate the transformation of the ladder operators in both representations, i.e.

$$U^\dagger a_m U = \sum_n \left( \alpha_{mn}^* a_n - \beta_{mn}^* a_n^\dagger \right), \quad (\text{D.10})$$

where the right-hand side was given by Equation (2.37). We use Equation (D.9), along with the Baker-Campbell-Hausdorff formula for two arbitrary operators  $O_1$  and  $O_2$ :

$$e^{O_1} O_2 e^{-O_1} = \sum_{k=1}^{\infty} \frac{1}{k!} [O_1, O_2]_k \quad (\text{D.11})$$

where  $[O_1, O_2]_0 := O_2$  and  $[O_1, O_2]_k := [O_1, [O_1, O_2]_{k-1}]$ . This gives

$$X_{mn}^{(1)} = -\frac{\theta_m - \theta_n}{e^{-i\theta_m} - e^{-i\theta_n}} \alpha_{mn}^{(1)*} \quad (\text{D.12a})$$

$$Y_{mn}^{(1)} = \frac{\theta_m + \theta_n}{e^{-i\theta_m} - e^{i\theta_n}} \beta_{mn}^{(1)*} \quad (\text{D.12b})$$

and hence, given Bogoliubov coefficients written in the form of Equations (D.1), i.e. the form used throughout this thesis, one can find the unitary transformation of the field state by substituting Equations (D.12) into Equation (D.8), and in turn substituting that into Equation (D.9), which we leave as an exercise to the reader. Following this recipe, one can confirm that the vacuum state transforms according to Equation (2.48) to first order.